

UNIVERSITÀ
DI PAVIA

Dipartimento di Biologia e Biotecnologie
"Lazzaro Spallanzani"

Laurea Magistrale in Molecular Biology and Genetics

Towards A Mechanistic Understanding of Gammaretrovirus Recognition of Host Receptors

Supervisor:
Professor Francesca Magnani

Experimental thesis by
Sara Al Tamam

Academic Year 2025/2026

Abstract

Feline leukemia virus (FeLV) enters host cells by exploiting multipass solute carriers as receptors: the heme exporter FLVCR1a (SLC49A1) for FeLV-C and the phosphate transporter PiT-1 (SLC20A1) for FeLV-B. It remains unclear whether the viral glycoprotein recognises a specific conformational state of these transporters, and whether cargo occupancy, by biasing the conformational equilibrium, modulates that recognition. No structure of FLVCR1a or PiT-1 in complex with a viral envelope protein has yet been reported.

This thesis combined biophysical analyses, membrane-protein production, and antibody-based tool development to address these questions. Building on established protocols for the purification of human FLVCR1a, reported to bind to the FeLV-type C, I used microscale thermophoresis and nano-differential scanning fluorimetry to show that hemin binds purified human FLVCR1a and increases the affinity of the FeLV-C surface-unit receptor-binding domain for the receptor by approximately sixfold. To my knowledge, this is the first biophysical evidence that substrate occupancy can influence the activity of FLVCR1a as a retroviral receptor, consistent with a conformational model of regulation that remains to be tested directly. Size-exclusion chromatography supported complex formation under these conditions, although the chromatographic conditions require further optimisation before the complex can be isolated as a homogeneous species. In parallel, in order to improve the affinity between the FeLV-type B-SU and the receptor, the feline orthologue was expressed and purified.

Two further strands of work were undertaken to enable future studies. To extend the approach beyond a single receptor–envelope pair, I produced the FeLV-B receptor-binding domain together with its receptor, PiT-1, establishing the groundwork for a comparative analysis of FeLV receptor engagement. To support structural work on FLVCR1a, a panel of 16 monoclonal antibodies against human FLVCR1a was characterised, and seven clones bound the native receptor. One of these, 339F1, appears to recognise a conformational epitope and is therefore a promising candidate as a fiducial marker for cryo-EM.

In conclusion, these results link transporter-substrate occupancy to retroviral receptor function *in vitro* and provide reagents and a methodological basis for future structural studies of FeLV receptor engagement.

Table of Contents

1. Introduction……6

1.1 Retroviruses and receptor usage……6

1.1.1 Multipass solute carriers as retroviral entry receptors……..6

1.1.2 Sequence divergence of viral envelope proteins vs. conservation of host receptor…….12

1.2 Feline Leukemia Virus (FeLV)……..12

1.2.1 FeLV subgroups A, B, C: host range and receptor usage……13

1.2.2 The FeLV Env glycoprotein: SU and TM subunits……14

1.2.3 Domain organization of the SU protein: signal peptide, RBD, VRA/VRB/VRC, PRR, and C-domain……15

1.2.4 Sequence comparison across FeLV-A/B/C and recombinant strains……15

1.3 FLVCR1a……..18

1.3.1 FLVCR1a as a heme exporter/transporter (SLC49 family)……..18

1.3.2 FLVCR1a as the receptor for FeLV-C……...21

1.3.3 Structural topology and known functional sites……24

1.4 fFLVCR1a: the feline orthologue of FLVCR1a……27

1.4.1 Identification of fFLVCR1a as the feline form of hFLVCR1a……27

1.4.2 Sequence and structural conservation between feline and human FLVCR1a……..28

1.4.3 Relevance of fFLVCR1a as a model system for studying FeLV receptor biology……..29

1.5 SLC20 family transporters and FeLV-B receptor usage……30

1.5.1 SLC20A1 (PiT-1) and SLC20A2 (PiT-2): phosphate transporters as retroviral receptors..30

1.5.2 FeLV-B RBD interaction with SLC20A1/PiT-1……..33

1.5.3 Critical residues in FeLV-B Env required for PiT-1 binding……34

1.5.4 PiT-1 extracellular loops as determinants of Env recognition……..38

1.5.5 Mutational studies comparing PiT-1 and PiT-2 receptor usage……43

1.6 Antibodies as structural biology tools……43

1.6.1 Bivalent scFv-Fc versus Fab antibody formats……44

1.6.2 Linear versus conformational epitopes and their relevance to cryo-EM……..47

1.7 Aims of the thesis……..51

2. Materials and Methods……..……..53

2.1 Molecular cloning……..……53

2.1.1 Cloning of the FeLV-B SU receptor-binding domain (RBD)……..……..54

2.1.2 Cloning of fSLC20A1 constructs……..……56

2.1.3 Cloning of the fFLCR1a construct……57

2.1.4 hFLVCR1a-GFP construct (Data from Professor Francesca Magnani)……58

2.1.5 hFLVCR1a construct (Strep-FLAG-Strep tag, purification protocol development)……58

2.2 Protein expression……59

2.2.1 Transient transfection of HEK293F cells (hFLVCR1a-GFP, pEGBacMam)……..…..59

2.2.2 Expression system(s) for fFLVCR1a……60

2.2.3 Expression system(s) for FeLV-B SU RBD……..62

2.2.4 Expression system(s) for fSLC20A1……63

2.3 Protein purification……64

2.3.1 Affinity chromatography……..64

2.3.2 Size-exclusion chromatography (Superose 6, DDM/CHS buffer system)…….……..…66

2.3.3 Purification quality control (SDS-PAGE, western blot)……..……..67

2.4 Antibody generation……68

2.4.1 Bivalent scFv-Fc monoclonal antibodies against hFLVCR1a (raised by F. Bertoglio, TU Braunschweig) (Data from Prof. Francesca Magnani)……69

2.4.2 Fab 339-F1 generation and format……70
2.5 Binding and biophysical characterization methods……..70
2.5.1 Microscale thermophoresis (MST) (Data from Prof. Francesca Magnani)……..71
2.5.2 Nano differential scanning fluorimetry (nDSF) (Data from Prof. Francesca Magnani……71
2.5.3 Gel filtration chromatography / SEC-based complex formation assay (all binding experiments) (Data from Prof. Francesca Magnani)…… ……72
2.5.4 Magnetic pulldown assay (hFLVCR1a and FeLV-C SU)……72
2.5.5 ELISA screening (Data from Prof. Francesca Magnani)……..73
2.5.6 SDS-PAGE and western blotting (anti-human Fc-HRP and GFP fluorescence detection) (Data from Prof. Francesca Magnani)……74

3. Results……..75
3.1 Binding of porphyrins to hFLVCR1a (Data from Professor Francesca Magnani)……75
3.1.1 Hemin binding to hFLVCR1a by MST……75
3.1.2 Coproporphyrin I binding to hFLVCR1a by MST……76
3.1.3 Thermal stability of hFLVCR1a in the apo state and in the presence of hemin and coproporphyrin I (nDSF)……..77
3.2 Characterization of the hFLVCR1a–FeLV-C SU interaction…….……78
3.2.1 Heme dependence of FeLV-C SU binding to hFLVCR1a (Data from Professor Francesca Magnani)……..79
3.2.2 Complex formation of FeLV-C SU and hFLVCR1a assessed by size-exclusion chromatography (SEC)……80
3.2.3 Validation of the interaction by magnetic pulldown assay…….……..84
3.3 Cross-reactivity of bivalent scFv-Fc monoclonal antibodies with murine FLVCR1a (Data from Professor Francesca Magnani)……90
3.4 Characterization of the hFLVCR1a–Fab 339F1 interaction…….……..91
3.4.1 Complex formation assessed by gel filtration chromatography (SEC)……91
3.5 Expression and purification of feline FLVCR1a…….……..95
3.5.1 Construct design……95
3.5.2 Small-scale expression by transient transfection……..96
3.5.3 Baculovirus generation…….……97
3.5.4 Large-scale expression and purification……97
3.6 Cloning, expression, and purification of FeLV-B SU RBD……..99
3.6.1 Cloning strategy…….……100
3.6.2 Expression optimization……..102
3.6.3 Purification and quality control…….……..103
3.6.4 Recloning of the RBD cassette into pEG BacMam……107
3.6.5 Signal peptide substitution: FeLV-B-RBD with the μ-phosphatase signal peptide……108
3.6.6 Small-scale expression and affinity-capture test of the native SP and μ-phosphatase SP constructs……110
3.7 Cloning, expression, and purification of fSLC20A1 (PiT-1)……..111
3.7.1 Cloning strategy……..112
3.7.2 Expression optimization……..114
3.7.3 Purification and quality control…….……..116
3.7.4 Redesign of the PiT-1 construct: repositioning the TwinStrep tag to the N-terminus……118
3.7.5 Verification of N-terminus-fSLC20A1 clones and bacmid generation……..……119
3.7.6 Expression test of fSLC20A1-C-terminus and N-terminus-fSLC20A1……120

4. Discussion……..122
4.1 Overview……122

4.2 hFLVCR1a substrate recognition: hemin binds and stabilises; coproporphyrin I does not……..……122
4.3 Heme as a switch for viral receptor engagement……123
4.4 Heme-dependent co-elution of FeLV-C SU with hFLVCR1a in SEC…..……..……124
4.5 An antibody and Fab toolkit for hFLVCR1a…….……..125
4.6 Successful optimization of RBD expression through expression in mammalian cells ……..…..……..128
4.7 fFLVCR1a expression and purification…….……..……129
4.8 fSLC20A1 (PiT-1) cloning and expression……..129
4.9 Lessons from an iterative membrane-protein production pipeline…..…..……131

5. Conclusions and Future Perspectives……..132
5.1 Conclusions…….132
5.2 Future Perspectives……133

6. References……..……137

1. Introduction

This thesis asks how two feline leukemia virus (FeLV) receptors, FLVCR1a and PiT-1, engage the viral envelope, and whether the transport state of the receptor influences that engagement. The Introduction builds the case in a deliberate order. It moves from the general principle that retroviruses use multipass solute carriers as receptors (1.1) to the virus (1.2), then to the two receptors studied here (1.3–1.5), and ends with the antibody-based tools chosen to make them accessible to cryo-EM (1.6). Each section supplies the background needed for a specific group of experiments in Chapter 3, and the gaps identified along the way lead directly to the aims in Section 1.7.

1.1 Retroviruses and receptor usage

The central question of the thesis, whether a transporter's conformational and ligand-occupancy state affects its role as a viral receptor, only makes sense if these receptors are understood as dynamic transporters rather than passive docking sites. Section 1.1.1 therefore establishes how widespread the use of multipass SLC proteins as retroviral receptors is, and how Env-mediated fusion depends on receptor binding as its first step. Section 1.1.2 then sets the evolutionary asymmetry between a variable viral RBD and a conserved host receptor, which is the framework used later to interpret the receptor-binding experiments (Section 3.2).

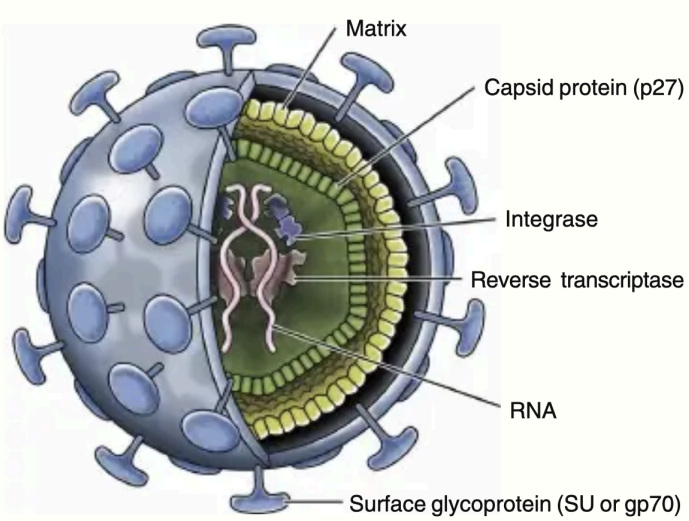
1.1.1 Multipass solute carriers as retroviral entry receptors

Retroviral entry begins when the viral envelope glycoprotein’s surface (SU) subunit recognizes a receptor on the host cell. This interaction determines which cell types, tissues, and species the virus can infect. In several well-studied gammaretroviruses, deltaretroviruses, and disulfide-linked betaretroviruses, these receptors belong to an unexpected group: instead of using single-pass or GPI-anchored surface proteins, as many retroviruses and other enveloped viruses do, they use polytopic, multipass membrane transporters from the solute carrier (SLC) superfamily [78].

One of the best-known examples is PiT1 (SLC20A1), a sodium-dependent phosphate transporter. PiT1 was first identified as the receptor for gibbon ape leukemia virus (GALV) and was later shown to function naturally as a type III Na^+/Pi cotransporter [58, 78]. It is now known to act as the entry receptor for several viruses, including GALV, woolly monkey virus (WMV), feline leukemia virus subgroup B (FeLV-B), FeLV-T, 10A1-MLV, and koala retrovirus subtype A (KoRV-A). Because the receptor-binding domains of these viruses share relatively little sequence similarity, their independent use of PiT1 is a striking example of convergent evolution among gammaretroviruses

[78]. PiT2 (SLC20A2), a closely related transporter with approximately 60% amino acid identity to PiT1, serves as the main receptor for amphotropic murine leukemia virus (A-MLV). It can also act as a secondary receptor for 10A1-MLV and, in certain rodent cell lines, for GALV and KoRV-A [78].

The use of SLC transporters is not limited to PiT1 and PiT2. Figure 1.1, adapted from Greenwood et al. (2018) [78], summarizes the range of SLC-family transporters known to function as retroviral receptors. These include phosphate transporters such as PiT1, PiT2, and the phosphate exporter XPR1; vitamin transporters such as SLC19A2/THTR1, which transports thiamine and serves as the receptor for FeLV-A and KoRV-B; and SLC5A1/HuPAR-2, a riboflavin transporter used by PERV-A. Other examples include the amino acid transporters SLC1A4/ASCT2 and SLC1A5/ASCT1, which are used by RD-114, baboon endogenous virus, and several human endogenous retroviruses; the cationic amino acid transporter SLC7A1/MCAT, used by ecotropic MLV; and the heme transporter SLC49A1/FLVCR1a, used by FeLV-C [78].



Virus(es)	Transporter gene name (product)	Transporter function
KoRV-A, GALV, FeLV-B, 10A1-MLV, FeLV-T, WMV	*slc20a1 (previously GLVR1; now PiT1)*	Sodium-dependent phosphate transporter
KoRV-B, FeLV-A	*slc19a2 (THTR1)*	Thiamine/folate transporter
A-MLV, 10A1-MLV, GALV, FeLV-B	*slc20a2 (previously GLVR2; now PiT2)*	Sodium-dependent phosphate transporter
E-MLV, BLV	*slc7a1 (MCAT)*	Cationic amino acid transporter
M813, HEMV	*slc5a3 (Smit1)*	Sodium/myoinositol cotransporter
RD-114, BaEV, REV, SRVs 1 to 5, HERV-W	*slc1a5 (ASCT1)*	Glutamate/neutral amino acid transporter
BaEV, HERV-W	*slc1a4 (ASCT2)*	Glutamate/neutral amino acid transporter
FeLV-C	*slc49a1, slc49a2*	Heme importer and exporter
X-MLV, P-MLV	*Xpr1 (ND)*	Phosphate exporter
PERV-A	*slc5a1 (huPAR-2)*	Riboflavin transporter
GLN MLV	*slc19a1*	Thiamine/folate transporter
ALV-J	*slc9a1 (NHE-1)*	Sodium/hydrogen exchanger
HTLV	*slc2a1 (Glut-1)*	Glucose transporter

Figure 1.1. Several retroviruses use multipass solute carrier proteins as receptors to enter host cells. The figure shows the basic structure of a gammaretroviral particle—including the matrix, capsid, integrase, reverse transcriptase, RNA genome, and surface glycoprotein (gp70)—alongside a table summarizing retroviruses that use SLC-family transporters as entry receptors. The table identifies each transporter gene, its normal physiological transport function, and the virus or viruses that use it for cell entry. Adapted from Greenwood, Ishida, O'Brien, Roca, and Eiden, *Microbiology and Molecular Biology Reviews* (2018).

FeLV-C's use of FLVCR1a (SLC49A1), a heme exporter required for normal red blood cell development, is particularly relevant to this thesis. Infection with FeLV-C is associated with severe,

and often fatal, aplastic anemia. This disease outcome differs markedly from the leukemia, lymphoma, and tumor formation associated with FeLV-B, which uses a phosphate transporter, and the immunosuppression and lymphoma associated with FeLV-A, which uses a thiamine transporter (Figure 1.2). These differences suggest a relationship between the receptor a virus uses, the transporter's normal physiological function, and the disease it causes. In FeLV-C infection, for example, the disruption of a heme exporter is linked to anemia, whereas targeting a phosphate transporter is associated with phosphate- and growth-signalling abnormalities. This recurring pattern among FeLV subgroups supports the central premise of this thesis: understanding FeLV receptor engagement at the molecular and structural levels requires viewing these transporters not simply as passive docking sites, but as dynamic proteins that cycle through distinct conformational states and whose extracellular surfaces are remodelled by that cycle. Since the loops presented to the virus differ between outward-open, occluded, and inward-open states, the determinants of RBD recognition may themselves be transient, and substrate occupancy could modulate receptor availability by shifting the conformational equilibrium.

FeLV subgroup	Receptor	Associated disease
FeLV-A	Putative thiamine transporter THTR1 (SLC19A2)	Macrocytic anemia Immunosuppression Lymphoma
FeLV-B	Inorganic phosphate transporters PiT1 and PiT2 (SLC20A1/A2)	Leukemia Lymphoma Tumor formation
FeLV-C	Heme exporter FLVCR1a (SLC49A1)	Aplastic anemia
FeLV-T	Inorganic phosphate transporter PiT1 (SLC20A1) + co-receptor FeLIX (enFeLV-derived)	Feline acquired immunodeficiency syndrome (FAIDS)

Figure 1.2. Viral tropism influences disease outcomes. Summary of the four recognized FeLV subgroups—FeLV-A, FeLV-B, FeLV-C, and FeLV-T—their cellular receptors, and the clinical syndromes associated with each. FeLV-A, which is thought to use the thiamine transporter THTR1 (SLC19A2), is associated with macrocytic anemia, immunosuppression, and lymphoma. FeLV-B uses the phosphate transporters PiT1 and PiT2 (SLC20) and is associated with leukemia, lymphoma, and tumor formation. FeLV-C uses the heme exporter FLVCR1a (SLC49A1) and causes aplastic anemia. FeLV-T uses PiT1 together with the co-receptor FeLIX, an endogenous FeLV-derived protein, and causes feline acquired immunodeficiency syndrome (FAIDS). This work is motivated by the broader goal of understanding the molecular basis of retroviral receptor tropism.

The structural mechanism by which SU–receptor binding initiates membrane fusion is conserved across the gamma-type Env family, which includes gammaretroviruses, alpharetroviruses, and deltaretroviruses [79]. Mature Env is produced as a trimeric precursor and cleaved at a furin site into two disulfide-linked subunits: the surface (SU) subunit and the transmembrane (TM) subunit. SU contains the signal peptide, receptor-binding domain (RBD), three variable regions (VRA–VRC), and a proline-rich region (PRR). TM contains the fusion peptide, two heptad-repeat regions (HR1 and HR2) surrounding an immunosuppressive domain (ISD), a membrane-spanning domain, and a cytoplasmic tail that ends in a YXXL motif and an R-peptide (Figure 1.3) [79]. SU and TM remain covalently connected through an intersubunit disulfide bond, formed by the CXXC–$C(X)_6CC$ motif, until the virus binds its receptor. Receptor engagement then initiates a series of coordinated conformational changes. First, the RBD binds the cellular receptor, triggering extension of TM and insertion of the fusion peptide into the target-cell membrane. In gamma- and deltaretroviruses, cellular or viral thiol isomerases catalyse rearrangement of the SU–TM disulfide bond, allowing SU to dissociate from TM. TM then folds into a six-helix bundle that pulls the viral and cellular membranes together. The membranes subsequently fuse, releasing the viral core into the cytoplasm (Figure 1.4) [79]. This mechanism makes receptor binding the essential first step—and a potential rate-limiting point—within a larger conformational cascade. Consequently, any factor that affects the affinity or kinetics of RBD–receptor binding, including the receptor's conformational or ligand-bound state, could influence every later stage of viral entry.

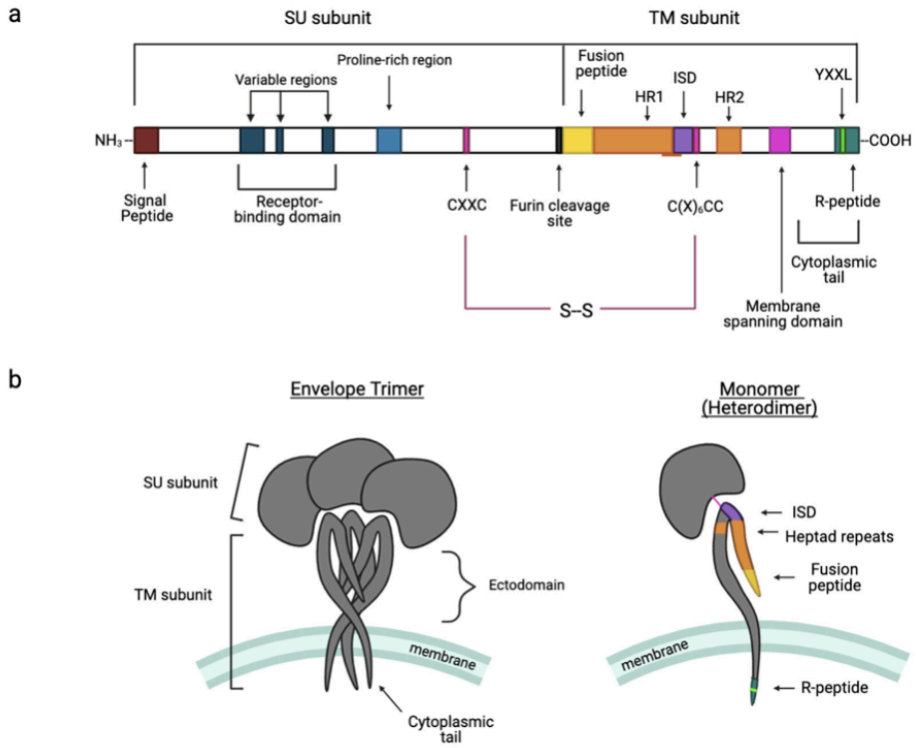


Figure 1.3. Domain architecture of a gamma-type retroviral envelope glycoprotein. (a) Linear domain map of the SU and TM subunits. SU contains the signal peptide, receptor-binding domain, three variable regions, and proline-rich region. SU is linked to TM by a CXXC/C(X)$_6$CC disulfide pair spanning the furin cleavage site. TM contains the fusion peptide, heptad repeats 1 and 2 (HR1/HR2), the immunosuppressive domain (ISD), the membrane-spanning domain, and a cytoplasmic tail ending in a YXXL motif and R-peptide. (b) Quaternary organization of the Env trimer (left) and a single SU–TM heterodimer (right), showing the ectodomain, membrane-spanning region, and cytoplasmic tail. Adapted from Hogan and Johnson, Viruses (2023).

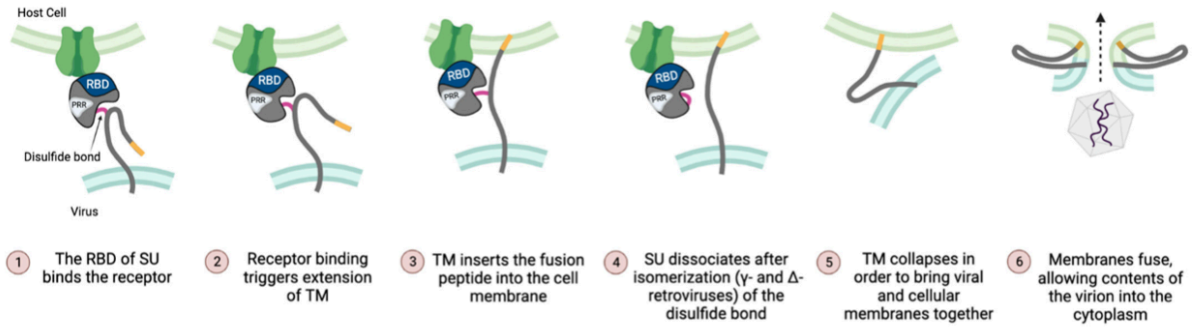


Figure 1.4. Receptor binding initiates a stepwise gamma-type Env fusion cascade. (1) The SU receptor-binding domain binds the cellular receptor. (2) Receptor binding triggers extension of TM. (3) TM inserts its fusion peptide into the target-cell membrane. (4) SU dissociates from TM following rearrangement of the intersubunit disulfide bond. (5) TM folds into a six-helix bundle, bringing the viral and cellular membranes together. (6) The membranes fuse, releasing the viral core into the cytoplasm. Adapted from Hogan and Johnson, Viruses (2023).

1.1.2 Sequence divergence of viral envelope proteins and conservation of host receptors

The SU–receptor relationships described above reveal a pronounced asymmetry in the evolutionary constraints acting on the two binding partners. Host SLC receptors are generally ancient, essential proteins that are subject to strong purifying selection. PiT1 (SLC20A1), for example, is a widely expressed and highly conserved phosphate symporter, and complete loss of the gene is embryonically lethal in mice [76, 78]. Similarly, FLVCR1a is required for the expansion of committed erythroid progenitors, whereas its mitochondrial isoform FLVCR1b (Section 1.3.2) contributes to expansion and is required for differentiation [88]. FLVCR1a also contributes to systemic heme and iron balance [3, 17]. The viral RBD follows a very different evolutionary path. It is one of the most variable regions of Env because it determines host range and cellular tropism while also serving as a major target of neutralizing antibodies [11, 13].

The viral RBD therefore evolves under very different constraints from the receptor it engages. Comparison of FeLV-A, -B and -C SU sequences shows that variation is concentrated in the signal peptide and the RBD, particularly VRA, whereas the C-domain and membrane-proximal region are highly conserved (Section 1.2.4; Figure 1.5) [11–14]. Localized changes in VRA can be sufficient to redirect receptor choice: a single glutamine-to-arginine substitution at VRA position 73 helps determine whether FeLV-B can use PiT2 in addition to PiT1 (Section 1.5.3) [82]. A variable receptor-binding module on a conserved Env scaffold, directed at an essential and highly conserved host transporter, is a general feature of gammaretroviruses [80, 81]. This tension between a rapidly diversifying binding domain and a constrained receptor motivates the central question of this thesis: whether the receptor's conformational and ligand-occupancy states, in addition to RBD sequence, contribute to the specificity and dynamics of receptor recognition (Section 3.2).

1.2 Feline Leukemia Virus (FeLV)

Because the thesis focuses on two FeLV subgroups, FeLV-C (via FLVCR1a) and FeLV-B (via PiT-1), this section introduces the virus and explains how the subgroups differ in origin, receptor and disease. It also describes the architecture of the Env glycoprotein and compares SU sequences across subgroups, which identifies the RBD and variable region A as the determinants of receptor choice. This background justifies the choice of the FeLV-C SU RBD as the viral ligand in the

binding assays (Section 3.2) and the FeLV-B RBD as the ligand for PiT-1, and it explains why the clinical severity of FeLV-C infection motivates a biophysical study of FLVCR1a.

1.2.1 FeLV subgroups A, B, C: host range and receptor usage

Feline leukemia virus (FeLV) is a gammaretrovirus of domestic cats that spreads horizontally between animals. It was originally classified into interference subgroups according to the ability of one virus to prevent superinfection by another and according to the results of neutralization assays [11]. Four subgroups are now recognized—FeLV-A, -B, -C, and -T. These groups are distinguished not by completely separate genomic lineages, but by the specific cell-surface receptors recognized by their envelope glycoproteins (Figure 1.2, Section 1.1.1). FeLV-A is the naturally transmitted, exogenous form of the virus and is found in essentially all naturally infected cats. It uses the putative thiamine transporter THTR1 (SLC19A2) as its receptor [78]. The precise receptor determinants of FeLV-A have not been defined as thoroughly as those of the other subgroups. Infection with FeLV-A is associated with macrocytic anemia, immunosuppression, and lymphoma. FeLV-B, which is the focus of much of this thesis, does not arise through simple point mutations in FeLV-A. Instead, it is generated in vivo through recombination between infectious FeLV-A and env sequences derived from endogenous FeLV (enFeLV) proviruses that are fixed in the domestic cat genome [11, 12, 85]. The incorporation of enFeLV-derived sequence into the SU receptor-binding domain changes receptor usage from THTR1 to the sodium-dependent phosphate symporters PiT1 and, in some isolates, PiT2 (SLC20A1 and SLC20A2, respectively) [46, 78, 82, 83]. FeLV-B infection is clinically associated with leukemia, lymphoma, and tumor formation. FeLV-C, in contrast, develops from FeLV-A mainly through the accumulation of point mutations and small insertions or deletions, rather than through extensive recombination [11, 13]. It uses the heme exporter FLVCR1a (SLC49A1) as its receptor [15, 16]. Infection with FeLV-C causes severe, often fatal, pure red cell aplasia or aplastic anemia. This distinctive clinical phenotype is the main reason for the subgroup's biological importance and provides the rationale for the biophysical studies of FLVCR1a presented in this thesis (Sections 3.1–3.2). FeLV-T adds another level of complexity to FeLV receptor usage. It uses PiT1 as its primary receptor but also requires a soluble coreceptor called FeLIX. FeLIX is encoded by a defective endogenous FeLV-B-related provirus and closely resembles the isolated FeLV-B SU receptor-binding domain (RBD), both in sequence and, as shown by crystallography, in three-dimensional structure [84]. FeLIX is secreted by feline T lymphocytes. Because its tissue distribution is more restricted than that of PiT1, FeLIX expression—not PiT1

expression alone—determines the T-cell tropism responsible for FeLV-T-associated feline acquired immunodeficiency syndrome (FAIDS) [78, 84].

This pattern of receptor usage is not unique to FeLV. PiT1 also serves as a receptor for gibbon ape leukemia virus (GALV), woolly monkey virus, 10A1-MLV, and koala retrovirus subtype A (KoRV-A). However, the receptor-binding domains of these viruses share only limited sequence identity with one another and with FeLV-B [78]. PiT2 is also used as a receptor by amphotropic MLV [78, 82]. The repeated, convergent use of a small group of essential host transporters by structurally and phylogenetically diverse viral envelope proteins is a defining feature of gammaretroviral receptor biology and has been examined in several comparative studies [78, 86].

1.2.2 The FeLV Env glycoprotein: SU and TM subunits

The FeLV envelope glycoprotein (Env) has the canonical gamma-type architecture described in Section 1.1.1 (Figures 1.3 and 1.4) [79]: mature Env is a homotrimer of SU–TM heterodimers generated by furin cleavage of a single precursor, in which SU lies entirely outside the viral membrane and mediates receptor binding, whereas TM anchors Env in the membrane and carries the fusion machinery.

For FeLV, important structural information about this architecture comes from the X-ray crystal structure of the isolated FeLV-B SU receptor-binding domain, which was determined at 2.5 Å resolution [84]. This structure differs substantially from that of the receptor-binding domain of ecotropic Friend Murine Leukemia Virus (Fr-MLV), which recognizes a different receptor, the cationic amino acid transporter mCAT1 [80, 84]. This difference is notable because both proteins perform comparable receptor-binding functions and belong to the same broad gammaretroviral Env family. Barnett et al. (2003) [84] also showed that the isolated FeLV-B RBD retains post-binding activity when supplied in trans as a soluble monomer, separate from the virion. Purified FeLV-B RBD can activate membrane fusion by mutant Env proteins whose own receptor-binding activity has been disrupted. Remarkably, the unrelated Fr-MLV RBD can also substitute for the FeLV-B RBD to activate FeLV-T infection in cells expressing the Fr-MLV receptor, while the FeLV-B RBD acts as a competitive inhibitor under these conditions [84]. This observation supports the biological model underlying the FeLIX coreceptor system described above (Section 1.2.1). It suggests that RBD engagement is coupled to a conserved, receptor-independent activation step within the fusion machinery. It also provides important structural and mechanistic precedent for the work presented

in this thesis, which examines whether receptor conformation itself—as opposed to the RBD alone—can further regulate this coupling.

1.2.3 Domain organization of the SU protein: signal peptide, RBD, VRA/VRB/VRC, PRR, and C-domain

Sequence and functional conservation within the SU subunit are highly unevenly distributed (Figure 1.3a) [79]. Immediately after the N-terminal signal peptide is the receptor-binding domain (RBD), which contains three distinct variable regions: VRA, VRB, and VRC. In the murine leukemia virus literature, VRA and VRB—and sometimes all three regions together—have historically been referred to as the "RBD"; this terminology was later adapted for FeLV studies [82]. Extensive mutagenesis and chimera studies involving MuLV and FeLV-B have shown that VRA is the main determinant of primary receptor specificity. When transferred from FeLV-B to an FeLV-A backbone, VRA alone is sufficient to confer PiT1 tropism. VRB and downstream sequences act as secondary determinants that can modify receptor usage but do not generally determine it on their own [46, 82]. The RBD is followed by the proline-rich region (PRR), which is thought to participate in the receptor-induced conformational changes in SU that are required for productive membrane fusion (Section 1.1.1) [79]. Downstream of the PRR is the C-domain, located immediately upstream of the SU–TM disulfide bond and the furin cleavage site. This linear domain organization (Figure 1.3a; the underlying multi-isolate alignment is shown in Section 1.2.4, Figure 1.5) provides the structural framework used throughout this thesis introduction to describe and interpret sequence variation among FeLV isolates.

1.2.4 Sequence comparison across FeLV-A/B/C and recombinant strains

To examine sequence relationships and domain organization in the SU envelope glycoprotein, the env-encoded amino acid sequences of four FeLV isolates representing distinct subgroups were aligned (data received from Prof. Francesca Magnani, personal communication): the prototype recombinant FeLV-B/Gardner-Arnstein (GenBank K01209), the horizontally transmitted prototype FeLV-A/Glasgow-1 (M12500), the anaemogenic prototype FeLV-C/Sarma (M14331), and the naturally occurring A/C mosaic isolate FeLV-A-C_FY981 (FJ436991.1). The alignment was interpreted in light of the established domain organization of gammaretroviral envelope proteins: the signal peptide (SP), the receptor-binding domain (RBD) with variable regions A–C (VRA,

VRB, VRC), the proline-rich region (PRR), the C-domain, and the downstream transmembrane (TM) segment [11–13].

SU length varies only slightly, from 639 aa (FeLV-C/Sarma and FeLV-A-C_FY981) through 642 aa (FeLV-A/Glasgow-1) to 662 aa (FeLV-B/Gardner-Arnstein). Pairwise identity ranges from 85.65% to 96.24% (Figure 1.5). FeLV-B/Gardner-Arnstein is the most divergent sequence, with 85.65–87.4% identity to the others. FeLV-A/Glasgow-1, FeLV-C/Sarma and FeLV-A-C_FY981 form a closely related group, with 92–96.24% identity among them. This pattern agrees with the known origins of the subgroups: FeLV-B arises by recombination between horizontally transmitted FeLV-A and endogenous FeLV (enFeLV), whereas FeLV-C usually arises from FeLV-A through point mutations and small insertions or deletions [11–13]. The 96.24% identity between FeLV-A/Glasgow-1 and FeLV-A-C_FY981 is also consistent with the latter being an A/C mosaic, as described by Stewart et al. (2012) [14] for naturally occurring anaemogenic isolates.

Variation is unevenly distributed across the domain map. The SP is the most divergent segment and is poorly conserved, as is typical for this region. Immediately downstream, the RBD (VRA, VRB and VRC) also shows low conservation, in line with its role in determining tropism [11, 13, 14]. VRA is particularly divergent and contains most of the substitutions specific to FeLV-C/Sarma, consistent with VRA being the main determinant of receptor specificity and VRB playing a supporting role [13, 14]. VRC, located further towards the C-terminus, also shows subgroup-specific divergence, in agreement with reported links between polymorphisms in this area and differences between FeLV-A and FeLV-C [14]. The PRR, which mediates receptor-induced conformational rearrangements of SU required for membrane fusion, shows length polymorphism: FeLV-B/Gardner-Arnstein carries additional PRR residues relative to the other three sequences. This fits the PRR being a frequent recombination site in FeLV-B env genes [12]. In contrast, the C-domain is highly conserved, with only conservative substitutions, which suggests a role in post-receptor-binding stages of entry [13]. The TM-proximal region is virtually identical across all four isolates, reflecting functional constraints on membrane anchoring and fusion.



Figure 1.5. The alignment and domain mapping of the SU envelope glycoprotein from representative FeLV-A, -B, and -C strains. The deduced amino acid sequences of the surface unit (SU) glycoprotein were aligned for four representative FeLV isolates: FeLV-B/Gardner-Arnstein (GenBank K01209; 662 amino acids), FeLV-A/Glasgow-1 (GenBank M12500; 642 amino acids), FeLV-C/Sarma (GenBank M14331; 639 amino acids), and the naturally occurring FeLV-A/C recombinant isolate FY981 (GenBank FJ436991.1; 639 amino acids). Identical residues are marked with asterisks (*), while conserved and semi-conserved substitutions are indicated by colons (:) and periods (.), respectively. The functional domains are shown above the alignment and color-coded for clarity: the signal peptide (SP, magenta), receptor-binding domain (RBD, black), including variable regions A, B, and C (VRA, VRB, and VRC), the proline-rich region (PRR, gold), the C-domain (black), and the transmembrane-proximal region (TM). The numbering on the right refers to residue positions in each unaligned mature protein. Gaps (–) were introduced to optimize the alignment and indicate potential insertion or deletion events, particularly within the PRR, where FeLV-B/Gardner-Arnstein contains additional residues relative to the other isolates. The inset matrix in the lower-right corner presents pairwise amino acid identities across the full-length SU sequences, ranging from 85.65% between FeLV-B and FeLV-C to 96.24% between FeLV-A and FY981. The alignment was performed using Clustal Omega Multiple Sequence Alignment (MSA).

1.3 FLVCR1a

This section is included because the interpretation of every FLVCR1a experiment depends on what is known, and still disputed, about the protein. It describes FLVCR1a as a heme exporter, an alternative choline/ethanolamine transporter, and the FeLV-C receptor, and it summarises its MFS topology, the available cryo-EM structures and the recombinant expression protocols. The unresolved question of its physiological substrate is what motivates testing porphyrin binding and then asking whether heme alters SU binding (Sections 3.1–3.2). The absence of any structure in an outward-facing or heme-bound state, together with the purification protocol, explains why a stable, purified preparation of the human receptor was the starting point for the biophysical work.

1.3.1 FLVCR1a as a heme exporter/transporter (SLC49 family)

Feline Leukemia Virus subgroup C Receptor 1a (FLVCR1a) is a polytopic plasma membrane protein belonging to the SLC49 branch of the Major Facilitator Superfamily (MFS) of transporters [4]. The gene was initially identified because it is exploited as an entry receptor by a pathogenic feline retrovirus (see Section 1.3.2). In 2004, Quigley and colleagues demonstrated—using ^{55}Fe-heme and the non-degradable heme analogue zinc mesoporphyrin (ZnMP)—that FLVCR1a mediates heme efflux from the cytosol to the extracellular space, establishing it as the first identified mammalian heme exporter [3]. This discovery was important because it provided the first evidence that eukaryotic cells can exchange heme, rather than handling it solely as a source of iron [4].

Heme is an essential but potentially cytotoxic cofactor. When present in excess, it promotes the formation of reactive oxygen species; therefore, its intracellular concentration must be tightly regulated through the coordinated control of heme synthesis, degradation and export [87]. FLVCR1a is considered an important component of this regulatory network. In mice, constitutive or tissue-specific deletion of Flvcr1a causes defective erythroid maturation, severe haemorrhaging and skeletal abnormalities, highlighting the essential role of this exporter in erythropoiesis—the cellular process with the highest rate of heme synthesis [88] (Fig. 1.6). Outside the erythroid compartment, high levels of FLVCR1a expression have also been reported in intestinal, hepatic and neuronal tissues, supporting a broader role in systemic heme homeostasis [4].

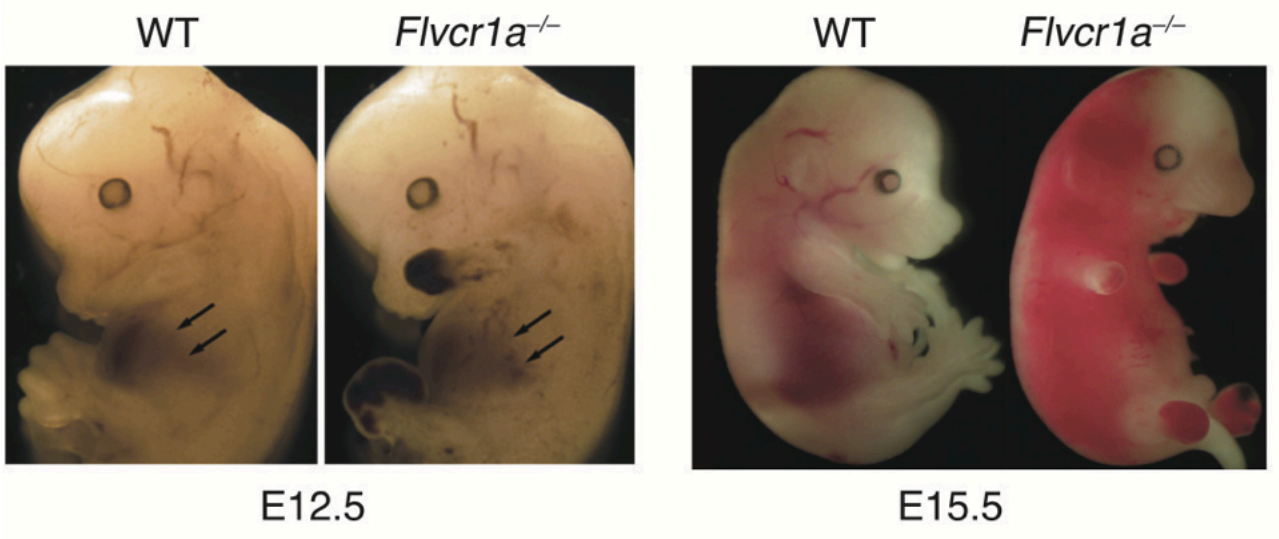


Figure 1.6. FLVCR1a is required for erythroid maturation in vivo. *Flvcr1a*-deleted mouse embryos (*Flvcr1a*$^{-/-}$) display severe hemorrhages at E12.5 and E15.5 and skeletal abnormalities of the limbs, axial skeleton and skull (Alizarin red/Alcian blue staining), compared with wild-type (WT) littermates. Adapted from Chiabrando et al. (2012), *J Clin Invest* 122(12).

FLVCR1a is proposed to function through the "rocker-switch" mechanism characteristic of MFS transporters. In this model, the protein alternates between outward-open, outward-occluded, inward-open and inward-occluded conformations to move its substrate across twelve transmembrane helices. These helices are arranged into two pseudo-symmetric six-helix bundles: an N-terminal domain comprising TM1–6 and a C-terminal domain comprising TM7–12 [4]. However, unlike many MFS transporters, the energetic driving force behind FLVCR1a-mediated heme efflux remains unclear. FLVCR1a is most closely related to the organic-phosphate antiporter and anion/cation symporter subfamilies of the MFS, both of which couple substrate transport to the movement of a specific ion. To date, however, no such coupled ion has been experimentally identified for FLVCR1a [87]. In addition, efficient heme export in biochemical assays requires an extracellular heme-binding protein, with hemopexin being considerably more effective than albumin at promoting FLVCR1a-dependent heme release [4].

More recently, this "canonical" model has been challenged by independent studies suggesting that FLVCR1a may also function as a high-affinity choline importer. This proposed activity is based on choline and phosphatidylcholine metabolite profiling, together with radiolabelled choline uptake assays performed in FLVCR1-knockout cell lines [4, 10, 110]. Consequently, the physiological substrate—or substrates—of FLVCR1a remains an open and actively debated question. It is still

unclear whether FLVCR1a transports heme, choline, or both in opposite directions. Several of the biochemical assays presented in this thesis were therefore designed to investigate these competing models (Fig. 1.7, Fig. 1.8).

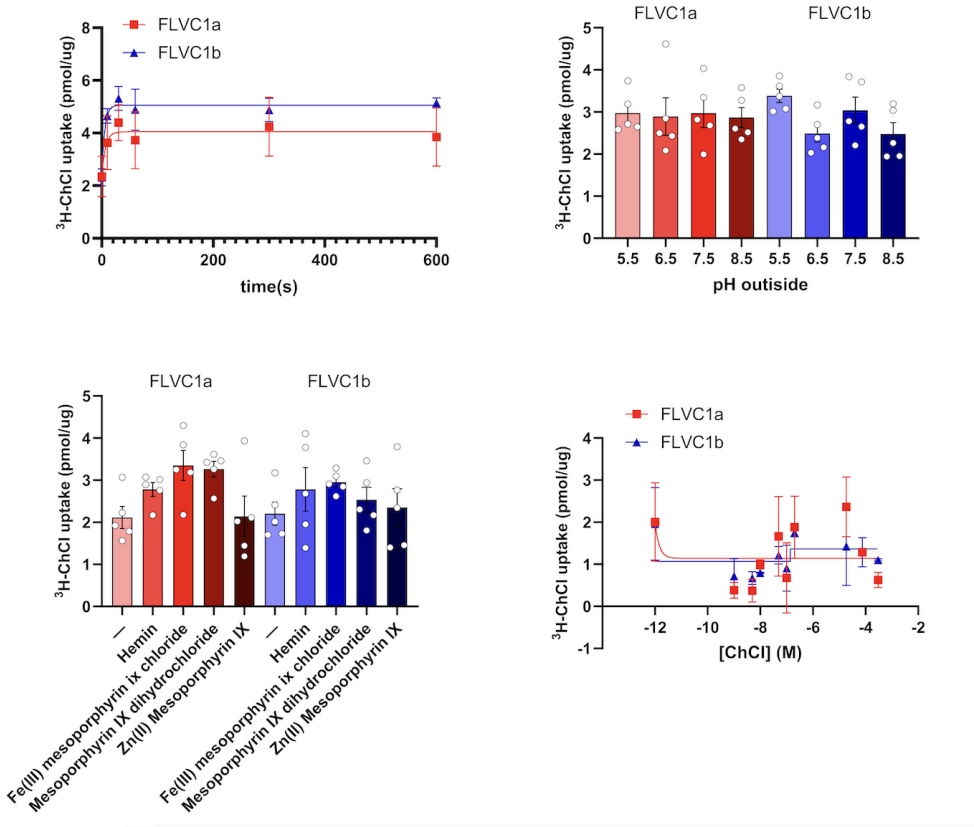


Figure 1.7. ^{3}H-choline uptake by FLVC1a and FLVC1b. (A) Time course of ^{3}H-ChCl uptake (0–600 s). (B) Effect of extracellular pH (5.5–8.5) on uptake. (C) Effect of pre-incubation with hemin and metalloporphyrins (Fe(III)-mesoporphyrin IX chloride, mesoporphyrin IX dihydrochloride, Zn(II)-mesoporphyrin IX) on choline uptake. (D) Competition of choline uptake by increasing concentrations of unlabelled choline chloride ([ChCl]). Data represent mean ± SEM. Data received from Prof. Matthias Quick (Columbia University, USA).

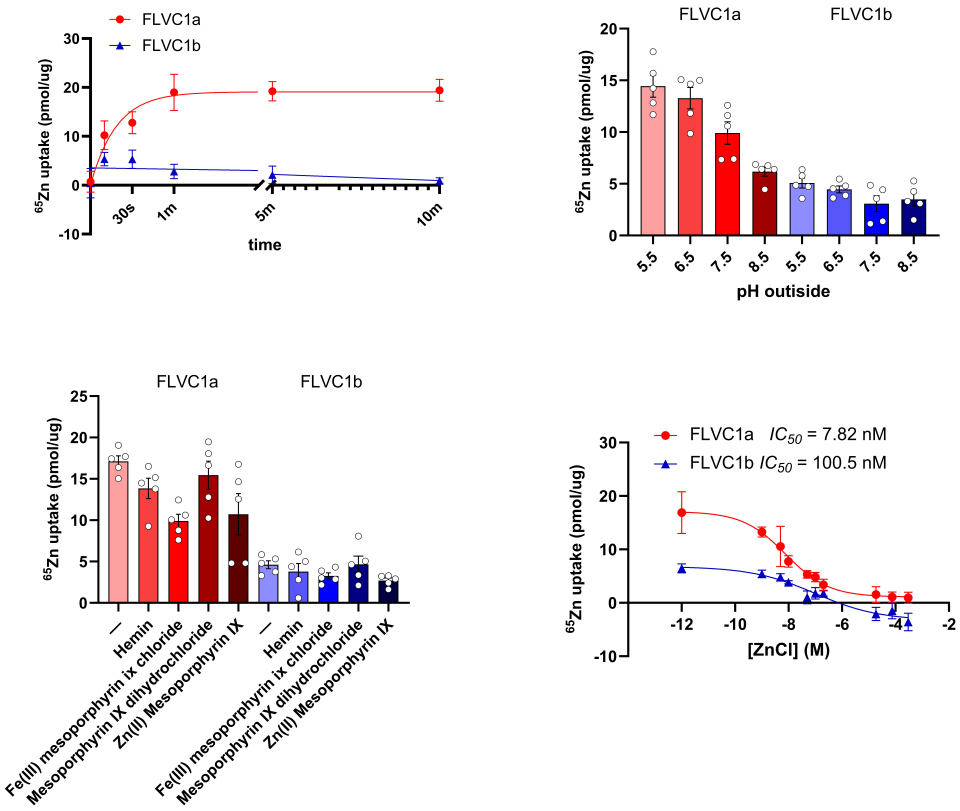


Figure 1.8. ^{65}Zn uptake by FLVC1a and FLVC1b. (A) Time course of ^{65}Zn uptake (0–10 min), showing markedly greater accumulation by FLVC1a than FLVC1b. (B) pH-dependence of ^{65}Zn uptake. (C) Effect of hemin and metalloporphyrin pre-treatment on ^{65}Zn uptake. (D) Concentration-dependent inhibition of ^{65}Zn uptake by unlabelled ZnCl, yielding IC_{50} values of 7.82 nM (FLVC1a) and 100.5 nM (FLVC1b). Data represent mean ± SEM. Data received from Prof. Matthias Quick (Columbia University, USA).

1.3.2 FLVCR1a as the receptor for FeLV-C

FLVCR1a was first identified in the late 1990s by two independent groups investigating the cellular receptor exploited by feline leukemia virus subgroup C (FeLV-C), a naturally occurring mutant of FeLV-A, to infect host cells [15, 16]. After cloning, the receptor was initially named FLVCR and subsequently renamed FLVCR1 to distinguish it from the paralogue FLVCR2; the "1a" designation was adopted once it became clear that the *FLVCR1* locus also encodes a second, shorter mitochondrial isoform, FLVCR1b, generated by alternative transcription initiation and lacking the first six transmembrane helices of FLVCR1a [88] (Fig. 1.9).

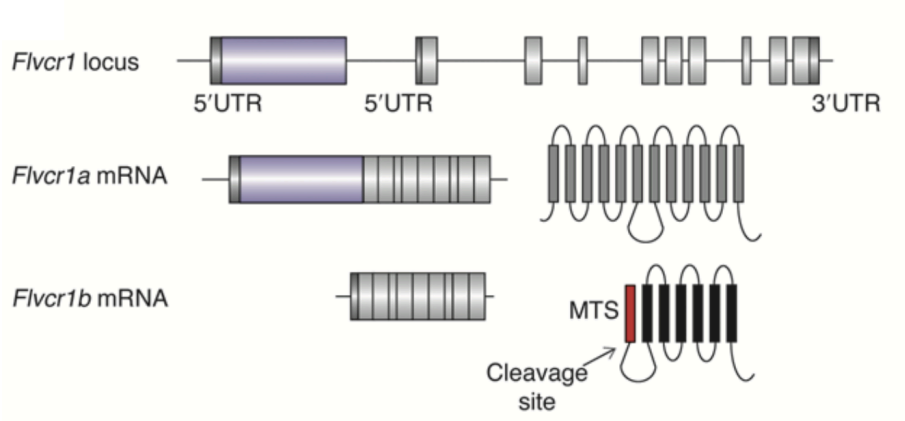


Figure 1.9. Genomic organisation of the *Flvcr1* locus and its two protein products. The *Flvcr1a* transcript retains the full 5′UTR and encodes the twelve-transmembrane-helix plasma-membrane exporter, whereas the *Flvcr1b* transcript initiates downstream and encodes a shorter product bearing a mitochondrial targeting sequence (MTS, red) and a proteolytic cleavage site, directing it to the mitochondrion. Adapted from Chiabrando et al. (2012), *J Clin Invest*.

FeLV-C infection is tightly associated with fatal pure red cell aplasia in cats, caused by depletion of erythroid colony-forming units and burst-forming units [15, 16]. FLVCR1a is highly specific for FeLV-C, conferring little or no susceptibility to FeLV-A, FeLV-B, amphotropic murine leukemia viruses, or the feline endogenous retrovirus RD114 [15, 16]. Receptor specificity is determined by a discrete variable region (vr1) near the N terminus of the receptor-binding domain (RBD) of the FeLV-C envelope surface (SU) glycoprotein: exchanging vr1 alone is sufficient to convert the receptor specificity of FeLV-A to that of FeLV-C [108, 109]. It has been proposed that aplastic anemia arises from the virus–receptor interaction itself, through interference with FLVCR1a function, rather than from the virus per se [15, 16].

Structural work on the FeLV-B RBD (Section 1.2.3 and 1.2.4) shows that, even though FeLV subgroups use unrelated multipass transporters as receptors, receptor diversity among gammaretroviruses is achieved by grafting variable, receptor-specific subdomains (VRA and VRB) onto an otherwise conserved β-sandwich RBD scaffold and a conserved fusion machinery [84] (Fig. 1.10).

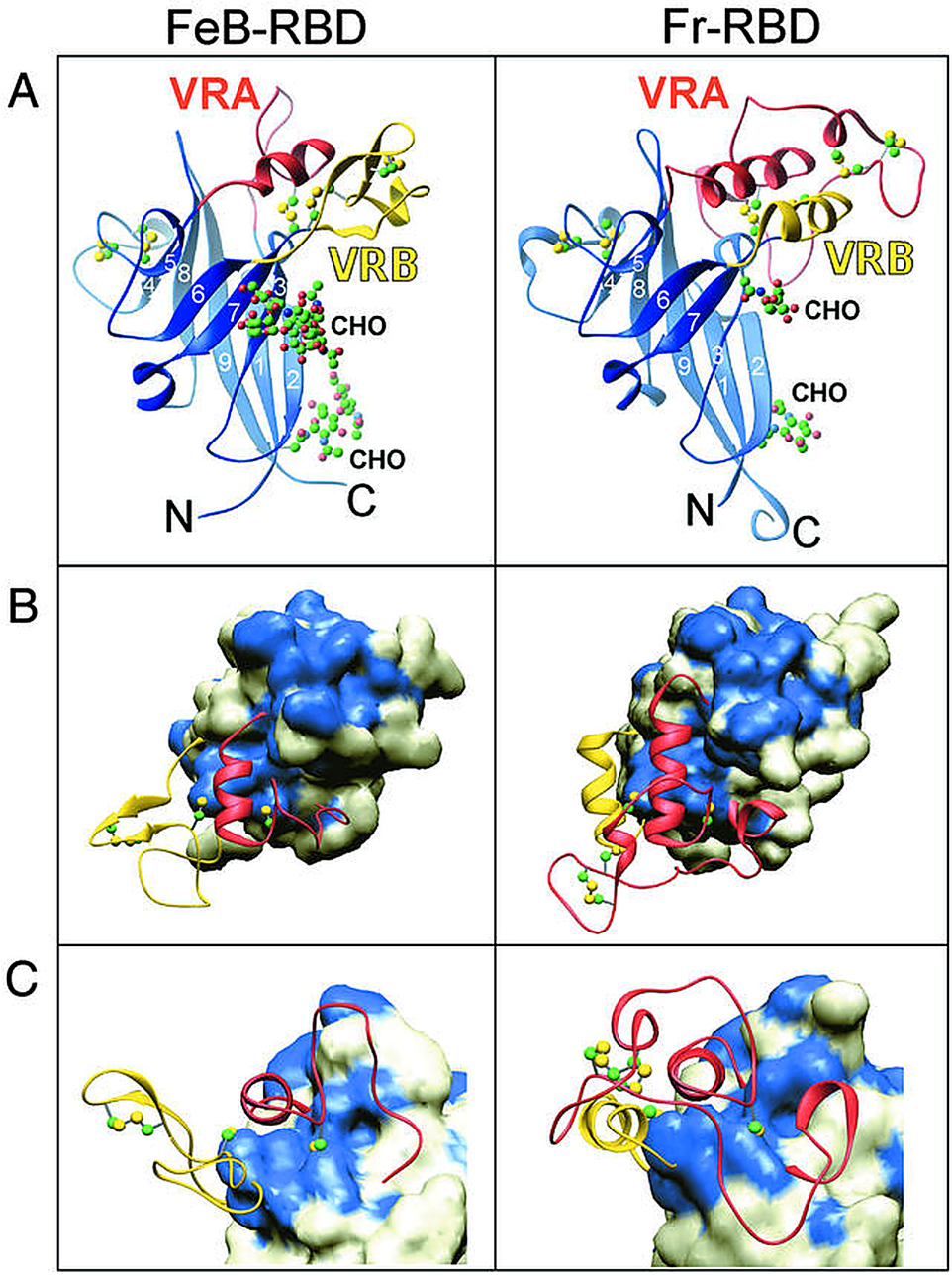


Figure 1.10. Structural comparison of the receptor-binding domains (RBDs) of FeLV-B (FeB-RBD) and Friend murine leukemia virus (Fr-RBD). Ribbon diagrams showing the conserved β-sandwich scaffold (blue) and the receptor-specific variable regions VRA (red) and VRB (yellow), which differ markedly in length, sequence and secondary structure between the two viruses despite occupying an equivalent structural position and converging on the same downstream fusion-activation mechanism. Adapted from Barnett et al. (2003), *J Virol* 77(4):2717–2729.

1.3.3 Structural topology and known functional sites

FLVCR1a is a glycoprotein comprising approximately 560 amino acids, with an apparent molecular mass of 55–70 kDa depending on its extent of glycosylation. The protein contains twelve hydrophobic transmembrane helices connected by six hydrophilic extracellular loops, while both the amino and carboxyl termini are located in the cytosol [4]. Three N-glycosylation sites have been identified: two are located within the third extracellular loop and one within transmembrane helix 11. Putative sites for protein kinase C and casein kinase II phosphorylation, as well as for N-myristoylation, have also been reported [4]. Among the extracellular loops, loops 1 and 6 appear to be particularly important for recognition by feline leukaemia virus subgroup C (FeLV-C) [4].

Consistent with the characteristic MFS fold, the twelve transmembrane helices are arranged into two structurally homologous six-helix bundles: an N-terminal domain and a C-terminal domain. Together, these domains form a central substrate-binding cavity composed of residues from both halves of the protein [4]. This architecture has been confirmed by cryo-EM structures of human FLVCR1 in the inward-facing conformation, in the apo state (PDB 8QCS) and bound to choline (PDB 8QCT, 8UBW and 8UBZ) or ethanolamine (PDB 8R8T) [10, 110]. In these structures, the substrate is bound within the central cavity by conserved aromatic residues, with selectivity for choline and ethanolamine conferred by cation–π interactions [10]. No structure has yet been reported for FLVCR1a in an outward-facing state or bound to heme.

Nevertheless, recombinant expression and purification protocols have enabled the biophysical characterisation of FLVCR1a. A C-terminally tagged protein, but not an N-terminally tagged version, retains heme-export activity. Furthermore, detergent and lipid screening identified conditions—including DDM supplemented with cholesterol hemisuccinate and elevated NaCl—that produce a stable, monodisperse and glycosylated transporter with an approximate particle diameter of 8 nm, making it suitable for subsequent structural studies [87] (Fig. 1.11, Fig. 1.12).

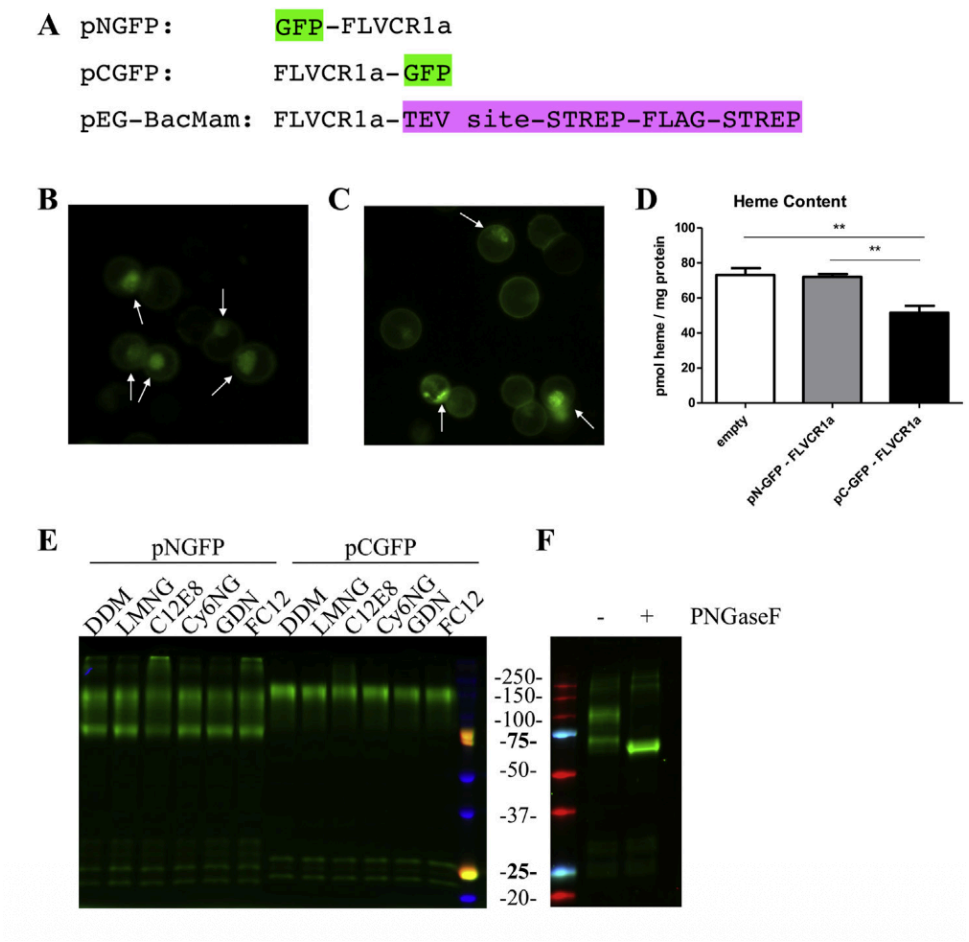


Figure 1.11. Construct design and expression screening for recombinant FLVCR1a. N- and C-terminally GFP-tagged (pNGFP/pCGFP) and Strep-FLAG-tagged (pEG-BacMam) constructs used for mammalian expression. Only the C-terminally tagged construct supports heme-export activity, consistent with the N- and C-termini being cytosolic. Adapted from Chiabrando et al. (2020), *Protein Expr Purif* 172:105637.

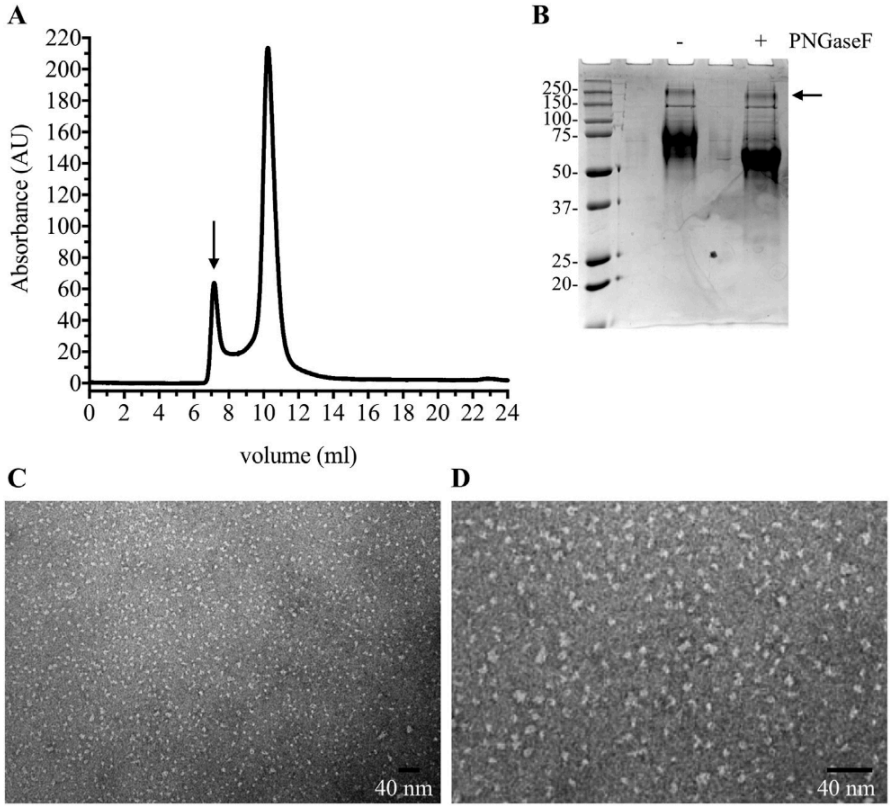


Figure 1.12. Purification and biophysical characterisation of recombinant FLVCR1a. Size-exclusion chromatography and negative-stain electron microscopy of detergent-solubilised, Strep-FLAG-tagged FLVCR1a purified from HEK293-F cells, showing a monodisperse elution profile (optimised with DDM/ cholesterol hemisuccinate and 300 mM NaCl) and homogeneously dispersed particles of ~8 ± 2 nm diameter, consistent with a properly folded monomeric transporter suitable for structural studies. Adapted from Chiabrando et al. (2020), *Protein Expr Purif* 172:105637.

Disease-associated mutations provide additional insight into the functional regions of FLVCR1a. Loss-of-function variants in FLVCR1 are associated with two distinct human disorders: Posterior Column Ataxia (PCA) without or with Retinitis Pigmentosa (PCARP), which is typically caused by homozygous missense mutations affecting highly conserved residues required for correct folding, intracellular trafficking, or cell-surface expression of FLVCR1a; and Hereditary Sensory and Autonomic Neuropathies (HSANs), which are genetically more heterogeneous and are associated with transporter proteins that retain partial function [111]. Notably, erythropoiesis is preserved in patients with these disorders, unlike the severe erythroid failure observed in Flvcr1-null animal models. This difference indicates that the consequences of impaired FLVCR1a function depend strongly on both the affected tissue and the specific mutation involved (for a comprehensive review of FLVCR1-related diseases, see [40]).

1.4 fFLVCR1a: the feline orthologue of FLVCR1a

FeLV-C infects cats, so the native receptor-virus pair involves the feline protein, yet nearly all functional and structural information on FLVCR1a comes from the human protein. This section is therefore included to establish how closely the two orthologues are related and what is, and is not, known about the feline protein. It provides the rationale for expressing and purifying fFLVCR1a (Section 3.5), and for placing the heme-dependent binding data, which were obtained with hFLVCR1a, in the context of the native feline receptor in the Discussion (Chapter 4).

1.4.1 Identification of fFLVCR1a as the feline form of hFLVCR1a

Feline FLVCR1a (fFLVCR1a) is the feline orthologue of the human heme/choline–ethanolamine transporter discussed in Section 1.3. Historically, feline FLVCR1a provided the original context for research into FLVCR1 biology. It is the native receptor used by FeLV-C to cause pure red cell aplasia in domestic cats and was cloned and functionally characterised in feline cells before the human orthologue was studied in detail (see Section 1.3.2) [15, 16].

The fFLVCR1a plasmid construct for expression in mammalian cells was designed as described above for the human homologue (Section 1.3.3): the coding sequence was cloned into the pEG BacMam vector with a C-terminal TEV protease cleavage site and Twin-Strep tag (Figure 1.13).

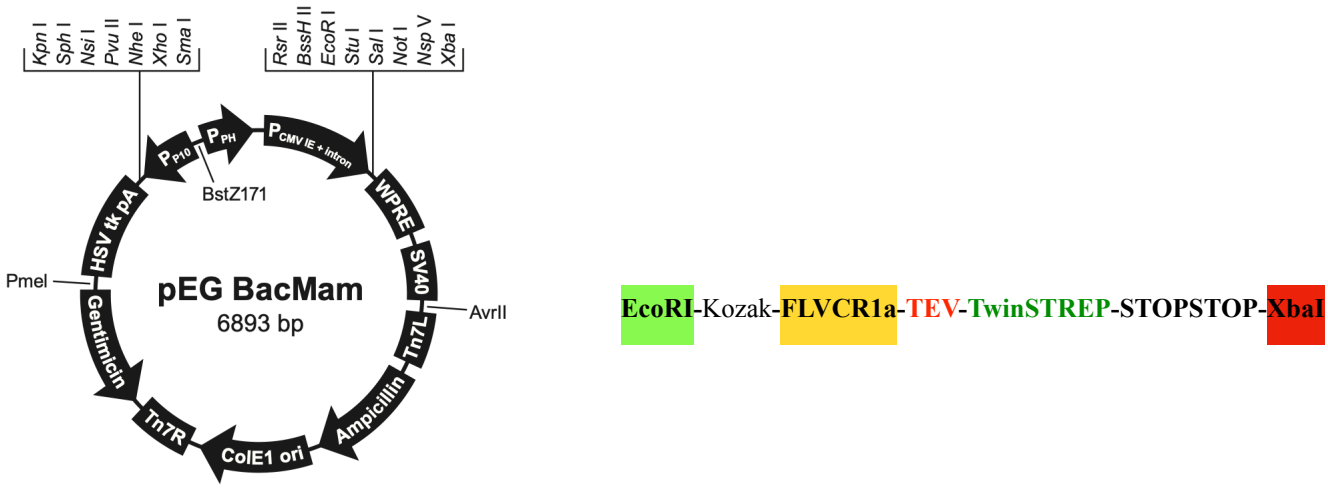


Figure 1.13. Expression cassette of the fFLVCR1a construct. The insert architecture EcoRI–Kozak–FLVCR1a–TEV–TwinStrep–STOP STOP–XbaI was cloned into the pEG BacMam vector between EcoRI and XbaI sites (no internal NotI site upstream of the TEV cleavage site). The tag consists of a TEV protease cleavage site (ENLYFQ↓G) followed by a Gly/Ser linker and two tandem Strep-tag II repeats (SAWSHPQFEK-GGGSGGGSGGS-AWSHPQFEK). The tagged construct (599 amino acids, including tag) has a calculated molecular weight of 64,445 Da, an extinction coefficient of 87,780 $M^{-1}cm^{-1}$, and an Abs 0.1% (1 g/L) of 1.40.

1.4.2 Sequence and structural conservation between feline and human FLVCR1a

The feline and human FLVCR1a orthologues are highly conserved. Their coding sequences share approximately 88% nucleotide identity, while feline FLVCR1a is 85% identical and 89% similar to the human protein at the amino-acid level (Figure 3.10) [4, 16]. Both orthologues are predicted to adopt the canonical major facilitator superfamily (MFS) fold, consisting of 12 transmembrane helices arranged into two structurally homologous six-helix bundles: an N-terminal domain comprising TM1–6 and a C-terminal domain comprising TM7–12. The N- and C-termini are predicted to face the cytoplasm, while the substrate-binding cavity is formed at the interface between the two domains [4]. This is consistent with the architecture described for human FLVCR1a in Section 1.3.3.

The strong conservation between the two proteins also extends to the extracellular loops implicated in FeLV-C receptor function. In particular, loops 1 and 6 occupy equivalent positions in the feline and human orthologues [31]. Both proteins have also been proposed to operate through the same

two-state rocker-switch mechanism, alternating between outward-open/occluded and inward-open/occluded conformations. This conformational cycle is thought to underlie substrate translocation in MFS transporters generally (Section 1.3.1) [4].

The two orthologues remain subject to the same unresolved debate regarding substrate identity, as discussed in Section 1.3.1. Both have been associated with heme export and, more recently, with choline and ethanolamine transport. The latter proposal is supported primarily by cryo-EM structures of human FLVCR1 captured in inward-facing conformations (PDB accession ID: 8QCS) (Section 1.3.3), together with functional assays measuring choline, ethanolamine and Zn^{2+} uptake [10, 110] (Figures 1.7 and 1.8).

No structure or high-resolution functional dataset is currently available specifically for the feline transporter. Accordingly, this thesis adopts the working assumption that the mechanistic principles established for human FLVCR1a are likely to extend to fFLVCR1a, although this has not yet been formally demonstrated.

1.4.3 Relevance of fFLVCR1a as a model system for studying FeLV receptor biology

The central biophysical finding of this thesis—that heme increases the binding affinity of the FeLV-C SU receptor-binding domain (RBD) for its receptor by approximately sixfold—was established using the human orthologue, hFLVCR1a, rather than the feline receptor. FeLV-C binds to both feline and human cells, although infection of human cells is not productive [15, 16], so hFLVCR1a is a suitable receptor for binding studies. The choice was also practical: hFLVCR1a was the construct for which a robust purification protocol had already been established (Section 2.1.5, Section 3.1–3.2). It therefore provided the platform for developing the porphyrin-binding assays, including MST and nano-differential scanning fluorimetry (nDSF), as well as the assays used to study SU–receptor complex formation (Section 3.2).

The feline orthologue is directly relevant to the viral–receptor interactions examined in this thesis because FLVCR1a was originally identified as a retroviral receptor in its natural feline context. FeLV-C causes pure red cell aplasia specifically in domestic cats, and it is feline FLVCR1a—not the human orthologue—that the virus engages in vivo [4, 15, 16] (Section 1.3.2). Similarly, structural and functional studies of gammaretroviral receptor engagement, including biochemical

reconstitution studies of the related FeLV-B/FeLV-T system, have historically used feline cell lines such as AH927 feline embryonic fibroblasts. This reflects the potential for receptor–envelope interactions to depend on species and orthologue [84].

The heme-dependent increase in FeLV-C SU–hFLVCR1a affinity identified in this thesis (Sections 3.2.1 and 4.3) was therefore measured with a human surrogate receptor. Whether it extends to the native feline FLVCR1a–FeLV-C pair, for which fFLVCR1a was expressed and purified in this project, is addressed in the Discussion (Chapter 4).

1.5 SLC20 family transporters and FeLV-B receptor usage

PiT-1 is the second receptor studied here, and the thesis aims to prepare it for structural work. This section reviews what is known about the PiT-1/PiT-2 pair, including the viral and receptor determinants of FeLV-B recognition and the revised topology that places both termini outside the cell. This background is needed for two reasons. First, the revised topology is the reason that tag position was treated as an open variable when the fSLC20A1 constructs were designed (Chapter 3). Second, the history of region A shows that a genetic determinant does not necessarily mark a direct contact point, which is a methodological precedent for interpreting the heme-dependent binding data (Section 3.2.1; Section 4.3).

1.5.1 SLC20A1 (PiT-1) and SLC20A2 (PiT-2): phosphate transporters as retroviral receptors

SLC20A1 (PiT-1) and SLC20A2 (PiT-2) are the two mammalian members of the type III sodium-dependent inorganic phosphate (Na^+/Pi) symporter family. They share approximately 60% amino acid sequence identity and are predicted to contain twelve transmembrane helices [58, 82, 89]. Although both proteins are expressed widely across mammalian tissues, their roles as retroviral receptors were identified before their physiological function as phosphate transporters was established.

PiT-1, initially termed GLVR1, was first cloned as the human receptor that confers susceptibility to gibbon ape leukemia virus (GALV) infection [90]. PiT-2, or GLVR2, was subsequently identified as the receptor for amphotropic murine leukemia virus (A-MuLV), largely because of its sequence similarity to PiT-1 [89]. Later studies demonstrated that both proteins function as physiological Na^+/

Pi cotransporters [89]. Together with FLVCR1a (Section 1.1.1), they therefore represent early examples of a broader phenomenon in which gammaretroviral receptors are “moonlighting” solute carriers that viruses have adapted for cell entry [78, 86].

Despite their shared ancestry and considerable sequence similarity, PiT-1 and PiT-2 are not interchangeable as viral receptors. PiT-1 supports entry by GALV and FeLV-B but not A-MuLV, whereas PiT-2 supports A-MuLV entry but generally does not support GALV or FeLV-B infection [58, 82]. Because specific sequence differences between these closely related paralogues can switch receptor specificity, the PiT-1/PiT-2 pair has become one of the most extensively studied models of gammaretroviral receptor recognition. It also provides the structural and functional context for the FeLV-B receptor interaction that must be experimentally examined in the future.

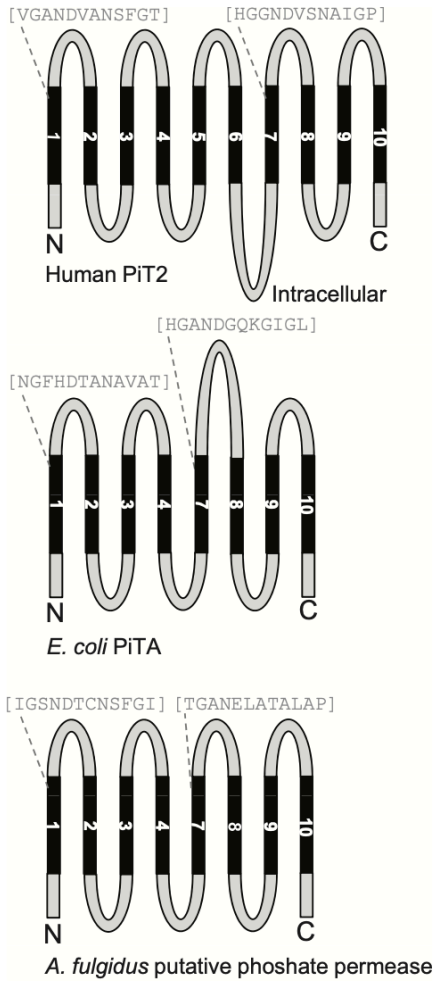


Figure 1.14. Predicted topologies of H. sapiens PiT2, E. coli PiTA, and the putative phosphate permease from A. fulgidus.Schematic representations of the predicted membrane topologies of H. sapiens PiT2, E. coli PiTA, and the A. fulgidus putative phosphate permease are shown. Transmembrane (TM) domains were predicted using the TMHMM server for H. sapiens PiT2 and the DAS server for E. coli PiTA and A. fulgidus putative phosphate permease. Cited from Bøttger, P., & Pedersen, L. (2011). Mapping of the minimal inorganic phosphate transporting unit of human PiT2 suggests a structure universal to PiT-related proteins from all kingdoms of life. *BMC biochemistry*, *12*, 21.

The coding sequence of mature feline SLC20A1 (UniProt O97596), comprising 681 residues with a calculated molecular mass of approximately 74 kDa, was synthesised with a C-terminal affinity and cleavage cassette (construct fSLC20A1-tag) and cloned into the pEG BacMam expression vector [24, 41], as previously described for fFLVCR1a (Section 2.1.3). The resulting expression cassette—EcoRI–Kozak–SLC20A1–TEV–Twin-Strep–STOP STOP–XbaI—contains a 2,200 bp insert, measured from EcoRI to XbaI and including both restriction sites, within the 9,037 bp full-length pEG BacMam vector. It encodes a 720-residue fusion protein with a calculated mass of

approximately 78 kDa, in which fSLC20A1 is followed at its extreme C-terminus by a tobacco etch virus (TEV) protease cleavage site and a Twin-Strep-tag II affinity tag.

The fSLC20A1 sequence contains three consensus N-glycosylation sequons (N-X-S/T, X ≠ Pro): Asn100, Asn375 and Asn419 (numbering from Met1, UniProt O97596), corresponding to Asn96, Asn371 and Asn415 of human SLC20A1; the fourth human sequon (Asn497) is not conserved in the cat. Based on the PHD-predicted topology of human PiT1, in which the N- and C-termini are extracellular, Asn100 lies in extracellular loop 1 and is therefore the only expected glycosylation site, whereas Asn375 and Asn419 fall within the large intracellular loop [93]. All three sites lie in the receptor, 581, 306, and 262 residues upstream of the TEV cleavage site. The 39-residue TEV–Twin-Strep-tag II cassette at the C-terminus contains no sequon, so the tag is not expected to be glycosylated. These assignments are sequence-based predictions and have not been verified experimentally for the feline protein.

Unlike FLVCR1a, whose N- and C-termini are both predicted to face the cytoplasm (Section 1.3), current topological models of PiT1 and PiT2 place both termini on the extracellular side of the membrane. These models are based on epitope tagging, glycosylation-site mapping and substituted-cysteine accessibility studies [58, 91, 92]. Consequently, a C-terminal tag on PiT1 cannot, a priori, be assumed to have no effect on the extracellular surface involved in retroviral envelope or antibody binding. This contrasts with the C-terminal tag selected for fFLVCR1a. To address this uncertainty, constructs carrying the tag at either terminus (fSLC20A1-tag and tag-fSLC20A1) were generated in parallel and compared (Chapter 3).

1.5.2 FeLV-B RBD interaction with SLC20A1/PiT-1

As described in Section 1.2.1, FeLV-B arises by recombination between exogenous FeLV-A and endogenous FeLV (enFeLV) envelope sequences [12, 85], and essentially all naturally occurring FeLV-B isolates can use PiT-1 as a receptor [46, 82].

As in GALV, the FeLV-B receptor-binding domain (RBD), which contains the variable regions VRA and VRB (Section 1.2.3), is required for PiT-1 recognition. When the FeLV-B RBD is transferred onto an FeLV-A envelope backbone, it is also sufficient to confer PiT-1 specificity. These findings identify VRA, in particular, as the main viral determinant of PiT-1 tropism [82].

The crystal structure of the isolated FeLV-B RBD provides the only currently available high-resolution structural information about any component of this interaction [84] (Section 1.2). However, no structure has yet been reported for the FeLV-B RBD in complex with PiT-1, or for PiT-1 itself in any conformational state. This lack of structural information remains particularly relevant to the biophysical questions addressed later in this thesis.

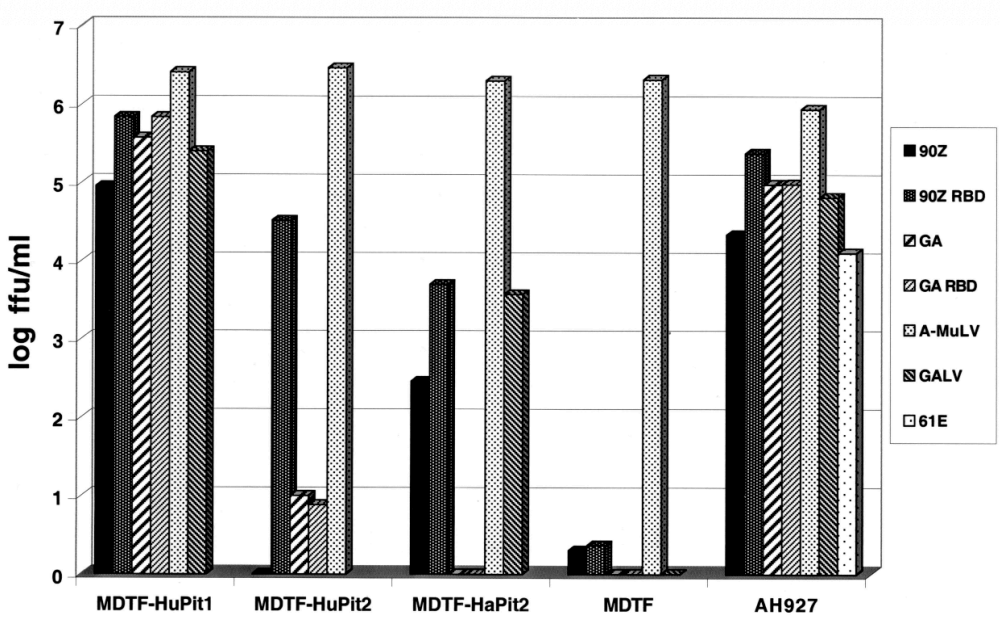


Figure 1.15. Receptor-usage profile of FeLV-B isolates. Infection of MDTF cells expressing HuPit1, HuPit2, and HaPit2 with FeLV-B-GA, FeLV-B-90Z, and control envelopes. It shows directly that FeLV-B-GA infects HuPit1-expressing cells but not HuPit2 or HaPit2. Cited from Sugai, J., Eiden, M., Anderson, M.M., Van Hoeven, N., Meiering, C.D. and Overbaugh, J. (2001) 'Identification of envelope determinants of feline leukemia virus subgroup B that permit infection and gene transfer to cells expressing human Pit1 or Pit2', *Journal of Virology*, 75(15).

1.5.3 Critical residues in FeLV-B Env required for PiT-1 binding

Although PiT-1 usage is a near-universal feature of FeLV-B isolates, the ability to use the related receptor PiT-2 is not. Comparisons between FeLV-B isolates that can or cannot use PiT-2 have therefore been central to identifying Env residues involved in productive receptor engagement [46, 82].

These effects have been examined most extensively in the FeLV-B/PiT1/PiT2 system by Sugai et al. (2001) [82]. Sugai et al. (2001) compared two independently derived, naturally occurring FeLV-B

isolates: FeLV-B-90Z, which can use human PiT2 in addition to PiT1, and FeLV-B-Gardner-Arnstein (FeLV-B-GA), which cannot. Only three residues differed between the RBDs of the two isolates. Of these, a single non-conservative substitution—a glutamine-to-arginine change at VRA position 73—was required, although not sufficient on its own, for PiT2 usage. Introducing this substitution into the FeLV-B-GA envelope produced detectable PiT2 binding and infectivity. However, a chimeric envelope containing arginine 73 together with the wild-type C-terminal SU sequence from FeLV-B-90Z was still unable to infect PiT2-expressing cells. This result showed that C-terminal SU sequences outside the canonical RBD, including the VRA–VRB region, can exert a dominant effect on PiT2-mediated entry. The effect is likely to occur after the initial receptor-binding step [82]. Sequence alignment placed arginine 73 within a short helical element located nine residues upstream of a highly conserved FYVCP motif. This motif is retained even in the otherwise weakly homologous RBD of ecotropic MuLV. Thus, despite the limited overall sequence identity between divergent gammaretroviral RBDs, important receptor-contact residues may recur within structurally analogous elements of the VRA helix across the gammaretroviral family [80, 82]. The same arginine at position 73 is also conserved in GALV, which uses receptors related to PiT1 and PiT2. However, GALV cannot use human PiT2. This finding demonstrates that arginine 73 is necessary but not sufficient for PiT2 usage across gammaretroviruses. Additional determinants, including virus-specific sequences outside VRA and VRB, must further restrict receptor choice [82].

This single-residue switch, which distinguishes between receptor paralogues, provides the clearest experimental example in this system of the broader evolutionary pattern introduced in Section 1.1.2. Localized sequence changes within an otherwise conserved SU framework can repeatedly modify recognition of a small and deeply conserved group of host transporters. The FeLV-A/B/C comparison presented in Section 1.2.4 (Figure 1.5) extends this principle across FeLV subgroups rather than examining variation within FeLV-B alone. The alignment shows that the RBD—particularly VRA—is the most divergent region of SU among FeLV-A, -B, and -C, whereas the C-domain and membrane-proximal region remain highly conserved. These patterns are consistent with, and provide further comparative support for, the receptor-switching mechanisms established at single-residue resolution by Sugai et al. (2001) [82] and Boomer et al. (1997) [46] in the FeLV-B/PiT1/PiT2 system.

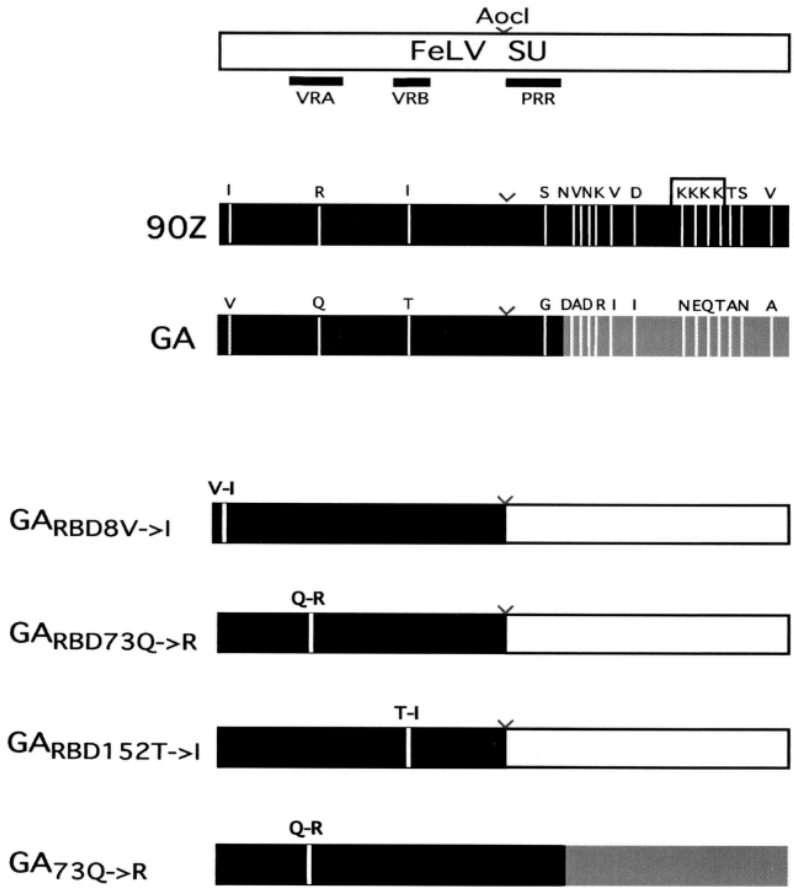


Figure 1.16. Schematic representation of the sequence differences between FeLV-B-90Z SU and FeLV-B-GA SU, marking the three residues that differ between the isolates, including VRA position 73 (Q in GA, R in 90Z). The cluster of lysine residues unique to FeLV-B-90Z SU is highlighted by a box. Cited from Sugai, J., Eiden, M., Anderson, M.M., Van Hoeven, N., Meiering, C.D. and Overbaugh, J. (2001) 'Identification of envelope determinants of feline leukemia virus subgroup B that permit infection and gene transfer to cells expressing human Pit1 or Pit2', *Journal of Virology*, 75(15).

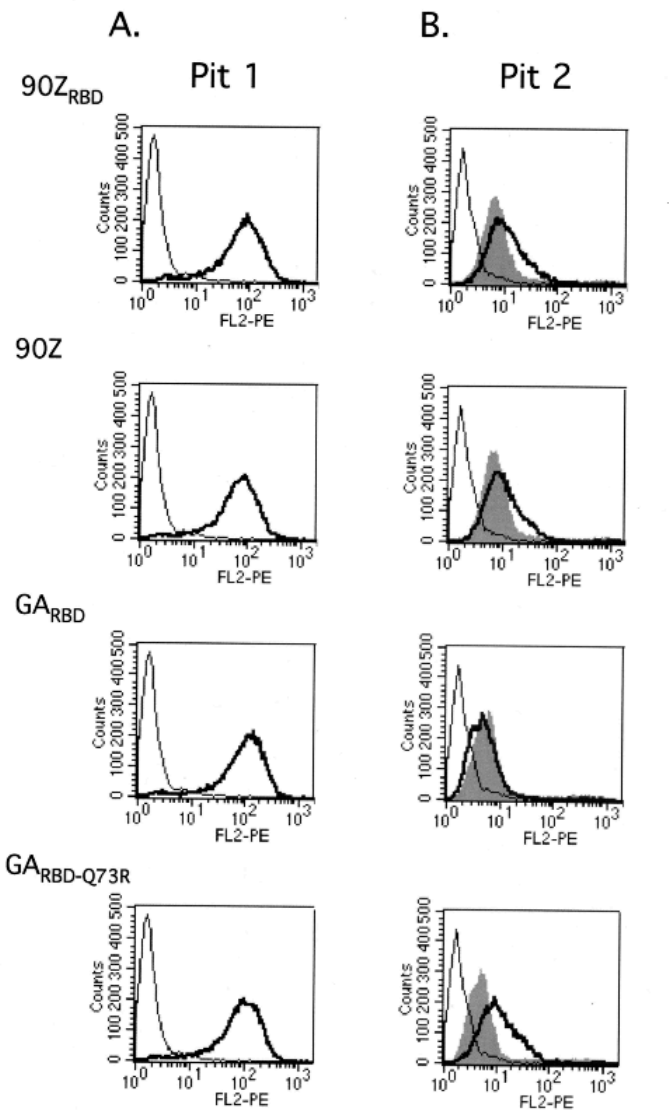


Figure 1.17. Flow-cytometric histograms of HA-tagged FeLV-B SU binding to MDTF-HuPit1 versus MDTF-HuPit2 cells. Envelope binding to MDTF-HuPiT1 and MDTF-HuPiT2 cells, where MDTF cells expressing the indicated PiT receptors were incubated with conditioned medium containing HA-tagged FeLV-B SU. Bound SU was detected by staining with the HA.11 monoclonal antibody, which recognizes the HA epitope. In each panel, fluorescence intensity is shown on the x-axis on a logarithmic scale, while the y-axis represents the number of events. Cells incubated with medium alone are represented by thin black lines, whereas the gray-filled histograms indicate background SU binding to naïve MDTF cells. Binding of SU to MDTF cells expressing HuPiT1 (A) and HuPiT2 (B) is shown by bold black lines. Cited from Sugai, J., Eiden, M., Anderson, M.M., Van Hoeven, N., Meiering, C.D. and Overbaugh, J. (2001) 'Identification of envelope determinants of feline leukemia virus subgroup B that permit infection and gene transfer to cells expressing human Pit1 or Pit2', *Journal of Virology*, 75(15).

1.5.4 PiT-1 extracellular loops as determinants of Env recognition

On the receptor side, efforts to identify the determinants distinguishing PiT-1 from PiT-2 have focused largely on the transporters' predicted extracellular loops. An early and influential study used chimeras between human PiT-1, which functions as a GALV and FeLV-B receptor, and murine PiT-1, which does not. This work identified a nine-residue polymorphic segment in the C-terminal portion of the predicted fourth extracellular loop, termed "region A" and corresponding to PiT-1 residues 550–558, as critical for both GALV and FeLV-B receptor activity [90, 94].

Subsequent studies confirmed and extended the importance of this region. Chimeras between PiT-1 and PiT-2, or between PiT-1 and rat PiT-2, reproduced the requirement for region A [93]. In addition, changing the first residue of PiT-2 region A from lysine to glutamate was sufficient to confer partial GALV receptor activity [95]. Remarkably, transferring the PiT-1 region A sequence into the distantly related fungal phosphate transporter Pho-4 was also sufficient to generate a functional GALV receptor from an otherwise non-receptor scaffold [96].

Studies of PiT-2 identified the second extracellular loop as an additional determinant specifically required for A-MuLV receptor function [97, 98]. Together, residues in loops 2 and 4 appear to determine the receptor-specificity profiles of PiT-1, PiT-2, and their chimeras [96]. For FeLV-B, a minimal 13-amino-acid PiT-1-specific sequence in loop 4—including tyrosine 546 and valine 548 in addition to the original nine-residue region A—was sufficient to confer FeLV-B receptor activity on otherwise non-permissive PiT-2 [99]. This finding parallels the identification of VRA as the main viral determinant of PiT-1 tropism described in Section 1.5.3.

However, subsequent work from the same group substantially changed the interpretation of the loop-4/region-A model. Chaudry and Eiden (1997) [112] tested whether region A mutations that eliminated GALV and FeLV-B infectivity also prevented virus binding. They found that PiT-1 receptors carrying infectivity-null mutations in region A could still bind the virus. Moreover, region A could be altered substantially, including changes in its overall charge and hydrophobicity, without disrupting GALV entry. These findings challenged the idea that region A functions as a simple, direct virus-binding motif.

Further work using epitope tagging, glycosylation analysis, and computational topology modelling led Farrell, Russ, Murthy and Eiden (2002) [93] to propose a revised topology for PiT-1. In this

model, both the N- and C-termini are extracellular rather than cytoplasmic, as assumed in the original topology model. Region A is consequently located in a cytoplasmic loop rather than an extracellular one. Its role was therefore reinterpreted as regulating receptor topogenesis and the accessibility of the true extracellular virus-binding surface, potentially through an intramolecular interaction with a second determinant, region B, spanning residues 232–260.

A later biochemical and computational reassessment of the full extracellular architecture of PiT-1/SLC20A1 independently supported this revised topology [58]. This work placed both termini outside the cell and identified a separate extracellular loop EC4, as the region most likely to contact the FeLV-B/GALV RBD directly.

To consider, these studies demonstrate that identifying a genetic determinant through chimeras or mutagenesis does not, by itself, prove that the determinant makes direct physical contact with the viral RBD. Instead, the determinant may influence folding, topology, receptor accessibility, or a later stage of entry.

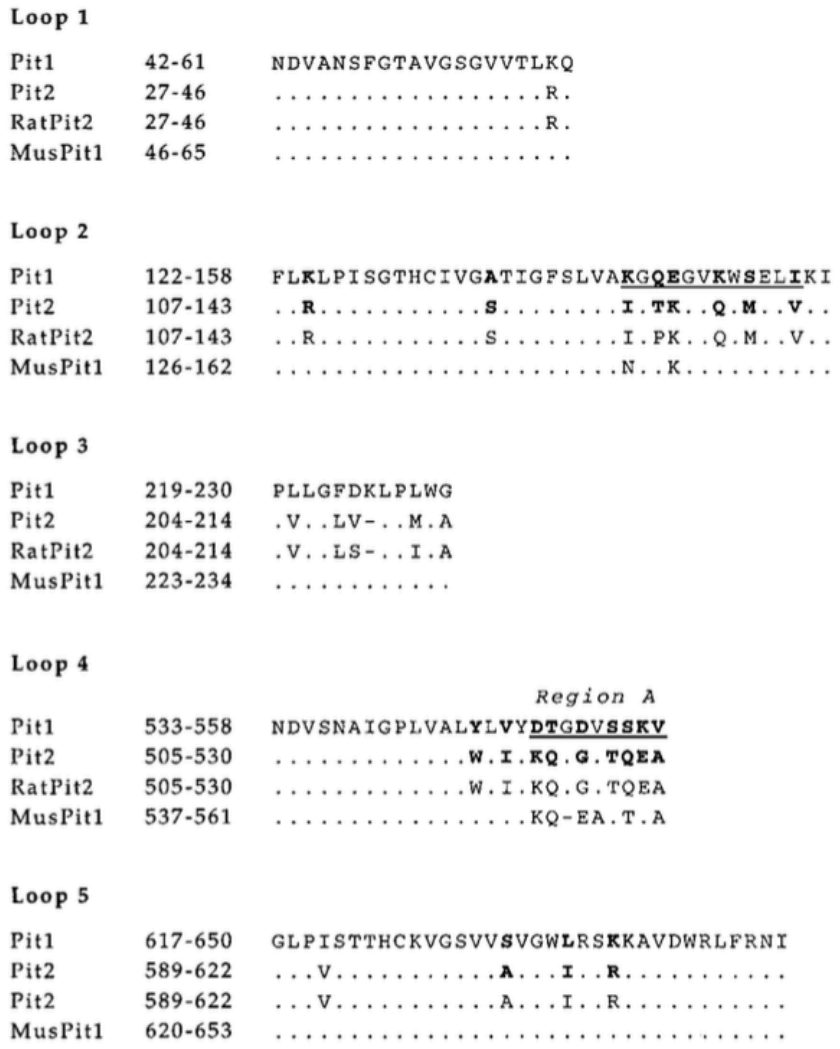


Figure 1.18. Alignment of the putative extracellular loop sequences of PiT1, PiT2, RatPiT2, and MusPiT1. The numbers on the left indicate the positions of the first and last amino acids shown in each sequence. Dots denote residues identical to those in PiT1, while dashes represent gaps introduced to optimize the alignment. Underlined sequences correspond to region A and the loop 2 sequence modified in the A1, A2, and A3 chimeric receptors. Residues subjected to mutagenesis in this study are highlighted in bold. This is the visual definition of region A and the 13-residue extension (Y546, V548). Cited from Dreyer, K., Pedersen, F. S., & Pedersen, L. (2000). A 13-amino-acid Pit1-specific loop 4 sequence confers feline leukemia virus subgroup B receptor function upon Pit2. *Journal of virology*, *74*(6).

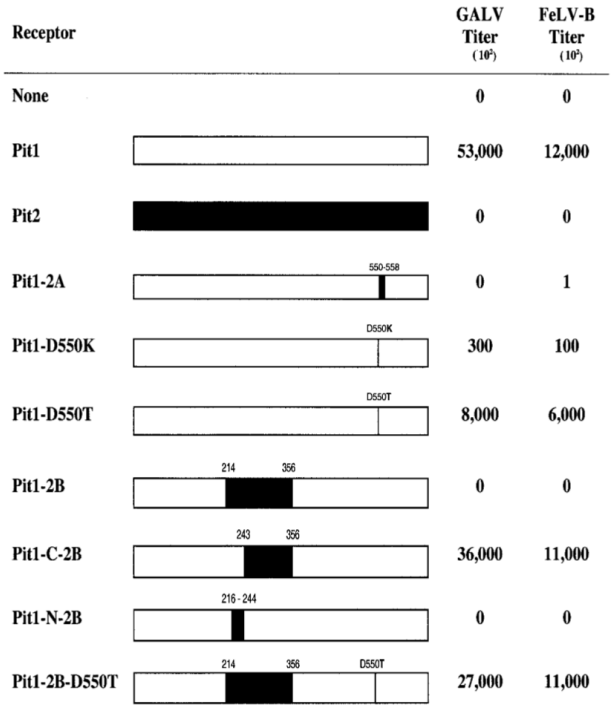


Fig 1.19. Infection of MDTF cells stably expressing PiT1, PiT2, or chimeric or mutant PiT1 receptors with GALV- and FeLV-B-enveloped retroviral vectors. Bars represent schematic depictions of the receptors, with PiT1 shown in white and PiT2 in black. The positions of introduced mutations or substitutions are indicated. Viral titers were determined from at least three independent experiments and are presented as mean numbers of β-galactosidase-expressing cells. Cited from Farrell, K. B., Russ, J. L., Murthy, R. K., & Eiden, M. V. (2002). Reassessing the role of region A in Pit1-mediated viral entry. *Journal of virology*, *76*(15).

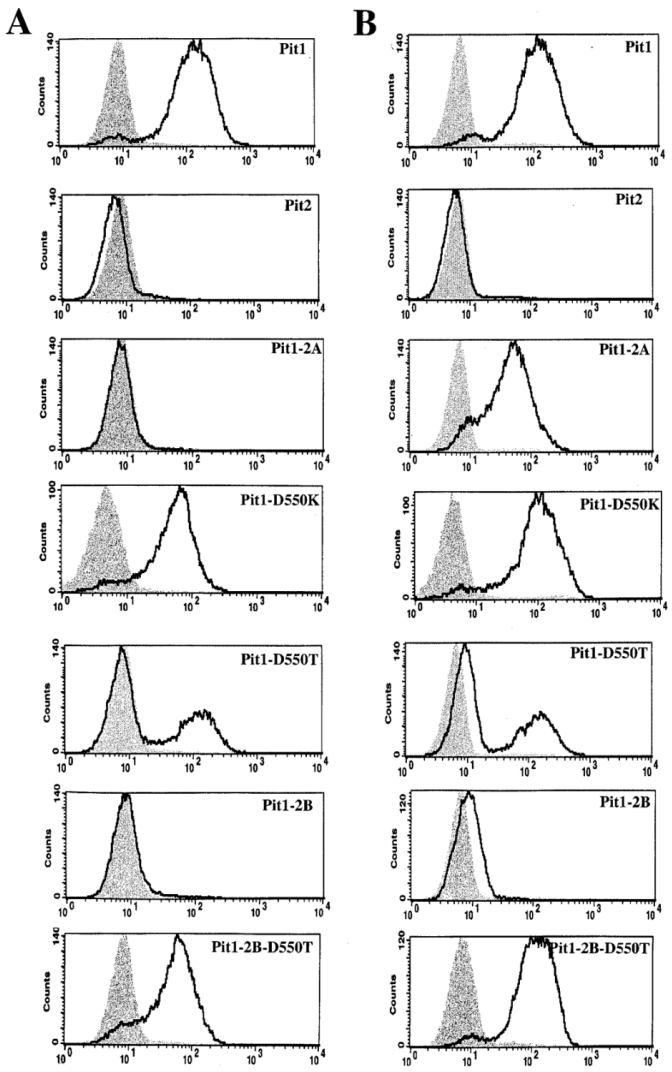


Figure 1.20. Histograms showing the flow-cytometric analysis of cells stained with the fluorescein-conjugated monoclonal antibody HA.11, which recognizes soluble HA-tagged GALV SU (A) and FeLV-B SU (B) glycoproteins. Fluorescence intensity is shown on the x-axis on a logarithmic scale, while cell number is shown on the y-axis. Shaded regions represent negative-control MDTF cells incubated with the HA-tagged glycoproteins, whereas the regions beneath the bold lines represent MDTF cells stably expressing the corresponding receptors following incubation with the HA-tagged glycoproteins. Cited from Farrell, K. B., Russ, J. L., Murthy, R. K., & Eiden, M. V. (2002). Reassessing the role of region A in Pit1-mediated viral entry. *Journal of virology*, *76*(15).

1.5.5 Mutational studies comparing PiT-1 and PiT-2 receptor usage

The PiT-1/PiT-2 chimera and point-mutation studies summarized above (Sections 1.5.3–1.5.4) show that receptor specificity within this transporter pair depends on multiple determinants rather than on a single residue or sequence element on either side of the interaction.

On the receptor side, PiT-1-specific residues in loop 4—including region A and its 13-residue extension—are required for GALV and FeLV-B usage. However, these residues are now thought to act primarily by influencing receptor topology or accessibility rather than by forming direct contacts with the viral RBD [93, 99]. Similarly, PiT-2-specific residues in loop 2 are required for A-MuLV usage [97, 98].

On the viral side, arginine at VRA position 73 is necessary but not sufficient for FeLV-B usage of PiT-2. Additional C-terminal SU determinants are required for productive entry, even when receptor binding can occur [82]. Thus, mutations that disrupt infection may act at several different stages: receptor binding, a distinct post-binding step, or receptor folding and accessibility. It emphasizes that receptor engagement by gammaretroviruses should not generally be reduced to a single, static protein–protein interface.

1.6 Antibodies as structural biology tools

Once embedded in a detergent micelle or lipid nanodisc, small membrane proteins, such as the ones discussed in this thesis, are often challenging to solve by cryo-EM and too flexible for X-ray crystallography. In addition to their well-established role in humoral immunity, antibodies and engineered antibody fragments have become valuable tools in structural biology. Antibody-derived binders can act as crystallisation chaperones, stabilise a protein in a defined conformational state and, in cryo-EM, increase the effective molecular mass of a particle. They can also introduce asymmetric, well-ordered surface features—known as fiducial markers—that improve particle alignment during image processing [66, 100]. This strategy has been especially useful for solute carriers and other polytopic membrane transporters in the 40–60 kDa range. Work from the Reyes laboratory illustrates this principle. The cryo-EM structure of the blood–brain barrier lysophospholipid transporter MFSD2A was determined using antibody Fab fragments, which increased the size of the complex and improved particle alignment [74]. This work built on a similar strategy used to determine cryo-EM structures of full-length CD20 bound to therapeutic Fab fragments [101]. In another example, the conformation-selective nanobody Nb469 was used to

stabilise the amino-acid transporter ASCT2 in a single inward-facing state, allowing its structure to be resolved at 2.3 Å resolution [75].

Human FLVCR1a, the subject of this thesis, is a similarly compact multi-pass membrane transporter of approximately 60 kDa. A dedicated monoclonal antibody (mAb) panel, the FBE series, was therefore generated by F. Bertoglio (TU Braunschweig) as a first step towards using antibody fragments as structural biology tools for this protein. Two properties are particularly important when evaluating antibodies for this purpose: (i) their molecular format, which influences their size, rigidity and behaviour during single-particle image processing, and (ii) the nature of the epitope they recognise, which determines whether binding depends on the native folded structure of the antigen. These two properties are considered below, together with the preliminary characterisation of the FBE panel by size-exclusion chromatography (SEC) and western blotting, which was performed by Professor Francesca Magnani and is presented here as unpublished data (Professor Francesca Magnani, personal communication). Experimental procedures are described in Materials and Methods, and further characterisation of the panel is presented in Discussion.

1.6.1 Bivalent scFv-Fc versus Fab antibody formats

A full-length immunoglobulin G (IgG) is a Y-shaped glycoprotein of approximately 150 kDa. It consists of two identical heavy chains and two identical light chains, arranged into two antigen-binding Fab (fragment antigen-binding) arms and one Fc (fragment crystallisable) stem, which are connected by a flexible hinge region [102, 103]. Each Fab arm, which is approximately 50 kDa, contains a variable domain pair, VH and VL, that together form the Fv and determine antigen specificity. It also contains a constant domain pair, CH1 and CL, which helps stabilise the structure. This modular architecture has enabled the development of a range of engineered antibody formats from a single parental clone, including minimal Fv fragments, single-chain Fv (scFv), Fab fragments and full bivalent IgG molecules [104]. Two formats were directly relevant to the anti-FLVCR1a antibody panel characterised in this thesis: bivalent scFv-Fc molecules and Fab fragments (Figure 1.21).

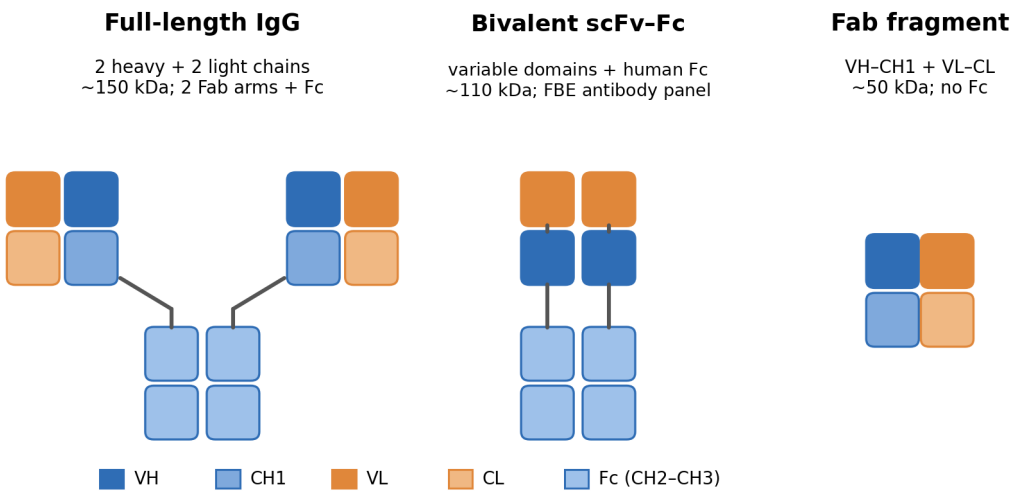


Figure 1.21. Antibody formats relevant to this thesis. Schematic comparison of a full-length IgG, the bivalent scFv-Fc format in which the FBE monoclonal antibody panel was generated and screened (antibody variable domains fused to a dimeric human Fc region), and a Fab fragment. Approximate molecular masses are indicated; domains are not drawn to scale. VH/VL, variable domain of the heavy/light chain; CH1/CL, constant domain 1 of the heavy chain/constant domain of the light chain; Fc, fragment crystallisable (CH2–CH3).

The bivalent, Y-shaped structure of IgG is well suited to antigen capture in assays such as ELISA and western blotting. Its two identical binding arms provide avidity, while the Fc region allows straightforward detection using anti-Fc secondary reagents. However, the flexibility that enables the two Fab arms to move independently of the Fc can be problematic for cryo-EM. The hinge permits a wide range of inter-domain angles, meaning that an intact IgG bound to a relatively small antigen may produce poorly resolved density—or no reliably interpretable density—outside the immediate paratope–epitope interface [105]. For this reason, Fab fragments are generally preferred to intact IgG molecules as cryo-EM fiducial markers. Fabs lack both the Fc region and the flexible hinge, forming comparatively rigid, well-folded modules of approximately 50 kDa. Their position relative to the antigen can therefore be modelled with greater confidence, reducing conformational heterogeneity within the complex [66, 101]. Even smaller single-domain formats, such as camelid nanobodies of approximately 14 kDa, can reduce flexibility further, although they contribute less additional mass to the overall particle [66, 75].

In practice, monoclonal antibody discovery campaigns rarely produce Fab fragments directly. The anti-FLVCR1a mAb panel was generated, expressed and screened by F. Bertoglio at TU Braunschweig as bivalent scFv-Fc molecules, in which variable domains identified through

antibody display technologies were fused to a dimeric human Fc region (see Materials and Methods). This format was selected for the primary screening stages because it allowed straightforward detection with standard anti-human-Fc secondary reagents in ELISA and western blotting. Its bivalency also increased apparent affinity through avidity, which was advantageous during the initial identification of binding clones. Conversion to a monovalent Fab format, lacking the flexible hinge and Fc region, is an important step before using the antibodies in downstream structural applications such as cryo-EM, and was considered only after individual clones had been shown to bind hFLVCR1a specifically and with high affinity.

Complex formation of the FBE panel with hFLVCR1a by SEC. Binding to the native, detergent-solubilised receptor was assessed for 15 of the 16 clones of the panel (344C1 was not tested) by analytical SEC on a Superose 6 5/150 GL column (Professor Francesca Magnani, personal communication). SEC is widely used to detect antibody–antigen complex formation in solution, where complex formation is typically indicated by a new, higher-molecular-weight species that elutes earlier than either individual component [28, 29]. This approach is also applicable to membrane protein–antibody complexes in detergent, because the additional mass of an antibody of approximately 110 kDa relative to the receptor micelle can still produce a measurable shift towards earlier elution [29, 30]. Complex formation was assessed by a leftward shift of the mixture trace relative to the free mAb and free hFLVCR1a, increased absorbance at the putative complex peak and a corresponding reduction of the free mAb peak (Figure 1.22). Seven clones (339C1, 339F1, 339H11, 340C1, 340D3, 341F5 and 345E9) showed clear complex formation. For the remaining eight clones (339B6, 339B9, 339C8, 339D6, 339H8, 340E7, 341A6 and 341D4), the shift was modest or ambiguous, and the apparent complex peak often overlapped with that of the free mAb or free hFLVCR1a. Because the components were injected immediately after mixing, without pre-incubation, the absence of a clear shift does not exclude binding, particularly for lower-affinity clones [18]. The epitope type recognised by each clone was assessed in addition to complex formation, as described in Section 1.6.2 and summarised in Table 1.1.

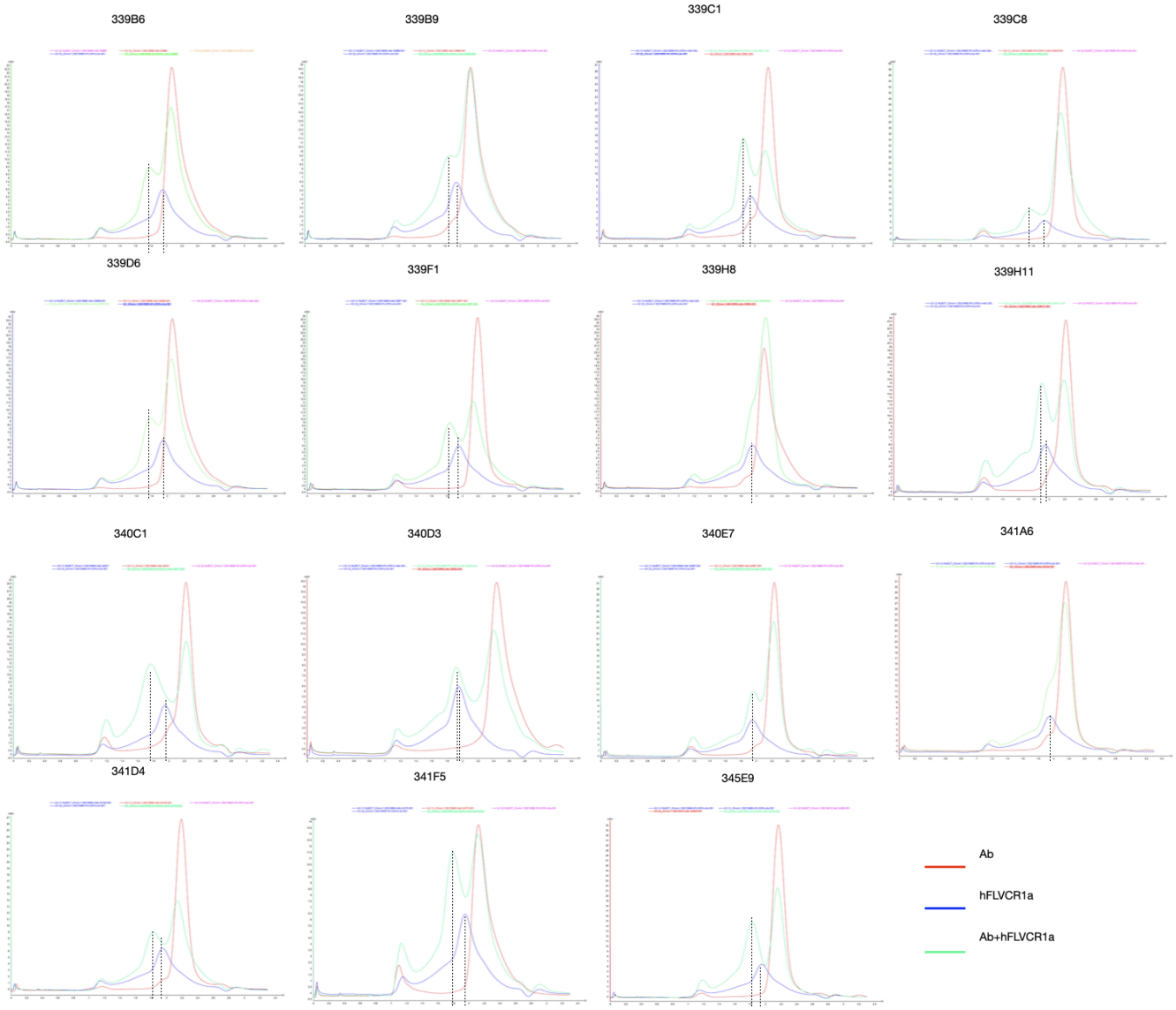


Figure 1.22. Analytical SEC screening of 15 anti-hFLVCR1a mAb clones for complex formation with purified hFLVCR1a. Each panel shows three traces obtained on a Superose 6 5/150 GL column equilibrated with 50 mM HEPES, 150 mM NaCl, 0.026% DDM and 0.005% CHS: mAb alone (red), hFLVCR1a alone (blue) and a 1:1.5 mAb:hFLVCR1a mixture injected immediately after mixing (green). UV absorbance (mAU) is plotted against elution volume (ml). Data: Professor Francesca Magnani (unpublished).

1.6.2 Linear versus conformational epitopes and their relevance to cryo-EM

An epitope is described as linear, or continuous, when the residues that contact the antibody paratope form an uninterrupted stretch of the primary amino acid sequence. By contrast, a conformational, or discontinuous, epitope consists of residues from separate regions of the polypeptide chain—or, in some cases, from different subunits of an oligomeric antigen—that are brought together only after the protein folds into its native structure [106, 107]. Most epitopes

recognised by antibodies raised against folded, native protein antigens are thought to be conformational rather than linear, with estimates commonly approaching 90% [106, 107].

This distinction is important when selecting antibodies for cryo-EM. Antibodies that recognise linear epitopes will retain binding activity when the target protein has been unfolded or denatured, such as after SDS-PAGE and transfer to a membrane for western blotting. Their recognition depends primarily on the amino acid sequence rather than the protein's tertiary structure. Such antibodies are generally less useful for cryo-EM because their linear epitopes often represent flexible portions of the protein and do not impose a fixed spatial relationship between the Fab and the remainder of the antigen—the very property required of an effective fiducial marker. By contrast, antibodies that recognise conformational epitopes depend on the correct three-dimensional arrangement of the target protein. They are therefore expected to preferentially recognise the natively folded antigen and to form more rigid interfaces, because multiple discontinuous contact points constrain the relative orientation of the Fab and antigen. This rigidity is central to fiducial-based cryo-EM approaches. A Fab or nanobody bound to a conformational epitope can transfer positional and rotational information from a small antigen to a larger mass that is easier to align. This principle has been demonstrated for the ASCT2–Nb469 complex [75], the MFSD2A–Fab complex [74] and Fab-bound CD20 [101].

Distinguishing conformational-epitope binders from linear-epitope binders was therefore an early and important step in characterising the FBE mAb panel. A positive SEC result alone cannot distinguish between these epitope classes, since antibodies recognising either type of epitope can potentially form stable complexes with a natively folded antigen in solution. Each candidate was therefore also tested by SDS-PAGE and western blotting against denatured hFLVCR1a (F. Magnani, personal communication, unpublished). Under these conditions, a positive western blot signal indicates recognition of a linear (or denaturation-resistant) epitope, because the epitope remains accessible after loss of tertiary structure. Conversely, failure to detect denatured hFLVCR1a is consistent with—but does not by itself prove—recognition of a conformational epitope.

Nine mAbs (339-B6, 339-B9, 339-C1, 339-D6, 339-F1, 340-C1, 341-F5, 344-C1 and 345-E9) were probed against lysates of HEK293F cells expressing hFLVCR1a-GFP-6×His or mock-transfected with the empty vector, using an HRP-conjugated anti-human Fc secondary antibody (Figure 1.23). 339-B6, 339-B9, 340-C1 and 344-C1 gave a band specifically in the hFLVCR1a lane. 339-C1 gave bands in both lanes, so its signal could not be attributed to hFLVCR1a, and no signal was detected for 339-D6, 339-F1, 341-F5 and 345-E9. Three further clones were assessed in the human/murine

comparison described in Section 3.3 (Figure 3.8): 339C8 gave a signal for human but not murine FLVCR1a, 341D4 detected both orthologues, and 339H11 gave no signal.

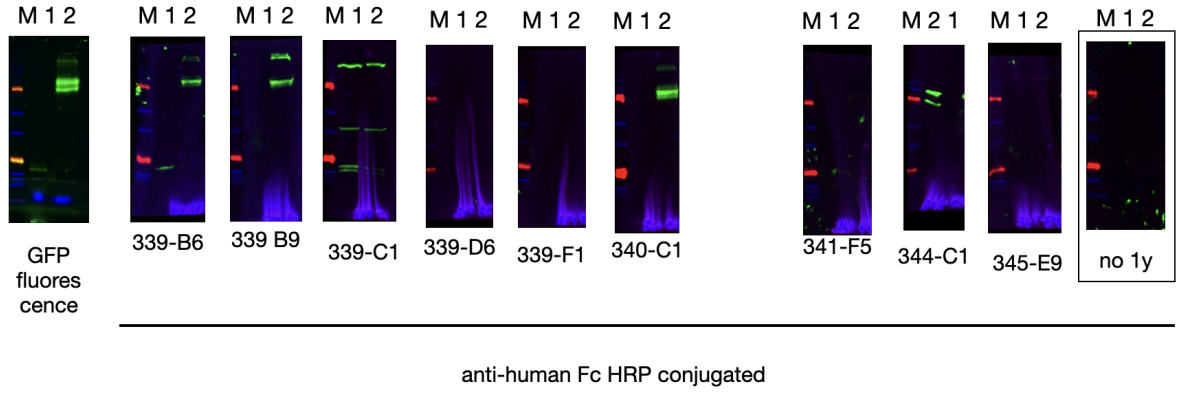


Figure 1.23. Western blot analysis of FBE mAbs against denatured hFLVCR1a-GFP-6×His. Each panel contains a molecular-weight marker (M), a lysate of mock-transfected HEK293F cells carrying the empty pEGBacMam vector (lane 1) and a lysate of HEK293F cells expressing hFLVCR1a-GFP-6×His (lane 2). The leftmost panel shows GFP fluorescence as an expression control; the following panels show chemiluminescent signals obtained with the indicated mAb as primary antibody, detected with an HRP-conjugated anti-human Fc secondary antibody (#A0170, Merck). The rightmost panel ("no 1y") is the no-primary-antibody control. Data: Professor Francesca Magnani (unpublished).

Combining the western blot and SEC data (Table 1.1), six clones (339B6, 339B9, 339C8, 340C1, 341D4 and 344C1) were detected by western blot and are therefore consistent with linear or denaturation-resistant epitopes. Four clones (339F1, 339H11, 341F5 and 345E9) formed complexes with native hFLVCR1a but were not detected by western blot, making them candidates for conformational epitopes. The remaining six clones could not be assigned: 339C1 formed a complex but also gave a western blot signal in the mock-transfected control, 340D3 formed a complex but was not tested by western blot, and 339D6, 339H8, 340E7 and 341A6 gave ambiguous SEC profiles without a positive western blot signal. These assignments indicate the character of the epitope rather than definitive epitope mapping.

mAb clone	Western blot (denatured hFLVCR1a)	SEC (native hFLVCR1a)	Inferred epitope type
339B6	Positive	Ambiguous	Linear / denaturation-resistant
339B9	Positive	Ambiguous	Linear / denaturation-resistant
339C1	Signal in mock and hFLVCR1a lanes	Complex	Not assigned
339C8	Positive (human only)	Ambiguous	Linear / denaturation-resistant
339D6	Negative	Ambiguous	Not assigned
339F1	Negative	Complex	Conformational (candidate)
339H8	Not tested	Ambiguous	Not assigned
339H11	Negative	Complex	Conformational (candidate)
340C1	Positive	Complex	Linear / denaturation-resistant
340D3	Not tested	Complex	Not assigned
340E7	Not tested	Ambiguous	Not assigned
341A6	Not tested	Ambiguous	Not assigned
341D4	Positive	Ambiguous	Linear / denaturation-resistant
341F5	Negative	Complex	Conformational (candidate)
344C1	Positive	Not tested	Linear / denaturation-resistant
345E9	Negative	Complex	Conformational (candidate)

Table 1.1. Summary of western blot and SEC results and inferred epitope type for the FBE mAb clones. Western blot: signal specific for hFLVCR1a on denatured, SDS-PAGE-separated lysates (Figure 1.23; for 339C8 and 341D4, the orthologue assay shown in Figure 3.8, Chapter 3). SEC: complex formation with purified, native hFLVCR1a (Figure 1.22), classified as clear complex formation (“Complex”) or modest/ambiguous shift (“Ambiguous”). Data: Professor Francesca Magnani (unpublished).

Antibodies that formed stable, shifted complexes with detergent-solubilised hFLVCR1a by SEC and showed no western blot signal were therefore regarded as putative conformational-epitope binders and prioritised for progression towards structural studies, since a stable and relatively rigid antibody–antigen complex is essential for effective particle alignment in cryo-EM. Selected clones were subsequently tested for cross-reactivity with the murine FLVCR1a orthologue, which assesses species specificity and provides an additional, independent indication of epitope characteristics before conversion to the Fab format (see Results, Section 3.3).

1.7 Aims of the thesis

The preceding sections reveal a consistent theme in FeLV receptor biology. A small group of essential and evolutionarily conserved SLC-family transporters—including FLVCR1a (SLC49A1) and PiT-1/PiT-2 (SLC20A1/A2)—have been independently and repeatedly co-opted as entry receptors by FeLV and related gammaretroviruses (Sections 1.1–1.5). However, the structures of FLVCR1a and PiT-1 in complex with viral ligands remain unresolved (Sections 1.3 and 1.5). Moreover, before this study, no functional evidence had demonstrated that binding of a receptor's physiological substrate could modulate its activity as a viral receptor (Sections 1.3–1.5). This thesis was therefore designed to address these gaps.

The primary aim of this work was to characterise the molecular basis of FeLV-C receptor engagement, with a focus on FLVCR1a, and to establish whether the transport substrate(s) of this protein affects its function as a viral entry receptor. Alongside these studies, the work aimed to develop the expression, purification, and structural biology methods required for future high-resolution determination of receptor–ligand complexes of FLVCR1a and PiT-1.

This overall aim was addressed through four specific objectives:

1. To establish recombinant expression and purification methods for the feline orthologue fFLVCR1a, PiT-1/SLC20A1, and the FeLV-B receptor-binding domain (see Results, Chapter 3). These preparations were required to achieve the yield, purity, and homogeneity necessary for subsequent biophysical analyses (Sections 3.5–3.7).
2. To investigate whether the physiological FLVCR1a substrates hemin and the related porphyrin coproporphyrin I bind to the purified transporter. MST and nano-differential scanning fluorimetry (nDSF) were used to distinguish between simple ligand binding and productive interactions that stabilise the protein (Section 3.1).
3. To determine whether heme binding to the FLVCR1a substrate site alters the affinity of the FeLV-C SU receptor-binding domain for FLVCR1a. This was examined using MST, size-exclusion chromatography, and magnetic pulldown assays, with the findings interpreted in relation to the proposed conformational cycle of the transporter (Section 3.2).
4. To characterise a panel of monoclonal antibodies and antibody fragments against hFLVCR1a, as potential fiducial markers for future cryo-EM studies (Sections 3.3–3.4).

Collectively, these objectives were intended to extend the study of FeLV receptor tropism beyond a primarily genetic and sequence-based framework. The aim was to develop a biophysical—and ultimately structural—model in which receptor engagement is viewed as an active, ligand-

dependent process rather than as a static docking interaction. The results are presented in Chapter 3, the wider significance of the findings and their limitations are discussed in Chapter 4, and the conclusions and future perspectives are given in Chapter 5.

2. Materials and Methods

The experiments in this thesis were designed to study how FeLV Env engages its receptors, FLVCR1a and PiT-1, and to build the reagents needed for future structural work. The methods are organised in the order in which a protein is produced and then used: constructs are cloned (2.1), expressed (2.2), and purified (2.3). Binders are generated (2.4), and the purified proteins are tested in binding and biophysical assays (2.5). The central methodological challenge throughout is that both receptors are multipass membrane proteins, which have to be extracted in detergent while staying folded and monodisperse. Many choices described below (construct design, the DDM/CHS system, Superose 6 analytical SEC and the pulldown format) follow from this. Where experiments were performed by collaborators, this is stated in the corresponding subsection heading.

2.1 Molecular cloning

PCR amplifications were performed in 50 µL reactions containing 0.5 µL each of forward and reverse primers (10 µM), 0.5 µL of template DNA (30 ng/µL), 25 µL of 2× high-fidelity DNA polymerase master mix, and 23.5 µL of nuclease-free water. Reactions were run on a thermal cycler with an initial denaturation step at 98 °C for 10 s, followed by 30–35 cycles of 98 °C for 10 s, 55 °C for 5–15 s, and 72 °C for an extension time scaled to amplicon length (approximately 5 s/kb, with empirical adjustment for individual amplicons). A final hold was performed at 10 °C.

PCR products and restriction digests were resolved on 1% agarose gels alongside a GeneRuler DNA Ladder Mix (Thermo Fisher Scientific). Products intended for downstream cloning were gel-purified using a silica-membrane-based PCR/gel extraction kit. Excised gel slices were weighed before purification so that reagent volumes could be adjusted according to sample mass. DNA concentrations were measured spectrophotometrically throughout the workflow.

PCR fragments were seamlessly assembled into linearized acceptor vectors using an In-Fusion-based cloning enzyme. This system joins DNA fragments containing short (~15 bp) primer-encoded terminal homology overlaps, eliminating the need for restriction digestion or ligase-mediated insert joining [54]. The assembled products were transformed into Stellar chemically competent Escherichia coli, a $recA^-$, $endA^-$ strain optimized for In-Fusion cloning. Briefly, competent cells were thawed on ice, the complete In-Fusion reaction was added, and the cells were incubated on ice for 30 min. Cells were then heat-shocked at 42 °C for 2 min, returned to ice, and recovered in 600 µL of SOC medium pre-warmed to 42 °C for 1 h at 37 °C.

Recovered cells were plated at three densities—5 µL, 50 µL, and the pelleted remainder of the culture—on LB agar containing 1× ampicillin and incubated at 37 °C for 1–2 days. Individual colonies were expanded overnight at 37 °C in 5 mL LB broth containing 1× ampicillin. Plasmid DNA was purified using the QIAprep Spin Miniprep Kit (Qiagen) according to the standard alkaline lysis and silica-membrane spin-column protocol, including resuspension in Buffer P1, alkaline lysis in Buffer P2, neutralization and high-salt binding in Buffer N3, washing with Buffer PE, and elution in Buffer EB [56].

Clones were verified by restriction digestion. For each clone, the volume corresponding to 200 ng of plasmid DNA was calculated from the measured concentration using V = m/C. This volume was digested in a 10 µL reaction containing 0.5 µL of each of two restriction enzymes, 1 µL of 10× FastDigest Green Buffer, and nuclease-free water to the final volume. Digested products were analyzed by agarose gel electrophoresis.

Where recombinant baculovirus generation was required, verified plasmids were transformed into DH10Bac E. coli to generate recombinant bacmid DNA through site-specific Tn7-mediated transposition [48]. Recombinant clones were identified by blue/white screening on Bluo-gal/IPTG/ antibiotic-selective agar. Successful transposition disrupts the bacmid-encoded lacZα reporter, resulting in white colonies. Bacmid DNA was subsequently isolated from positive clones for downstream transfection of mammalian cells.

2.1.1 Cloning of the FeLV-B SU receptor-binding domain (RBD)

Three sequential constructs containing the FeLV-B SU receptor-binding domain (RBD) were generated during this work.

FeLV-B_RBD in pFAstBAc1. The initial construct was based on the receptor-binding domain of the feline leukemia virus subgroup B (FeLV-B) surface unit (SU) envelope glycoprotein (PDB 1LCS, chains A/B). The construct comprised the native RBD signal peptide and ectodomain, consisting of 271 amino acids, with a calculated molecular weight of 30,299.97 Da, an extinction coefficient of 72,015 $M^{-1}cm^{-1}$, and an Abs 0.1% (1 g/L) value of 2.401.

A synthetic gene was designed with the architecture Kozak–RBD–TEV site–6His–GS–6His–STOP STOP. The sequence was reverse-translated and codon-optimized while excluding internal recognition sites for EcoRI, StuI, SalI, XbaI, KpnI, and XhoI to maintain compatibility with downstream subcloning. The gene was synthesized with flanking SalI and XbaI sites for directional cloning into pFastBac1.

FeLV-B_RBD in pEG BacMam. The FeLV-B_RBD in pFAstBAc1 cassette was subsequently subcloned from pFastBac1 into an open pEG BacMam acceptor vector [24], which had been linearized between the same SalI and XbaI sites to enable direct expression in mammalian cells. The cassette retained the native RBD signal peptide and was amplified from the pFastBac1 template using custom primers:

FelV020fw: 5′-aaaggcctacGTCGACgccaccatggagggtccaac-3′

FelV020rv: 5′-gactgcaggcTCTAGActattagtgatggtgatg-3′

These primers introduced SalI and XbaI sites, together with flanking bases to facilitate restriction digestion and provide In-Fusion-compatible overlaps. The resulting amplicon was gel-purified, quantified, and assembled with the linearized pEG BacMam vector using In-Fusion cloning. The reaction was then transformed into Stellar cells, and clones were verified as described above.

µSP-FeLV-B_RBD in pEG BacMam. To examine the effect of signal peptide identity on RBD expression, secretion, and receptor tropism, we generated a construct in which the native RBD signal peptide was replaced with the heterologous µ-phosphatase secretion signal peptide (MGILPSPGMPALLSLVSLLSVLLMGCVA↓ETG). The arrow indicates the predicted signal peptidase cleavage site. This signal peptide was originally described as part of a versatile mammalian/insect secretion vector suite [55]. Because the complete signal peptide-encoding sequence was too long to incorporate into a single primer, it was added to the 5′ end of the RBD coding sequence through three sequential overlapping PCR reactions using progressively longer forward primers:

FelV021fw1:

5′-GTCTGTGCTGCTGATGGGCTGTGTGGCAGAAACCGGAaacccatccccacaccaagtg-3′

FelV021fw2:

5′-

TCCAGGCATGCCAGCTCTGCTGTCTCTGGTGAGCCTGCTGTCTGTGCTGCTGATGGGCT-3′

FelV021fw3:

5′-aaggcctacGTCGACgccaccATGGGGATTTTGCCCTCTCCAGGCATGCCAGCTCTGC-3′

The FelV020rv reverse primer was used in all three reactions to retain the unmodified TEV–6His-GS-6His cassette at the 3′ end. The final amplicon was gel-purified, quantified, and assembled by In-Fusion cloning into a fresh aliquot of the SalI/XbaI-linearized pEG BacMam vector. Unlike FeLV020, the assembled FeLV021 construct was transformed into DH10Bac E. coli to generate

recombinant bacmid DNA through Tn7-mediated transposition. Recombinant clones were identified by blue/white selection on Bluo-gal/IPTG/antibiotic plates, and bacmid DNA was isolated from positive white colonies [48].

2.1.2 Cloning of fSLC20A1 constructs

Two constructs encoding the feline phosphate transporter SLC20A1 (PiT-1), the cellular receptor for FeLV-B, were generated. The constructs differed in the position of the affinity tag relative to the transporter sequence.

fSLC20A1 C-terminus. The feline SLC20A1 coding sequence (UniProt O97596, S20A1_FELCA, 681 amino acids with a molecular weight of 74kDa, extension coefficient of 101590 $M^{-1}cm^{-1}$, and an Abs 0.1% (1 g/L) value of 1.372) was synthesized with a C-terminal tag architecture: EcoRI–Kozak–SLC20A1–TEV–TwinStrep–STOP STOP–XbaI. The TwinStrep tag consisted of a TEV cleavage site followed by two Strep-tag II repeats separated by a Gly-Ser-rich linker (ENLYFQG-GS-SAWSHPQFEK-GGGSGGGSGGS-AWSHPQFEK), enabling single-step affinity purification using Strep-Tactin resin [43]. The cassette was cloned into an open pEG BacMam vector linearized between EcoRI and XbaI [24]. No internal NotI site was retained upstream of the TEV protease site.

N-terminus fSLC20A1. To determine whether relocating the affinity tag would improve expression and capture, a second construct was generated with the tag positioned at the N-terminus. This design was motivated by the location of the native SLC20A1 C-terminus near the final transmembrane helix in the protein's 12-transmembrane topology [58]. The resulting architecture was SalI–Kozak–STREP–STREP–TEV–SLC20A1–STOP STOP–NotI.

We assembled the construct using the existing pEG BacMam-based vector EROS004 (SalI–Kozak–STREP–FLAG–STREP–TEV–AgeI–mEROS–STOP STOP–NotI) as a scaffold. A two-step overlap-extension PCR strategy was used.

In PCR1, the EROS004 vector was used as the template to amplify the vector backbone with primers N-terminus fSLC20A1 fw1 (5′-AAGTACGTGATCCTGTAATAGGCGGCCGCTTTCGAATCT-3′) and fSLC20A1 N-terminus rv1 (5′-CGGACCCTCCCCCGCTTCCGCCGCCCTTCTCGAATTGAGGGTGGCTCCA-3′). This reaction removed the mEROS coding sequence and one of the three Strep-tag repeats while retaining the SalI site, Kozak sequence, N-terminal Strep-Strep-TEV segment, and STOP STOP–NotI region.

In PCR2, the fSLC20A1 C-terminus plasmid was used as the template to amplify the SLC20A1 coding sequence. Nested forward primers:

- N-terminus fSLC20A1 fw2-1

(5′-

GTTCGAAAAGGGCAGCGAGAACCTGTACTTCCAGGGCGCCTTCACCGGCGCTACCCTG-3′)

- N-terminus fSLC20A1 fw2-2

(5′-GCGGGGGAGGGTCCGGAGGATGGAGCCACCCCCAGTTCGAAAAGGGCAGCGA-3′)

with reverse primer N-terminus fSLC20A1 rv2

(5′- CAGGATCACGTACTTGAACACGGCCATGATGGCGGC-3′). These primers introduced sequence homologous to the TEV cleavage site at the 5′ end and to the vector's STOP STOP–NotI region at the 3′ end.

The PCR1 vector-backbone fragment and PCR2 SLC20A1 insert were gel-purified, quantified, and assembled by In-Fusion cloning to generate the final 9,040 bp N-terminus fSLC20A1 plasmid. Clones were verified by SalI/NotI digestion as described above, and positive clones were transformed into DH10Bac E. coli for recombinant bacmid generation.

2.1.3 Cloning of the fFLVCR1a construct

fFLVCR1a encodes feline FLVCR1a (UniProt Q9N1F2, FLVC1_FELCA), a 12-transmembrane heme/choline-ethanolamine transporter belonging to the major facilitator superfamily. The construct was synthesized with the architecture EcoRI–Kozak–FLVCR1a–TEV–TwinStrep–STOP STOP–XbaI. It encoded 599 amino acids, including the affinity tag, with a calculated molecular weight of 64,445 Da, an extinction coefficient of 87,780 $M^{-1}cm^{-1}$, and an Abs 0.1% (1 g/L) value of 1.40.

The construct incorporated the same TwinStrep tag architecture described for fSLC20A1 C-terminus. (ENLYFQG-GS-SAWSHPQFEK-GGGSGGGSGGS-AWSHPQFEK) [43]. The cassette was cloned into an open pEG BacMam vector linearized between EcoRI and XbaI [24], with no internal NotI site upstream of the TEV protease site. The verified plasmid was transformed into Top10 E. coli for propagation and, in parallel, into DH10Bac E. coli for recombinant bacmid generation through Tn7-mediated transposition, as described above [48].

2.1.4 hFLVCR1a-GFP construct (Data from Professor Francesca Magnani)

A GFP-fusion construct of the human FLVCR1a ortholog (hFLVCR1a) was generated for downstream antibody-validation studies and was distinct from the feline FLVCR1a–TwinStrep construct (fFLVCR1a) described in Section 2.1.3. The hFLVCR1a coding sequence was fused at its C-terminus to green fluorescent protein (GFP), followed by a hexahistidine (6×His) tag, and cloned into the pEG BacMam expression vector [24] for expression in HEK293F cells.

C-terminal GFP fusion is a well-established strategy for the study of eukaryotic membrane proteins. It was initially developed to facilitate fluorescence-detection size-exclusion chromatography (FSEC)-based expression screening directly from small-scale, unpurified cell lysates and to enable straightforward, antibody-independent confirmation of protein expression through in-gel or whole-cell fluorescence [59]. In the present study, the GFP moiety also served as a convenient, tag-independent internal reference for verifying successful transfection and expression before immunoblot-based screening of candidate monoclonal antibodies raised against FLVCR1a (Section 2.4.1; antibodies provided by Federico Bertoglio, Technische Universität Braunschweig). An empty pEG BacMam vector lacking the hFLVCR1a–GFP insert was maintained in parallel as a mock-transfected negative control.

2.1.5 hFLVCR1a construct (Strep-FLAG-Strep tag, purification protocol development)

A third FLVCR1a construct was generated using the human orthologue (hFLVCR1a; UniProt Q9Y5Y0, FLVC1_HUMAN), distinct from both the feline FLVCR1a construct (Section 2.1.3) and the hFLVCR1a-GFP-6xHis construct used for antibody validation (Section 2.1.4). This construct carried a C-terminal TEV-Strep-FLAG-Strep tripartite tag:

(AAA-ENLYFQG-GS-WSHPQFEK-GS-DYKDDDDK-GS-WSHPQFEK), comprising a TEV protease cleavage site followed by a single Strep-tag II repeat, a FLAG tag, and a second Strep-tag II repeat, each separated by short Gly-Ser linkers. The full-length tagged construct (605 amino acids) has a calculated molecular weight of 66,400 Da, an extinction coefficient of 89,000 $M^{-1}cm^{-1}$, and Abs 0.1% (1 g/L) = 1.37; following TEV cleavage, the untagged protein (555 amino acids, matching the native hFLVCR1a sequence) has a calculated molecular weight of 60,800 Da, an extinction coefficient of 75,000 $M^{-1}cm^{-1}$, and Abs 0.1% (1 g/L) = 1.23. This construct was used to establish and optimize the detergent solubilization, Strep-Tactin XT affinity capture, and

size-exclusion chromatography protocol described in Section 2.3, before its application, unmodified, to the orthologous feline FLVCR1a construct.

2.2 Protein expression

Membrane proteins and secreted glycoproteins need different expression strategies, and this section records the systems used for each. Mammalian cells (HEK293F/Expi293) were chosen for the receptors because they provide a human-like folding and glycosylation environment. Baculovirus transduction was run in parallel with direct plasmid transfection to see which route gave more material, and sodium butyrate was used to counter transgene silencing. The secreted FeLV-B RBD was expressed in both ExpiSf9 insect cells and mammalian cells, since yield and glycosylation could differ between hosts. A small-scale screen (2.2.4) was used to compare constructs before committing to a large-scale preparation. The transient transfection used for antibody validation (2.2.1) is described first because it generated the antigen source on which the antibody work depends.

2.2.1 Transient transfection of HEK293F cells (hFLVCR1a-GFP, pEGBacMam)

HEK293F cells, a suspension-adapted derivative of the human embryonic kidney 293 (HEK293) cell line [60], were used for expression of the hFLVCR1a-GFP-6xHis construct described in Section 2.1.4. These cells are optimized for high-density, serum-free, transient transfection. To generate a suitable antigen source for antibody validation, HEK293F cells were transiently transfected with either hFLVCR1a-GFP-6×His cloned into the pEGBacMam vector or the empty pEGBacMam vector, which served as a mock-transfected negative control. pEGBacMam is a mammalian expression vector optimized for high-level expression of membrane proteins, including GFP-fusion constructs [24, 25]. Transfections were performed using 0.5 µg of vector per 10^6 cells. To improve recombinant protein yield, sodium butyrate was added to a final concentration of 10 mM eight hours after transfection. This treatment exploits the established role of sodium butyrate as a histone deacetylase inhibitor that enhances transient gene expression in HEK293 cells [26, 27]. Cells were harvested 40 hours after transfection. Cell pellets containing 2×10^6 cells were solubilized in 200 µl of buffer containing 0.5% DDM–CHS, 50 mM HEPES, 150 mM NaCl, and a Roche protease inhibitor cocktail. The lysates were then clarified by centrifugation at 18,000 × g for 20 minutes at

4°C. Cleared lysates were separated on a 12% SDS-PAGE gel and transferred to a PVDF membrane for western blotting. The membrane was then cut into strips, with each strip corresponding to a single mAb, and blocked with milk before incubation with the primary antibodies. Each strip was incubated with one candidate mAb for one hour at room temperature, washed, and then incubated for a further hour at room temperature with an HRP-conjugated anti-human Fc secondary antibody (#A0170, Merck). This detection strategy took advantage of the human Fc region present in each IgG-like mAb. Chemiluminescent signal was subsequently developed. A strip incubated without a primary antibody was included as a control to confirm the absence of non-specific secondary-antibody signal (Figure 1.23, “no 1y”).

2.2.2 Expression system(s) for fFLVCR1a

fFLVCR1a (feline FLVCR1a–TwinStrep in pEG BacMam; Section 2.1.3) was expressed using two complementary approaches made possible by the dual plasmid/baculovirus-transfer-vector design of pEG BacMam [24, 41].

Direct mammalian plasmid expression. Plasmid DNA propagated in Top10 E. coli was used to transiently transfect suspension-adapted HEK293 cells. This approach was used initially for small-scale expression screening and subsequently at larger scale, using a 550 mL culture for full-scale purification (Section 2.3).

Baculovirus-mediated expression. The fFLVCR1a pEG BacMam plasmid was also transformed into MAX Efficiency DH10Bac chemically competent E. coli (Thermo Fisher Scientific). These cells contain the bMON14272 bacmid, which carries a mini-attTn7 target site and a kanamycin-resistance marker, together with a helper plasmid encoding Tn7 transposase and conferring tetracycline resistance. Recombinant bacmid was generated through site-specific Tn7-mediated transposition [48, 49].

Transformants were selected on LB agar containing 50 µg/mL kanamycin, 7 µg/mL gentamicin, 10 µg/mL tetracycline, 100 µg/mL Bluo-gal, and 40 µg/mL IPTG. Plates were incubated for 48 hours at 37 °C. Successful transposition disrupts the bacmid-encoded lacZα reporter, resulting in white colonies against a blue background of non-recombinant colonies. White colonies were restreaked onto fresh selective plates to confirm the phenotype, and recombinant bacmid DNA was isolated

from overnight liquid cultures grown in LB medium supplemented with kanamycin, gentamicin, and tetracycline.

Bacmid DNA was isolated using a column-free alkaline lysis method. Cell pellets were resuspended in Solution I (15 mM Tris-HCl, pH 8.0; 10 mM EDTA; 100 µg/mL RNase A), lysed with Solution II (0.2 N NaOH; 1% SDS), and neutralized with 3 M potassium acetate, pH 5.5. The clarified lysate was precipitated with isopropanol, washed with 70% ethanol, air-dried, and resuspended in sterile water. DNA concentration was determined spectrophotometrically.

Recombinant clones were verified by PCR using the pUC/M13 forward primer (5′-CCCAGTCACGACGTTGTAAAACG-3′) and reverse primer (5′-AGCGGATAACAATTTCACACAGG-3′), which flank the mini-attTn7 insertion site. PCR was performed using PrimeSTAR Max DNA Polymerase (Takara Bio; 2× premix, 0.2–0.3 µM of each primer, and <200 ng template) under the following conditions: 98 °C for 10 s, 55 °C for 5–15 s, and 72 °C for approximately 5 s/kb for 30–35 cycles. A bacmid containing the correctly transposed pEG BacMam vector was expected to produce a PCR product of approximately 4,200 bp plus the size of the insert, whereas the untransposed bacmid was expected to yield a product of approximately 300 bp.

Insect cell line. Baculovirus stocks were produced in ExpiSf9 cells, a non-engineered derivative of the Sf9 cell line adapted by Thermo Fisher Scientific for high-density suspension growth in ExpiSf CD Medium [61, 108]. Sf9 is a clonal isolate of the Sf21 cell line (IPLB-Sf21-AE), which was established from pupal ovarian tissue of the fall armyworm, *Spodoptera frugiperda* (Lepidoptera: Noctuidae), at the US Department of Agriculture laboratory in Beltsville, Maryland [109]. The Sf9 clone was isolated from Sf21 at Texas A&M University and has been widely adopted as a host for the baculovirus *Autographa californica* multiple nucleopolyhedrovirus (AcMNPV) and its derivatives [110]. In baculovirus expression systems, insect cells serve two roles. They allow recombinant bacmid DNA to be transfected into cells and amplified into infectious virus stocks (P0, P1, P2), and they act as a production host in which recombinant proteins are expressed from the viral genome during infection [51, 111]. In this thesis, ExpiSf9 cells were used mainly for the first role. Bacmid DNA was used to generate baculovirus stocks for transduction of mammalian cells (pEG BacMam constructs; Sections 2.2.2 and 2.2.4). ExpiSf9 cultures were also infected directly for secretion of the FeLV-B SU RBD (Section 2.2.3).

The verified recombinant bacmid was used to transfect ExpiSf9 insect cells [61] to generate a P0 baculoviral stock. ExpiSf9 cells were seeded the previous day at 1×10^6 cells/mL and grown to 2×10^6 cells/mL, with viability maintained above 90%. A 5 mL culture was transfected with a complex containing 2 µg bacmid DNA and 10 µL ExpiFectamine in 500 µL transfection buffer comprising 50 mM HEPES, pH 7.4, and 150 mM NaCl. Following a 96-hour incubation, cells were harvested by centrifugation at 1,000 × g for 10 min and protected from light. The P0 stock was then used to infect a 100 mL ExpiSf9 culture seeded at 1×10^6 cells/mL to generate an amplified P1 stock. The P1 stock was harvested using the same procedure and stored at 4 °C protected from light [61].

The functional titre of the P1 stock was assessed by transducing HEK293-6E cells with increasing proportions of P1 stock (0.5%, 1%, and 2%; duplicate cultures). One set of replicates was treated with 10 mM sodium butyrate 8 hours after transduction to reduce epigenetic silencing of the transgene and enhance expression [50]. Cells were harvested two days later. Because fFLVCR1a encodes a membrane protein, the cell pellets were retained for downstream analysis.

2.2.3 Expression system(s) for FeLV-B SU RBD

The three sequential FeLV-B SU RBD constructs described in Section 2.1.1 were expressed using two different platforms.

FeLV-B SU_RBD (pFastBac1). FeLV-B SU RBD (pFastBac1) was expressed using the conventional Bac-to-Bac baculovirus/insect-cell secretion system [48]. The verified pFastBac1 construct was transformed into DH10Bac E. coli, and a recombinant bacmid was generated, selected, verified, and isolated using the procedure described above for fFLVCR1a (Section 2.2.2). For a pFastBac1-derived bacmid, the expected PCR product was approximately 2,300 bp plus the size of the insert [49].

Recombinant bacmid was used to generate P0 and P1 baculoviral stocks through sequential transfection and infection of ExpiSf9 cells, following the ExpiFectamine-based protocol described above [61]. Large-scale ExpiSf9 cultures were subsequently infected with P1 and further amplified P2 baculoviral stocks to produce the secreted RBD. Because FeLV-B SU RBD (pFastBac1) encodes a secreted protein, cultures were harvested by low-speed centrifugation at 1,200 × g for 10 min at 4 °C, and the clarified supernatant was retained. This approach is consistent with the established use of baculovirus–insect-cell systems for producing secreted recombinant glycoproteins [51].

FeLV-B SU_RBD and μSP-FeLV-B_RBD (pEG BacMam). Both constructs were expressed by transient transfection of Expi293 cells [24] using PEI-mediated transfection at a DNA:PEI ratio of 1:5. Primatone peptone was added to a final concentration of 0.6% (w/v) 4–5 hours after transfection to enhance recombinant protein titres [57].

FeLV-B SU_RBD (pEG BacMam) was introduced as In-Fusion-cloned plasmid DNA propagated in Stellar cells. In contrast, μSP-FeLV-B_RBD (pEG BacMam) was introduced as recombinant bacmid DNA generated through DH10Bac transposition and blue/white screening, as described above [48]. This approach took advantage of the compatibility of the pEG BacMam platform with both plasmid- and bacmid-based transient transfection for initial expression screening [24].

2.2.4 Expression system(s) for fSLC20A1

Both SLC20 constructs—fSLC20A1 C-terminus and fSLC20A1 N-terminus (Section 2.1.2)—were processed through the same recombinant bacmid-generation pipeline. The constructs were transformed into DH10Bac E. coli, followed by blue/white selection on kanamycin/gentamicin/ tetracycline/Bluo-gal/IPTG plates. White colonies were restreaked to confirm the phenotype, and bacmid DNA was isolated using the column-free alkaline lysis method described above. The bacmid was then verified by PCR using the pUC/M13 Forward and Reverse primers with PrimeSTAR Max DNA Polymerase. A correctly transposed pEG BacMam–SLC20 bacmid was expected to yield a product of approximately 4,200 bp plus the size of the insert [48, 49].

Verified bacmid DNA was used in two parallel expression workflows. For small-scale screening, bacmid DNA was used to transiently transfect Expi293 cells seeded in Dynamis + Gln medium in a 6-well plate at 2 mL per well and 1×10^6 cells/mL. The following day, cells were transfected with 1 μg DNA per well at a DNA:PEI ratio of 1:3. DNA and PEI were diluted separately in 100 μL of transfection buffer, combined, briefly vortexed, and incubated for 10 minutes at room temperature before being added dropwise to the cells. Eight hours after transfection, sodium butyrate was added to a final concentration of 10 mM to enhance transgene expression [50]. Cultures were harvested after 2 days.

In parallel, bacmid DNA was used to generate P0 and P1 baculoviral stocks through ExpiFectamine-mediated transfection and infection of ExpiSf9 cells, following the protocol described in Section 2.2.2 [61]. This enabled direct comparison of material produced by plasmid transfection and by baculovirus-mediated expression.

Because SLC20A1/PiT-1 is a polytopic integral membrane transporter rather than a secreted protein, expression was assessed using the solubilized cell pellet rather than the culture supernatant. Cell pellets were extracted using a DDM/CHS-containing buffer to support detergent solubilization while helping preserve the native fold of the transporter (Section 2.3) [44].

2.3 Protein purification

The purification strategy was designed to keep detergent-solubilised receptors stable enough for downstream binding and structural work. Strep-Tactin XT capture was chosen for the receptors for its high affinity and gentle biotin elution, while the His-tagged RBD was captured by Ni-NTA. Small-scale magnetic-bead capture mirrors the large-scale protocol so that screening results transfer to preparative work. The DDM/CHS buffer system (2.3.2) was kept constant from solubilisation to analytical SEC, so that any change in the chromatogram reflects the sample rather than a change in buffer. Superose 6 Increase 5/150 GL was selected because it needs only small amounts of protein, which is the practical limit with membrane-protein preparations. SDS-PAGE and western blotting (2.3.3) confirm identity and purity, and they are the readout used to decide which fractions to carry forward.

2.3.1 Affinity chromatography

Two complementary affinity capture strategies were used across the constructs described in this thesis, matched to the affinity tag carried by each construct, and applied at both small (screening) and large (preparative) scale.

Strep-Tactin affinity chromatography (fFLVCR1a, fSLC20A1 C-terminus, fSLC20A1 N-terminus, hFLVCR1a). Constructs carrying a C- or N-terminal Strep-based affinity tag were purified on Strep-Tactin XT resin (IBA Lifesciences), a streptavidin mutein engineered for substantially higher (picomolar-range) binding affinity for the Strep-tag II/Twin-Strep-tag than earlier-generation Strep-Tactin, while retaining reversible, biotin-competitive elution under mild, near-physiological conditions well suited to purification of detergent-solubilized membrane proteins [43, 62]. fFLVCR1a, fSLC20A1 C-terminus and fSLC20A1 N-terminus each carried a TEV-TwinStrep tag:

(ENLYFQG-GS-SAWSHPQFEK-GGGSGGGSGGS-AWSHPQFEK, comprising a TEV cleavage site followed by two Strep-tag II repeats separated by a Gly-Ser-rich linker), positioned at the C-terminus for fFLVCR1a and fSLC20A1 C-terminus and at the N-terminus for fSLC20A1 N-terminus (Section 2.1.2). The human FLVCR1a construct (hFLVCR1a; Section 2.1.5), used to develop and validate this purification protocol before its application, unmodified, to the orthologous fFLVCR1a construct, instead carried a C-terminal TEV-Strep-FLAG-Strep tripartite tag (AAA-ENLYFQG-GS-WSHPQFEK-GS-DYKDDDDK-GS-WSHPQFEK), comprising a single Strep-tag II repeat, a FLAG tag, and a second Strep-tag II repeat downstream of the TEV cleavage site. Both tag formats are compatible with Strep-Tactin XT-based capture via their Strep-tag II moieties.

Cell pellets (from 1 L of culture) were solubilized in 40 mL of Buffer B (50 mM HEPES pH 7.4, 150 mM NaCl, 20% glycerol) supplemented with a protease inhibitor cocktail (leupeptin 1 µg/mL, aprotinin 1 µg/mL, pepstatin 1 µg/mL, benzamidine 120 µg/mL, PMSF 100 µM) and 0.5% DDM-CHS, gently resuspended to avoid foaming and homogenized by 20 strokes of a tight-fitting Dounce homogenizer. The solubilized extract was clarified by centrifugation (56,000 × *g*, 4 °C, 45 min) and filtered through a 0.8–1.2 µm nylon syringe filter before being loaded by gravity flow onto Strep-Tactin XT resin pre-equilibrated in Buffer B, with 2-hour end-over-end incubation at 4 °C. The resin was washed sequentially with 5 column volumes (CV, one CV is 2ml) of Buffer C (50 mM HEPES pH 7.4, 500 mM NaCl, 10% glycerol) containing 0.1% DDM-CHS, then 5 CV of Buffer D (50 mM HEPES pH 7.4, 500 mM NaCl, 5% glycerol) containing 0.026% DDM-CHS (approximately 3× the critical micelle concentration of DDM) [44], and bound protein was eluted with 8 CV of the same Buffer D/detergent mixture supplemented with 50 mM biotin (pH-adjusted with NaOH to aid solubility). The eluate was concentrated using a 50 kDa molecular-weight-cutoff centrifugal concentrator (2,000 × *g*, sequential 10–12 min runs) to 2–2.5 mg/mL. Where tag removal was required, the eluate was digested overnight on ice with TEV protease (1:10 w/w) [42], and the digested sample was subsequently passed over Ni-NTA resin (1 hour, on ice, end-over-end) to remove the His-tagged TEV protease and cleaved tag fragment by reverse IMAC, with the untagged target protein recovered in the flow-through and wash fractions.

Immobilized metal affinity chromatography (IMAC) (FeLV-B SU RBD constructs). Constructs carrying a hexahistidine (6xHis) tag were purified by IMAC on Ni-NTA resin, exploiting the coordination of the polyhistidine tag to immobilized nickel ions [47]. For the RBD pellet-based purification protocol, cell pellets were solubilized in Buffer B (150 mM HEPES pH 7.4, 25 mM

NaCl) supplemented with a protease inhibitor cocktail (cOmplete-type tablet, dissolved at 100X) and 0.5% DDM-CHS, resuspended gently, homogenized (20 strokes, tight-fitting Dounce pestle), and clarified by centrifugation (56,000 × *g*, 4 °C, 45 min). The clarified supernatant was filtered (0.8–1.2 µm nylon syringe filter) and loaded by gravity flow onto Ni-NTA excel His resin pre-equilibrated in Buffer B, with 2-hour end-over-end incubation at 4 °C. The resin was washed with 20 CV of Buffer B containing 10 mM imidazole and bound protein eluted with 10 CV of Buffer B containing 400 mM imidazole, before concentration with a 10 kDa molecular-weight-cutoff centrifugal concentrator (2,000 × *g*, 10–12 min runs) to 2–2.5 mg/mL.

For small-scale expression screening (Sections 2.2.3, 2.2.4), an analogous but miniaturized magnetic-bead format was used for both tag systems: culture supernatant or clarified detergent lysate (as appropriate to each construct) was incubated for 1 hour at room temperature with 25 µL of magnetic Ni-NTA or Strep-Tactin beads pre-equilibrated in PBS, with total input, unbound (flow-through), and imidazole- or biotin-eluted fractions each retained for SDS-PAGE and western blot analysis, using the same low- and high-imidazole (10 mM/400 mM) or biotin-based wash/ elution logic described above at reduced volume.

2.3.2 Size-exclusion chromatography (Superose 6, DDM/CHS buffer system)

Following affinity capture, samples were further analysed and polished by size-exclusion chromatography (SEC) using a Superose 6 Increase 5/150 GL column (Cytiva). This small-bed-volume analytical column was well suited to the limited sample quantities typically obtained from membrane-protein preparations.

The column was equilibrated in Buffer D (50 mM HEPES, pH 7.4, 150 mM NaCl, excluding glycerol) containing 0.026% DDM-CHS. This buffer matched the detergent/lipid-mimetic system used during solubilization and affinity purification, thereby helping to maintain the target protein in a stable, monodisperse detergent micelle throughout the run [44]. SEC is a standard component of eukaryotic membrane-protein expression and purification workflows and is closely related in principle to fluorescence-detection SEC (FSEC), which is commonly used for GFP-fusion constructs [59, 24].

Before injection, samples containing at least 10 µg of protein were filtered through a 0.2 µm centrifugal microfilter. Samples were injected through a 100 µL sample loop using a 25 µL Hamilton syringe. This configuration was appropriate for the small sample volumes and limited

amounts of purified membrane protein typically available from these preparations, while also enabling reproducible loading between runs.

The eluate was monitored by UV absorbance at 280 nm. The resulting chromatograms were used to assess sample homogeneity, distinguish void-volume or aggregate-associated material from the principal monodisperse peak, and select fractions for downstream analysis by SDS-PAGE and western blotting. These analyses were consistent with standard SEC-based approaches for assessing aggregation and oligomeric state in purified protein samples [45]. Following analysis, purified protein samples were adjusted to 20% glycerol, aliquoted, and flash-frozen in liquid nitrogen for storage.

2.3.3 Purification quality control (SDS-PAGE, western blot)

SDS-PAGE. Protein purity and identity were assessed by SDS-PAGE using the discontinuous Tris-glycine-SDS buffer system described by Laemmli (1970) [63]. A 10× SDS-PAGE running buffer containing 250 mM Tris, 1.92 M glycine, and 1% SDS at pH 8.3 was prepared by dissolving 30.2 g Tris, 144.1 g glycine, and 10 g sodium dodecyl sulfate in distilled water to a final volume of 1 L. The pH was adjusted to 8.3, and the stock solution was stored at room temperature and diluted to 1× before use.

Samples were prepared in 6× SDS-PAGE sample buffer containing 375 mM Tris-HCl, pH 6.8, 6% (w/v) SDS, 50% (v/v) glycerol, and 0.03% (w/v) bromophenol blue. SDS was dissolved by warming the buffer to 40 °C. For reducing conditions, 2-mercaptoethanol was added immediately before use to a final concentration of 5% (v/v). Gels were run alongside prestained protein molecular-weight standards (Precision Plus Protein Dual Color Standards, Bio-Rad; 250–10 kDa range). Reference bands at 75 and 25 kDa were highlighted in magenta and were used to estimate the apparent molecular weight of the analysed proteins.

Where total protein visualization was required, gels were stained with Coomassie Brilliant Blue R-250 following the method of Fazekas de St Groth, Webster and Datyner (1963) [64]. Briefly, 0.5 g Brilliant Blue R-250 was dissolved in 125 mL isopropanol, diluted to 350 mL with distilled water, and supplemented with 50 mL acetic acid to a final volume of 500 mL. Following staining, gels were destained in water.

Western blotting. Following SDS-PAGE, proteins were electrophoretically transferred to a membrane using a Bio-Rad Trans-Blot Turbo transfer system. Transfer buffer was prepared by

diluting 5× Trans-Blot Turbo Transfer Buffer (Bio-Rad) to 1× with ethanol and distilled water. High-molecular-weight transfer settings were used for 12 min, following the discontinuous-buffer electroblotting principle originally described by Towbin, Staehelin and Gordon (1979) [65].

Membranes were blocked in TBS containing non-fat milk for 30 min and then incubated for 1 h with the appropriate primary detection reagent. Depending on the affinity tag carried by the construct under analysis (Sections 2.1 and 2.3.1), detection was performed using an anti-His-HRP conjugate, a Ni-NTA-Atto fluorescent conjugate, or a Mab Strep-Tactin-HRP conjugate. Membranes were developed either by chemiluminescence using ECL or, in the case of fluorescent conjugates, by direct fluorescence imaging.

For anti-Strep-Tactin-HRP detection, membranes were blocked in TBS containing 3% (w/v) BSA and 0.5% (v/v) Tween-20 for 1 h at room temperature with gentle shaking or overnight at 4 °C. Membranes were then washed three times with TBS for 5 min per wash at room temperature with gentle shaking. The membranes were incubated with Mab Strep-Tactin-HRP conjugate diluted 1:4000 for 60 min at room temperature with gentle shaking, followed by two 1-min washes in PBS-Tween and two 1-min washes in PBS. Chemiluminescent detection was performed using ECL substrate. This antibody-independent approach is based on the interaction between the Strep-tag and Strep-Tactin and is consistent with established methods for detecting Strep-tagged fusion proteins [43].

Membrane reblotting. When membranes required reprobing with an alternative or repeat antibody, previously bound antibody was removed using stripping buffer containing 200 mM glycine-HCl, pH 2.2, and 1% SDS. The stripping buffer was warmed to 50 °C and applied to the membrane for 5–15 min. The membrane was then re-blocked and re-probed using the blocking, primary-reagent incubation, washing, and chemiluminescent detection procedures described above.

2.4 Antibody generation

FLVCR1a is a small membrane protein with little extramembrane mass, which makes it a difficult target for cryo-EM on its own. The antibody work in this section aims to provide binders that can serve as fiducial markers and conformational stabilisers. The scFv-Fc panel raised against hFLVCR1a (2.4.1) provided candidate clones, which were validated against transfected-cell lysates,

with GFP fluorescence as an antibody-independent expression control. Clone 339-F1 was then reformatted as a monovalent Fab (2.4.2), because avidity effects and the flexibility of an Fc-containing format would complicate both complex formation and structural analysis. Complex formation with hFLVCR1a was tested by analytical SEC in the same detergent system used for purification.

2.4.1 Bivalent scFv-Fc monoclonal antibodies against hFLVCR1a (raised by F. Bertoglio, TU Braunschweig) (Data from Prof. Francesca Magnani)

Recombinant monoclonal antibodies against human FLVCR1a were generated using phage display by Dr. Federico Bertoglio at the Institut für Biochemie, Biotechnologie und Bioinformatik, Technische Universität Braunschweig. Positive scFv clones were reformatted into a bivalent, human Fc-containing scFv-Fc format. In this configuration, the scFv is directly fused to a human IgG Fc domain rather than being reconstituted as a conventional four-chain IgG (Figure 1.21). The format preserves bivalent antigen binding and Fc-mediated detection while requiring expression of only a single recombinant polypeptide chain. It is also a well-established intermediate format in recombinant antibody-engineering workflows.

The scFv-Fc antibodies were expressed, and their binding to hFLVCR1a was evaluated by ELISA in the collaborating laboratory. Binding specificity was subsequently assessed by western blotting using lysates from HEK293F cells transiently transfected with hFLVCR1a-GFP-6xHis in pEG BacMam. Cells transfected with the empty pEG BacMam vector served as a mock-transfected negative control. Detection was performed using an anti-human Fc-HRP secondary reagent, as described in Section 2.5.6.

The candidate clones evaluated included 339-B6, 339-B9, 339-C1, 339-D6, 339-F1, 340-C1, 341-F5, 344-C1, and 345-E9. A no-primary-antibody control was included in parallel.

2.4.2 Fab 339-F1 generation and format

Clone 339-F1 was selected from the validated hFLVCR1a-binding scFv-Fc clones described in Section 2.4.1 and reformatted as a monovalent Fab fragment. The Fab comprised the light chain (VL-CL) paired with the heavy-chain Fd fragment (VH-CH1), without the Fc domain and hinge region present in the original scFv-Fc format. The monovalent Fab format was chosen for subsequent complex-formation and structural studies because it minimizes avidity effects and reduces the additional conformational flexibility associated with bivalent, Fc-containing formats. Fab fragments are also widely used as compact binding modules and fiducial markers in structural studies of small membrane proteins [66].

Complex formation between purified 339-F1 Fab and hFLVCR1a was assessed by analytical size-exclusion chromatography using the Superose 6 Increase 5/150 GL column and the DDM/CHS-based buffer system described in Section 2.3.2: 0.026% DDM, 0.005% CHS, 50 mM HEPES, and 150 mM NaCl. The Fab and hFLVCR1a were initially analyzed separately to establish their individual elution profiles. They were then mixed at a molar ratio of 1:1.5 (antibody:hFLVCR1a) and injected immediately, with a pre-incubation period. Finally, complex formation was evaluated by comparing the chromatogram of the mixed sample with the individual reference runs. A leftward shift and increased amplitude of the hFLVCR1a peak, accompanied by a reduction in the free Fab peak, were interpreted as evidence of a stable Fab–antigen complex.

2.5 Binding and biophysical characterization methods

The methods in this section address the central question of the thesis, whether the transport state of FLVCR1a influences recognition by the viral FeLV-SU, and test the antibody panel. They are chosen to be complementary. MST (2.5.1) gives solution-phase affinities, and nDSF (2.5.2) is an orthogonal, label-free readout of ligand-induced stabilisation, which confirms ligand binding independently of MST. SEC-based complex formation (2.5.3) tests all binding pairs in the same detergent system and is the method used to screen the antibody panel. The magnetic pulldown (2.5.4) provides a qualitative bead-based check of the FeLV-SU–receptor interaction, with the naked-bead and heme-only controls. ELISA and western blot (2.5.5–2.5.6) are the primary screening steps that identify which antibody clones recognise hFLVCR1a, including whether they cross-react with the mouse orthologue.

2.5.1 Microscale thermophoresis (MST) (Data from Prof. Francesca Magnani)

Binding affinities were measured by microscale thermophoresis (MST) using a Monolith instrument (NanoTemper Technologies). MST monitors the directed movement of molecules along a microscopic temperature gradient generated by an infrared laser. Ligand binding can change a molecule's size, charge, or hydration shell, thereby altering its thermophoretic mobility. These changes are detected as differences in the normalized fluorescence (Fnorm, ‰) of a fluorescently labelled binding partner [67].

Human FLVCR1a (hFLVCR1a) was covalently labelled at surface-exposed primary amines using the Monolith Protein Labeling Kit RED-NHS 2nd Generation (NanoTemper Technologies). The labelled protein was used at a fixed concentration of 20 nM in all experiments. It was titrated against a 16-point, two-fold serial dilution series of the unlabelled binding partner, and each mixture was loaded into standard-treated capillaries. The Fnorm (normalized fluorescence, ‰) was plotted as a function of the log10 of the ligand concentration (M) and fitting the data to a single-site binding model gave a Kd.

MST was used to address two related questions. First, we investigated whether the FeLV-C SU RBD binds hFLVCR1a with different affinity in the presence or absence of its substrate. To do this, the RBD alone or a pre-mixed RBD–heme complex was titrated against labelled hFLVCR1a. Second, we tested whether hFLVCR1a directly binds physiologically relevant porphyrin substrates by titrating hemin and coproporphyrin I against labelled hFLVCR1a. For each experiment, the resulting binding curves, expressed as Fnorm as a function of ligand concentration, were fitted to a single-site binding model to determine the equilibrium dissociation constant (Kd).

2.5.2 Nano differential scanning fluorimetry (nDSF) (Data from Prof. Francesca Magnani)

The thermal stability of purified hFLVCR1a was assessed using nano differential scanning fluorimetry (nDSF) on a Prometheus instrument (NanoTemper Technologies). Unlike conventional dye-based differential scanning fluorimetry, nDSF is a label-free method that measures the intrinsic fluorescence of tryptophan and tyrosine residues at 330 and 350 nm during a linear temperature ramp. As thermal unfolding exposes previously buried aromatic residues to the solvent, the ratio between these two emission wavelengths changes. The midpoint of this transition is reported as the melting temperature (Tm).

Samples were loaded into standard capillaries and measured in the apo state or in the presence of a saturating concentration (100 μM) of hemin or coproporphyrin I. Ligand-induced thermal stabilization, indicated by an increase in Tm, was used as an orthogonal, activity-independent

measure of ligand binding. These measurements complemented the MST experiments described in Section 2.5.1.

2.5.3 Gel filtration chromatography / SEC-based complex formation assay (all binding experiments) (Data from Prof. Francesca Magnani)

Complex formation between purified binding partners was assessed by analytical size-exclusion chromatography (SEC) using a Superose 6 Increase 5/150 GL column (Cytiva). The column was equilibrated with a buffer containing 0.026% DDM, 0.005% CHS, 50 mM HEPES, and 150 mM NaCl. This buffer was consistent with the purification conditions described in Section 2.3.2 and helped maintain the membrane protein targets in stable detergent micelles throughout the experiment [44].

This assay was used for all binding experiments in this thesis, including the analysis of the sixteen anti-hFLVCR1a antibody clones described in Section 2.4.1: 339B6, 339B9, 339C1, 339C8, 339D6, 339F1, 339H8, 339H11, 340C1, 340D3, 340E7, 341A6, 341D4, 341F5, and 345E9.

For each pair of binding partners, the individual proteins were first injected separately to establish their reference elution profiles. The proteins were then mixed at a defined molar ratio, typically 1:1.5, and injected without an extended pre-incubation period. Complex formation was assessed qualitatively by comparing the chromatogram of the mixed sample with the two individual reference runs. Evidence of complex formation included a leftward shift and increased amplitude of the target protein peak, accompanied by a corresponding reduction in the free binding-partner peak. These changes are consistent with established approaches for assessing complex formation and oligomeric or aggregation states by SEC [45, 59].

2.5.4 Magnetic pulldown assay (hFLVCR1a and FeLV-C SU)

The direct interaction between hFLVCR1a and the FeLV-C SU RBD, and the potential influence of heme on this interaction, was further investigated using a bead-based magnetic pulldown assay. His-tagged SU was used as the bait. A 12 mg/mL stock solution, corresponding to 20 µM, was immobilized on Ni-NTA magnetic beads through its hexahistidine tag by passive capture. This procedure relied on the same Ni^{2+}-chelation principle used during IMAC purification [47].

To start with, a 25% bead slurry was placed on a magnetic rack and washed to remove the storage ethanol. The beads were then incubated with SU in binding buffer for 30 min at room temperature. Following incubation, the beads were magnetized, and the unbound material was removed. A

separate batch of unloaded, or "naked," beads was prepared in parallel using the same procedure but without adding SU. These beads served as a negative control for non-specific binding.

The bait-loaded and naked beads were transferred to a 96-well magnetic bead plate. hFLVCR1a was used as the prey protein. A 4 mg/mL stock solution was diluted to a working concentration of 10 μM and added to the appropriate wells in the presence or absence of heme. Each condition was analysed in duplicate, giving six experimental conditions:

1. SU-loaded beads with hFLVCR1a and heme
2. SU-loaded beads with hFLVCR1a alone
3. SU-loaded beads with heme alone, without hFLVCR1a
4. SU-loaded beads with buffer only
5. Naked beads with hFLVCR1a and heme
6. Naked beads with hFLVCR1a alone

The plates were incubated for 1 h at 4 °C before being placed on a magnetic rack. The supernatant was removed, and the beads were briefly washed with buffer to remove unbound material. Bound proteins were then eluted using buffer containing 500 mM imidazole.

The eluted material was analysed by SDS-PAGE and western blotting, as described in Section 2.3.3. Co-elution of hFLVCR1a with the SU bait was interpreted as evidence of a direct interaction, while comparison across the different conditions was used to assess whether this interaction was affected by heme.

2.5.5 ELISA screening (Data from Prof. Francesca Magnani)

Initial screening for anti-hFLVCR1a antibody clones generated through the phage display selection campaign (Section 2.4.1) was performed using an enzyme-linked immunosorbent assay (ELISA). The assay was carried out by the collaborating laboratory at TU Braunschweig (F. Bertoglio) as part of their standard high-throughput phage display workflow.

This screening pipeline is used to identify scFv or scFv-Fc clones that bind to the immobilized target antigen before they are reformatted and subjected to further validation [68].

2.5.6 SDS-PAGE and western blotting (anti-human Fc-HRP and GFP fluorescence detection) (Data from Prof. Francesca Magnani)

Antibody clones identified by ELISA (Section 2.5.5) were further evaluated for binding to hFLVCR1a using SDS-PAGE and western blotting, following the general procedures described in Section 2.3.3. HEK293F cells were transiently transfected with either the hFLVCR1a-GFP-6×His construct (Section 2.1.4), cloned into pEG BacMam, or the empty pEG BacMam vector as a mock-transfected negative control. Transfections were performed using 0.5 μg of vector per 10^6 cells. Sodium butyrate was added to a final concentration of 10 mM 8 h after transfection, and the cells were harvested 40 h later.

Cell pellets containing 2×10^6 cells were solubilized in 200 μL of solubilization buffer containing 0.5% DDM-CHS, 50 mM HEPES, 150 mM NaCl, and Roche protease inhibitor cocktail. The lysates were clarified by centrifugation at 18,000 × g for 20 min at 4 °C.

Mock-transfected and hFLVCR1a-expressing lysates were separated on 12% SDS-PAGE gels. After electrophoresis and transfer, the PVDF membrane was cut into strips so that each strip could be probed in parallel with a different candidate IgG-like antibody clone in the scFv-Fc format (Section 2.4.1). The membrane strips were blocked with milk and incubated with the primary antibodies for 1 h at room temperature. After washing, the strips were incubated for a further 1 h at room temperature with an HRP-conjugated anti-human Fc secondary antibody (#A0170, Merck). This detection strategy made use of the human Fc domain retained in the scFv-Fc antibody format. The strips were then washed and developed using chemiluminescence.

In parallel, GFP fluorescence was used as an antibody-independent control for expression of the hFLVCR1a-GFP-6×His construct. This approach took advantage of the well-established intrinsic fluorescence of GFP [69] and was analogous to fluorescence-based detection methods used to assess GFP-tagged membrane protein constructs [59]. A subset of validated clones—FBE339-C1, FBE339C8, FBE339D6, FBE339H11, FBE340C1, FBE341D4, and FBE339F1—was subsequently tested using the same protocol against lysates from HEK293F cells expressing human or mouse FLVCR1a-GFP-6×His, alongside mock-transfected lysates (Section 3.3). The samples were run in parallel on the same membrane to determine whether individual antibody clones cross-reacted with the mouse orthologue or were specific for human FLVCR1a.

3. Results

This chapter presents the experiments in the order in which the scientific question develops. It begins with the question that motivates the thesis, whether the transport substrate of FLVCR1a influences its role as a viral receptor. Sections 3.1 and 3.2 test this directly with purified human FLVCR1a: first whether it binds hemin and coproporphyrin I (3.1), and then whether heme alters its interaction with the FeLV-C SU (3.2). Sections 3.3 and 3.4 turn to the antibody tools, assessing the orthologue specificity of the bivalent scFv-Fc clones (3.3) and whether the monovalent Fab 339F1 retains binding to the receptor (3.4), since a conformation-specific binder is the main route towards a structure of FLVCR1a. The remaining sections cover the reagents that these studies depend on and that future structural work will need: the cognate feline FLVCR1a (3.5), the soluble FeLV-B SU RBD (3.6) and the FeLV-B receptor SLC20A1/PiT-1 (3.7). Several of these preparations did not succeed on the first attempt, and these outcomes are reported together with the changes of construct, host or detection strategy they led to, because they define which parts of the pipeline are established and which remain open. The interpretation of how these results fit together is deferred to Chapter 4.

3.1 Binding of porphyrins to hFLVCR1a (Data from Professor Francesca Magnani)

hFLVCR1a has been indicated as a heme exporter [2]. To characterize its substrate recognition, it was therefore first tested whether purified hFLVCR1a binds hemin, its putative substrate, and whether this binding depends on the central iron atom, by comparison with the iron-free porphyrin coproporphyrin I. Binding was measured by microscale thermophoresis (MST), and the effect of each ligand on protein stability was assessed by nano-differential scanning fluorimetry (nDSF).

3.1.1 Hemin binding to hFLVCR1a by MST

Binding affinities were measured by MST. The dissociation constant is derived from the MST dose-response curves based on the thermophoretic movement of a fluorescently labeled protein in a temperature gradient upon ligand binding [1].

Hemin (iron(III)-protoporphyrin IX, the ferric oxidized form of heme b) was titrated against 20 nM fluorescently labelled hFLVCR1a (Figure 3.1A). The corresponding binding curve displayed a clear sigmoidal, saturable dose-response, with Fnorm decaying from a saturated plateau corresponding to

approximately 900 ‰ at low hemin concentrations to approximately 830 ‰ at saturating hemin, over a range of ligand concentrations spanning approximately 10^{-8} to 10^{-3} M. A fit to a single-site binding model provided a dissociation constant of Kd = 23 ± 0.6 μM (mean ± SE of 2–3 repetitions of the assay; the curve in Figure 3.1A is a single representative titration), indicating that hFLVCR1a binds hemin with moderate affinity (Kd in the tens-of-micromolar range). This is consistent with other published data indicating hFLVCR1a as a heme exporter whose substrate-binding site must release its cargo to the extracellular acceptor hemopexin, which itself binds heme with sub-picomolar affinity, thereby imposing the directionality of export [2].

3.1.2 Coproporphyrin I binding to hFLVCR1a by MST

Coproporphyrin I is a non-metalloporphyrin and a dead-end byproduct of heme biosynthesis: once formed, it cannot be used by cells and is excreted. Lacking the central iron atom of hemin, coproporphyrin I was titrated against the same 20 nM fluorescently labelled hFLVCR1a preparation (Figure 3.1B). The binding curve showed a sigmoidal dose-response, with Fnorm falling from approximately 700–750 ‰ at low coproporphyrin I concentrations to near zero at saturation, once again over a concentration range of approximately 10^{-8} to 10^{-3} M. Fitting gave an apparent Kd = 1.8 ± 0.1 μM (SE of 2–3 repetitions of the assay; representative curve shown).

The fall of Fnorm to near zero, a change much larger than that observed with hemin, is an important observation. It indicates that coproporphyrin I most probably quenched the fluorescence of the labelled hFLVCR1a, so that the apparent binding is likely an artifact of the increasing coproporphyrin I concentration rather than genuine binding. The apparent Kd of 1.8 μM should therefore not be interpreted as an affinity. This would also explain the lack of an effect of coproporphyrin I in the nDSF experiments described below (Section 3.1.3).

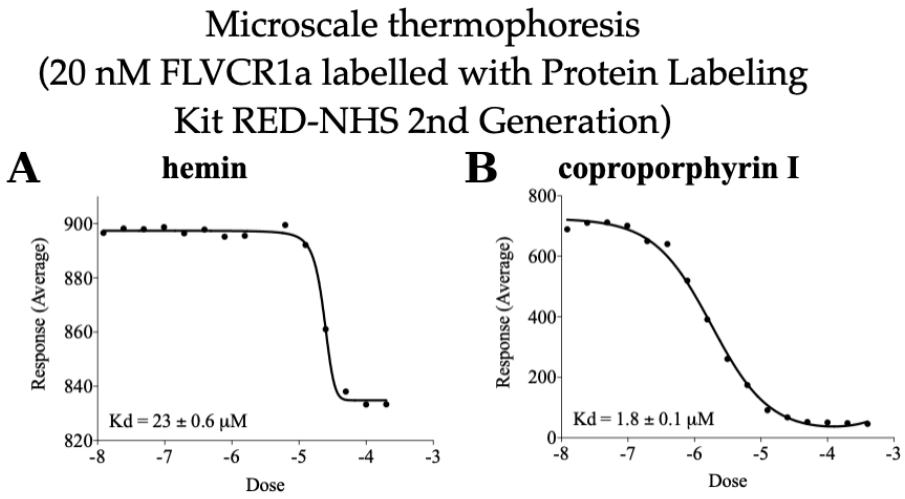


Figure 3.1. Binding of porphyrins to hFLVCR1a assessed by MST. (A) MST binding curve for hemin titrated against 20 nM hFLVCR1a labelled with Protein Labeling Kit RED-NHS 2nd Generation. Kd = 23 ± 0.6 µM. (B) MST curve for coproporphyrin I. Apparent Kd = 1.8 ± 0.1 µM; the decrease of Fnorm to near zero probably reflects quenching of the label fluorescence rather than binding (see text). Fnorm (‰) is plotted against $\log_{10}$ ligand concentration (M); solid line = single-site binding fit. Each plot shows one representative titration; Kd values are given as mean ± SE of 2–3 repetitions of the assay.

3.1.3 Thermal stability of hFLVCR1a in the apo state and in the presence of hemin and coproporphyrin I (nDSF)

To complement the MST affinity measurements and assess how porphyrin binding affects hFLVCR1a stability, nano-differential scanning fluorimetry (nDSF) was used. This technique monitors a protein's intrinsic tryptophan fluorescence as the temperature increases, with unfolding detected as a change in the fluorescence emission ratio (350/330 nm). Since nDSF does not require an external dye and is compatible with a broad range of buffer conditions, it is particularly well suited to detergent-solubilized membrane proteins [6,7]. The melting temperature (Tm) of hFLVCR1a was measured under three conditions: in the apo state without ligand, with 100 µM hemin, and with 100 µM coproporphyrin I.

Apo hFLVCR1a had a Tm of 53.8 ± 0.2°C (Table 3.1), establishing the baseline for the unliganded protein. Adding 100 µM hemin increased the Tm to 56.0 ± 0.0°C, corresponding to a thermal shift of ΔTm = +2.2°C relative to the apo state. By contrast, 100 µM coproporphyrin I produced a Tm of 53.75 ± 0.07°C, essentially unchanged from the apo state within experimental error (ΔTm ≈ 0°C). A

positive thermal shift is generally interpreted as evidence of ligand-induced stabilization, in which ligand binding increases the protein's thermodynamic stability by shifting the folding equilibrium toward the folded, ligand-bound state [8,9]. The +2.2°C shift therefore indicates that hemin binds to and stabilizes hFLVCR1a, whereas the absence of any shift with coproporphyrin I indicates that it likely does not bind to hFLVCR1a, in agreement with the fluorescence artifact suspected in the MST experiment (Section 3.1.2).

hFLVCR1a	Tm (°C)
apo	53.8 ± 0.2
100 µM hemin	56.0 ± 0.0
100 µM coproporphyrin I	53.75 ± 0.07

Table 3.1. Thermal stability of hFLVCR1a measured by nDSF. Melting temperatures (Tm) of hFLVCR1a in the apo state and in the presence of 100 µM hemin or 100 µM coproporphyrin I. Hemin produces a thermal shift of +2.2°C; coproporphyrin I produces no significant shift. Data received from Prof. Francesca Magnani.

3.2 Characterization of the hFLVCR1a–FeLV C SU interaction

FLVCR1a is both the cell-surface receptor of feline leukemia virus subgroup C (FeLV-C) and a heme exporter, which raises the question of whether its transport substrate influences its role as a viral receptor. This section therefore examines the interaction between hFLVCR1a and the surface unit (SU) of the FeLV envelope glycoprotein in vitro, and whether heme modulates it, using three approaches: microscale thermophoresis (MST) to measure binding affinity (Section 3.2.1), size-exclusion chromatography (SEC) to assess complex formation (Section 3.2.2), and a magnetic pulldown assay as an independent validation (Section 3.2.3). Unless stated otherwise, heme was used at a concentration of 40 µM.

3.2.1 Heme dependence of FeLV-C SU binding to hFLVCR1a (Data from Professor Francesca Magnani)

FLVCR1a was first identified as the cell-surface receptor for feline leukemia virus subgroup C (FeLV-C), mediating viral entry and contributing to the development of pure red cell aplasia in infected cats [15,16]. Independently, FLVCR1a was found to function as a heme exporter essential for erythroid differentiation, raising the possibility that its physiological substrate, heme, might influence its role as a viral receptor [3, 17]. Viral recognition of FLVCR1a is determined by a short variable region (vr1) within the SU subunit of the envelope glycoprotein [4]. However, whether heme occupancy of FLVCR1a modulates this interaction had not yet been directly investigated.

To investigate this possibility, SU binding to hFLVCR1a was measured by microscale thermophoresis (MST) [1] in the presence and absence of 40 μM heme. hFLVCR1a was fluorescently labeled using the Protein Labeling Kit RED-NHS 2nd Generation and maintained at a constant concentration of 20 nM, while SU was titrated over a range of approximately 1×10^{-10} to 1×10^{-5} M. In the absence of heme, SU bound hFLVCR1a with a dissociation constant (Kd) of 412 nM. The addition of 40 μM heme increased this affinity approximately sixfold, resulting in a Kd of 66.7 nM (Figure 3.2). Under both conditions, the normalized fluorescence (Fnorm) traces displayed clear, sigmoidal, and saturable binding curves, consistent with a specific single-site interaction.

These findings suggest that heme is not essential for FeLV-C SU–FLVCR1a binding but instead acts as a positive modulator, substantially increasing the affinity of the interaction. This interpretation is consistent with the broader model that FeLV-C envelope recognition depends on the conformational state of its multispan transmembrane receptor [4]. Considering the conventional solute carrier alternating-access mechanism of cargo translocation, it can be speculated, at this stage, that heme binding stabilizes a receptor conformation that is particularly favorable for high-affinity engagement by the viral spike. This would provide a possible, but still speculative, mechanistic link between substrate transport dynamics and viral receptor function.

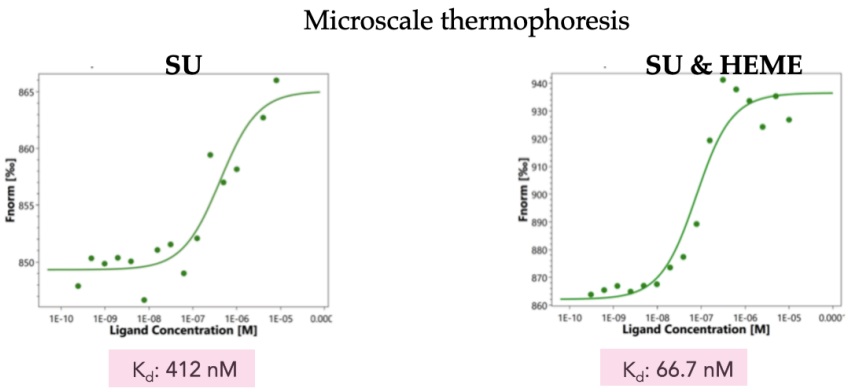


Figure 3.2. Heme increases the binding affinity of FeLV-C SU for hFLVCR1a. Microscale thermophoresis (MST) binding curves, based on the method described by Jerabek-Willemsen et al. (2011), show the interaction between the retroviral surface unit (SU) and hFLVCR1a in the absence (left) or presence (right) of 40 μM heme. hFLVCR1a (20 nM) was fluorescently labeled with the Protein Labeling Kit RED-NHS 2nd Generation, and unlabeled SU was titrated from approximately 1×10^{-10} to 1×10^{-5} M. Normalized fluorescence (Fnorm, ‰) is plotted against SU concentration, and the data were fitted to a single-site binding model to determine the dissociation constant (Kd). In the absence of heme, SU bound hFLVCR1a with a Kd of 412 nM. The addition of 40 μM heme increased the binding affinity approximately sixfold, resulting in a Kd of 66.7 nM. Each point represents an individual measurement, and the solid line indicates the fitted binding curve.

3.2.2 Complex formation of FeLV-C SU and hFLVCR1a assessed by size-exclusion chromatography (SEC)

To analyze whether heme promotes formation of a stable complex between FeLV-C SU and hFLVCR1a, size-exclusion chromatography (SEC) runs were performed on the same day under identical conditions (50 mM HEPES pH 7.4, 150 mM NaCl, 0.026% DDM/CHS buffer): SU alone, hFLVCR1a alone, hFLVCR1a incubated with SU, and hFLVCR1a incubated with SU in the presence of 40 μM heme [18-20]. Apparent molecular masses were estimated from the calibration of the column (Superose 6 Increase 5/150 GL).

SU alone eluted as a single, dominant, symmetric peak at 2.17 ml (apparent MW of 45,000 Da), accounting for 84.7% of the total peak area. Only minor void-volume (6.2%) and late-eluting (9.1%) species were detected, indicating that the preparation was largely monodisperse (Figure 3.3, red).

hFLVCR1a alone produced one dominant peak at 2.02 ml (apparent MW of 64,400 Da), representing 80.9% of the total area, together with minor void-volume (15.3%) and late-eluting (3.8%) species. The receptor eluted earlier than SU alone (2.02 ml versus 2.17 ml), consistent with the larger hydrodynamic size expected for a detergent-solubilized membrane protein–micelle particle compared with a soluble viral glycoprotein (Figure 3.3, blue).

In the absence of heme, the hFLVCR1a + SU mixture resolved into two similarly sized peaks at 1.98 ml (62.9%) and 2.16 ml (33.2%). These volumes closely matched those of hFLVCR1a alone (2.02 ml) and SU alone (2.17 ml), respectively. This profile indicates that the two proteins largely remained separate and eluted from the column as uncomplexed species (Figure 3.3, purple).

When 40 μM heme was included, the hFLVCR1a + SU mixture instead produced a single sharp, dominant peak at 2.00 ml, accounting for 70.2% of the total area. This peak was essentially coincident with the hFLVCR1a-alone peak, and no distinct shoulder was observed near the free-SU position at 2.17 ml. Minor peaks were detected at 1.15 ml (11.9%) and 3.83 ml (17.9%) (Figure 3.3, green).

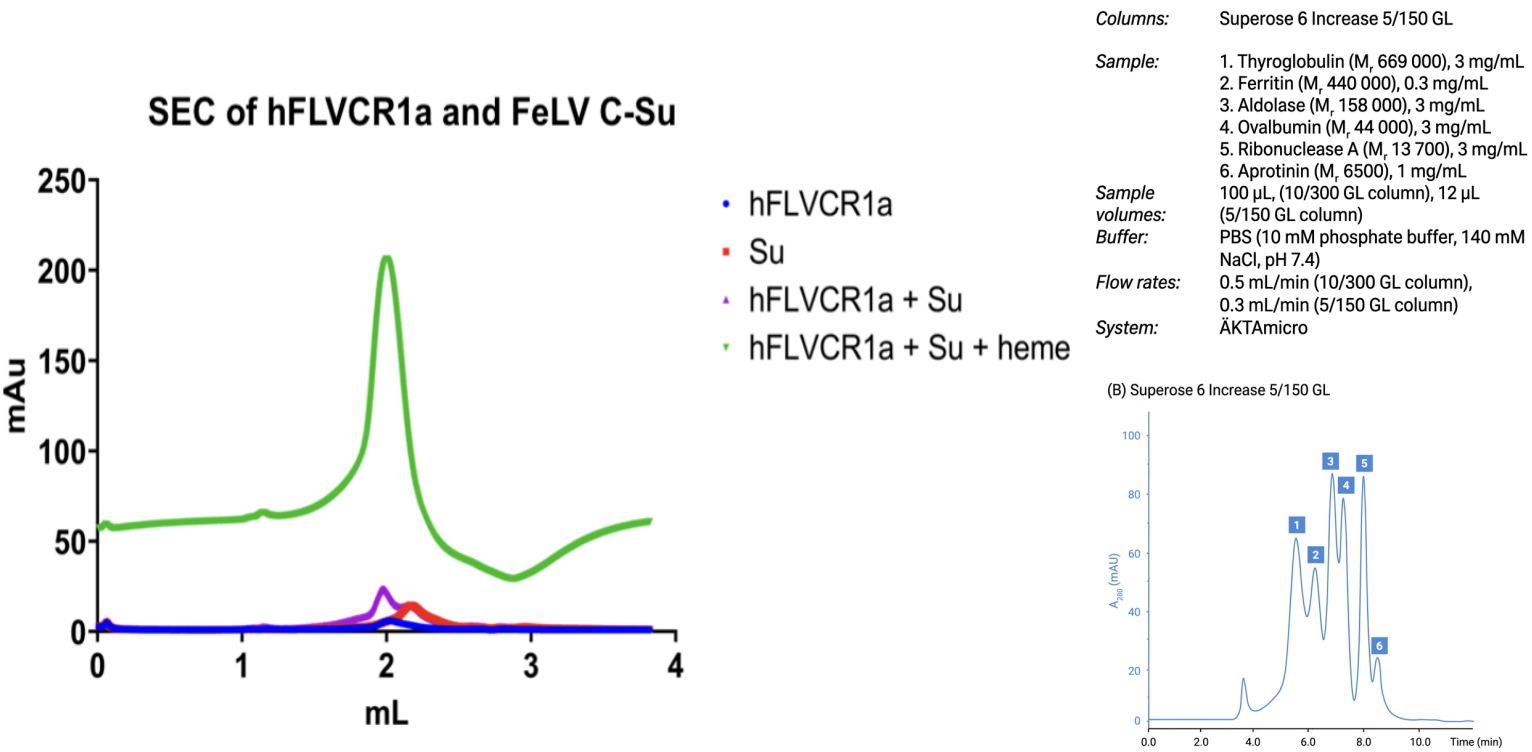


Figure 3.3. Heme promotes co-elution of FeLV-C SU with hFLVCR1a by SEC. (Red) SU alone. (Blue) hFLVCR1a alone. (Purple) hFLVCR1a + SU without heme. (Green) hFLVCR1a + SU in the presence of 40 µM heme. All runs were performed on Superose 6 Increase 5/150 GL in 50 mM HEPES pH 7.4, 150 mM NaCl, 0.026% DDM/CHS buffer, with UV absorbance (mAU) plotted against elution volume (ml). Free SU (red) eluted later (2.17 ml) than hFLVCR1a (blue) (2.02 ml). The mixture (purple) resolved into two peaks corresponding closely to the individual elution volumes of the two proteins. By contrast, (green) showed a single peak at the hFLVCR1a elution position, with no shoulder corresponding to free SU. On the right, the figure displays a high-resolution SEC of six standard proteins showing relative peak resolution on the 5/150 GL column.

Given the modest affinity of heme for hFLVCR1a (Kd = 23 µM; Figure 3.1A), in order to improve the SU–hFLVCR1a complex homogeneity, a second set of SEC runs was performed using a modified buffer in which heme (40 µM) was present throughout the run, rather than being added only during the incubation. Fractions were collected over an extended elution range and analyzed for absorbance at 414 nm (Figures 3.4 and 3.5):

– hFLVCR1a + heme alone, receptor-only control (Figure 3.4, blue). In the presence of heme, two major species were detected at 2.24 ml (40.5%) and 4.52 ml (53.9%), together with a minor peak at 2.70 ml (5.6%).

– SU + heme alone (Figure 3.4, red). Under the same buffer conditions, SU produced a major peak at 2.05 ml (65.5%), a minor peak at 2.54 ml (7.3%), and a broader, later-eluting peak at 3.42 ml (27.2%).

– hFLVCR1a + SU + heme, independent repeat (Figure 3.4, green). The complex sample produced a major peak at 2.09 ml (49.3%), a minor peak at 2.53 ml (4.2%), and a substantial later-eluting peak at 4.62 ml (46.5%).

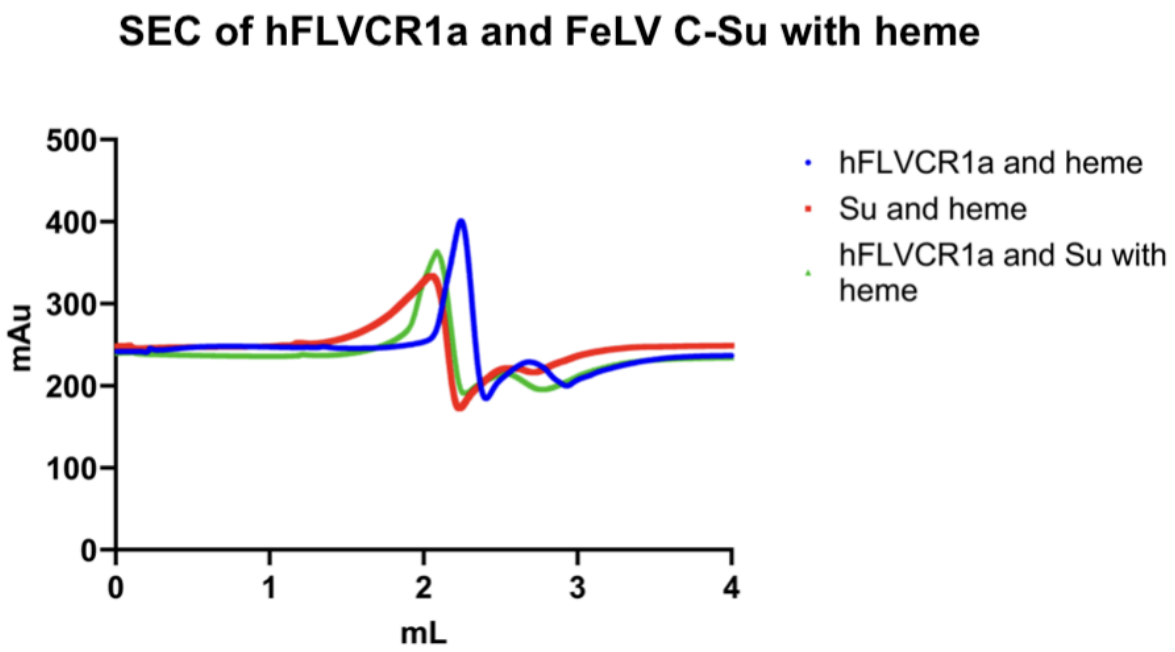


Figure 3.4. SEC of hFLVCR1a and heme, FeLV-C SU and heme, and their complex with heme in heme-containing running buffer (50 mM HEPES pH 7.4, 150 mM NaCl, 0.026% DDM/CHS, 40µM heme buffer). (Blue) hFLVCR1a and heme alone. (Red) SU and heme alone. (Green) hFLVCR1a + SU with heme. In contrast to Figure 3.3, where heme was included only during sample incubation, heme (40 µM) was present throughout the running buffer for all three runs. Fractions were collected over an extended elution range, and UV absorbance (mAU) was plotted against elution volume (ml). The peak positions and relative areas are reported in the main text. Column and calibration as in Figure 3.3 (Superose 6 Increase 5/150 GL in 50 mM HEPES pH 7.4, 150 mM NaCl, 0.026% DDM/CHS, 40µM heme buffer).

Under these heme-containing running conditions, the main peak in the complex sample (2.09 ml) was closer to the SU-alone peak (2.05 ml) than to the hFLVCR1a-alone peak (2.24 ml). This differs from the earlier dataset shown in Figure 3.3, in which the complex peak coincided more closely with the hFLVCR1a-alone peak. All three samples (hFLVCR1a alone, SU alone, and the complex) displayed a substantial, broader peak in the 3.4–4.6 ml range. The late peak in the complex sample

(4.62 ml, 46.5%) was closer to that of hFLVCR1a alone (4.52 ml, 53.9%) than to the corresponding SU peak (3.42 ml, 27.2%). Because a peak of comparable relative abundance appeared at a similar late elution position in all three samples, it cannot be confidently attributed to complex formation. Instead, it may reflect a feature of the heme-supplemented running buffer (e.g., formation of reactive oxygen species and protein degradation/aggregation, or protein degradation/unfolding caused by heme peroxidase activity). Accordingly, these results should be interpreted more cautiously than the earlier SEC dataset. On their own, they provide less direct evidence for heme-dependent complex formation than the results shown in Figure 3.3.

3.2.3 Validation of the interaction by magnetic pulldown assay

To validate the FeLV-C SU–hFLVCR1a interaction independently of the SEC (Section 3.2.2) results, a magnetic bead pulldown assay was performed. Pulldown assays are widely used in vitro to test predicted protein–protein interactions. In this approach, a tagged bait protein is immobilized on a solid support and used to capture a potential prey protein, which is then eluted and analyzed [21].

In this experiment, recombinant His-tagged SU served as the bait and was captured using Ni-NTA-functionalized magnetic beads. This represents a standard immobilized metal affinity chromatography (IMAC)-based method for isolating polyhistidine-tagged proteins and detecting co-purifying interaction partners. Tagged hFLVCR1a was used as the potential prey, and the assay was performed both in the absence and presence of 40 μM heme. For each condition, the unbound flow-through (FT) and bead-bound eluate (ELU) fractions were collected. The experiment was performed in technical duplicate as a quality-control measure.

Samples were separated by SDS-PAGE and analyzed by western blotting. In the first blot, an anti-histidine (anti-His) antibody was used to detect the His-tagged SU bait in each fraction (Figure 3.5). This served two purposes: first, to confirm that the antibody specifically recognized His-tagged SU and did not cross-react with untagged hFLVCR1a; and second, to verify that SU was efficiently captured by and recovered from the magnetic beads before assessing hFLVCR1a co-purification with a different antibody in a subsequent blot. The lanes were loaded in the following order: SU alone as a positive control, hFLVCR1a alone as a negative control for antibody specificity, a molecular-weight marker, flow-through and eluate fractions from the heme-free pulldown in

duplicate, a second molecular-weight marker, and flow-through and eluate fractions from the heme-supplemented pulldown in duplicate (Figure 3.5).

The SU-alone control produced a strong signal, confirming that the anti-His antibody recognized His-tagged SU. In contrast, the hFLVCR1a-alone control showed no corresponding signal, confirming that the antibody did not cross-react with untagged hFLVCR1a. Under heme-free conditions, no signal was detected in the flow-through fractions, whereas a clear and reproducible band was observed in both eluate replicates. This indicates that SU-His was efficiently captured by the beads and recovered in the eluate. Under heme-supplemented conditions (40 μM heme), bands were also detected in both eluate replicates.

Altogether, this blot confirms that the pulldown procedure performed as expected: the His-tagged SU bait was specifically detected and efficiently captured and eluted from the beads. These results establish the validity of the assay for assessing the co-purification of hFLVCR1a in the subsequent blot.

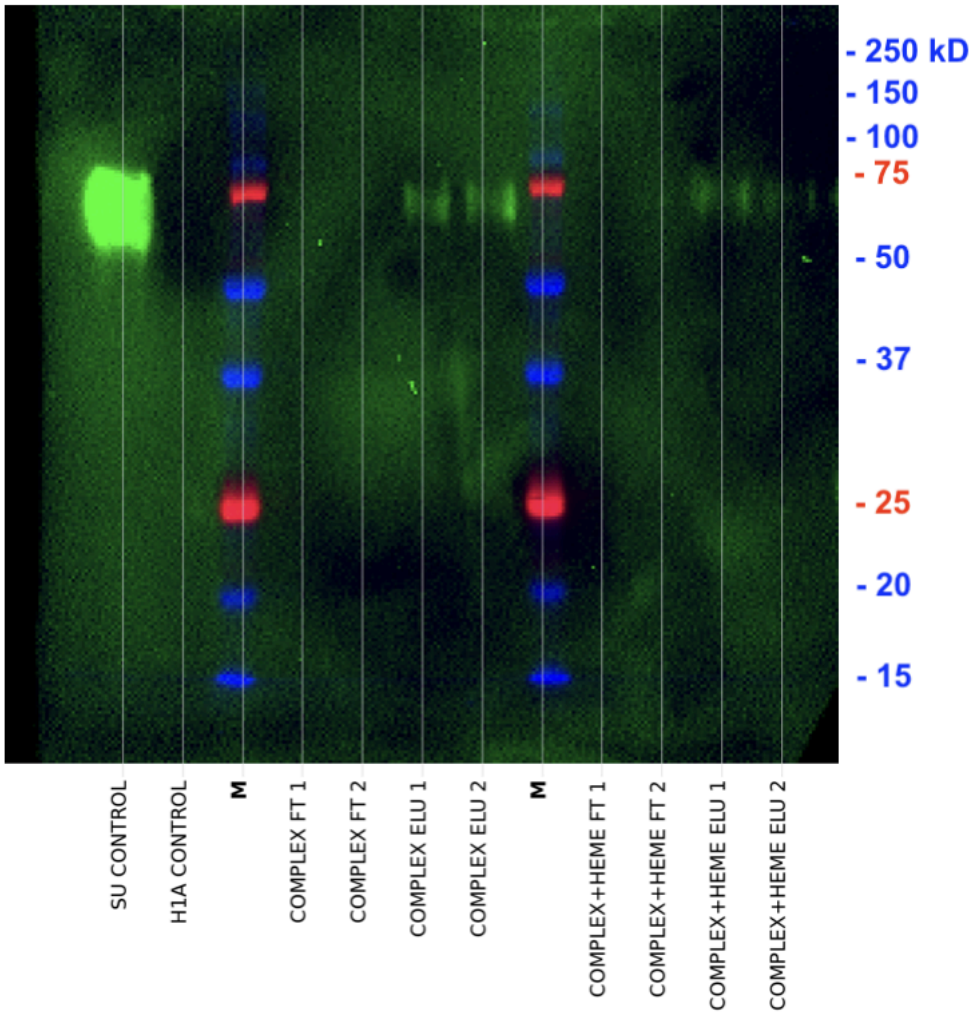


Figure 3.5. Detection of His-tagged FeLV-C SU across the magnetic pulldown fractions by anti-His western blot. Multichannel fluorescence western blot image showing the green anti-His antibody signal, with the red and blue bands corresponding to the fluorescent molecular-weight marker lanes. From left to right, the lanes contain SU alone (positive control), hFLVCR1a alone (negative control), a molecular-weight marker (M), flow-through fractions from the heme-free complex pulldown (FT 1 and FT 2), eluate fractions from the heme-free pulldown (ELU 1 and ELU 2), a second molecular-weight marker (M), flow-through fractions from the heme-supplemented (40 μM heme) complex pulldown (FT 1 and FT 2), and eluate fractions from the heme-supplemented pulldown (ELU 1 and ELU 2).

To assess directly whether hFLVCR1a co-purified with the His-tagged SU bait, the same pulldown fractions were analyzed by western blotting with an anti-FLAG antibody, which specifically recognizes FLAG-tagged hFLVCR1a (Figure 3.6). This blot provided the primary readout for determining whether hFLVCR1a physically associates with SU and whether the interaction is influenced by heme.

The hFLVCR1a-alone positive-control lane showed a strong, specific signal, confirming that the anti-FLAG antibody detected FLAG-tagged hFLVCR1a at the expected molecular weight (Figure 3.6, lane 1). Under heme-free conditions, hFLVCR1a was detected in both flow-through replicates (FT1 and FT2), indicating that some of the protein remained unbound in solution and was not retained by the SU. Moreover, no detectable anti-FLAG signal was observed in either eluate replicate (ELU1 or ELU2). This indicates that hFLVCR1a did not co-purify with SU-His in the absence of heme (Figure 3.6, lanes 3–6).

Under heme-supplemented conditions (40 μM heme), hFLVCR1a was again observed not detectably retained by the His-tagged SU bait under these conditions (Figure 3.6, lanes 8–11).

Therefore, under the conditions tested, the pulldown assay provided no detectable evidence that hFLVCR1a co-purified with FeLV-C SU. These results do not support the conclusion that the assay captured a stable, physically detectable interaction between FeLV-C SU and hFLVCR1a. Further optimization of the pulldown conditions, together with complementary experimental approaches, may be necessary to determine whether the interaction occurs and whether it is modulated by heme.

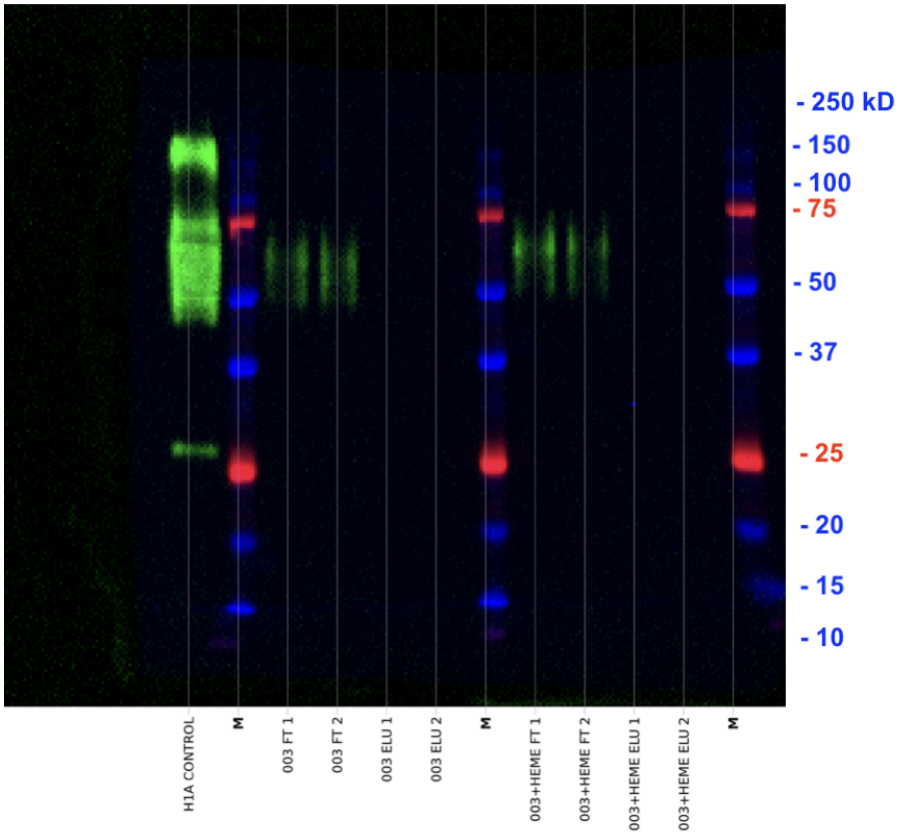


Figure 3.6. Detection of FLAG-tagged hFLVCR1a by anti-FLAG western blot across magnetic pulldown fractions. Multichannel fluorescence western blot showing the anti-FLAG signal for FLAG-tagged hFLVCR1a in green. The red and blue bands correspond to the fluorescent molecular-weight marker. From left to right, the lanes contain hFLVCR1a alone (positive control), a molecular-weight marker (M), flow-through replicates from the heme-free pulldown (003 FT1 and FT2), eluate replicates from the heme-free pulldown (003 ELU1 and ELU2), a second molecular-weight marker (M), flow-through replicates from the heme-supplemented (40 μM heme) pulldown (FT1 and FT2), eluate replicates from the heme-supplemented pulldown (003 ELU1 and ELU2), and a final molecular-weight marker (M). hFLVCR1a was detected in the flow-through fractions under both conditions but was not detected in either eluate by western blotting with the anti-FLAG antibody. Therefore, no detectable co-purification of hFLVCR1a with His-tagged SU was observed under the conditions tested, and this assay alone does not establish whether the interaction is heme-dependent.

To evaluate whether FLAG-tagged hFLVCR1a was recovered after the magnetic pulldown, the samples were analyzed by western blotting with an anti-FLAG antibody. The hFLVCR1a control produced a detectable anti-FLAG signal, confirming that the FLAG-tagged protein was present and could be detected under the assay conditions. By contrast, no detectable anti-FLAG signal corresponding to hFLVCR1a was observed in either of the duplicate complex eluates prepared

without heme. Similarly, no FLAG signal was detected in the eluate fractions from the heme-supplemented (40 µM heme) samples. The duplicate eluates therefore consistently lacked a detectable hFLVCR1a signal under both conditions. Anti-FLAG-reactive material was detected in the flow-through fractions, confirming that FLAG-tagged hFLVCR1a was present in the material that passed through the pulldown procedure. However, its absence from the corresponding eluates indicates that hFLVCR1a was not detectably recovered in the bead-bound fraction under the conditions tested (Figure 3.7). Conclusively, the anti-FLAG western blot showed no detectable recovery of hFLVCR1a in the complex eluates, either in the absence or presence of heme. Therefore, based on anti-FLAG detection alone, this experiment did not provide direct evidence that FLAG-tagged hFLVCR1a was recovered in the pulldown eluate.

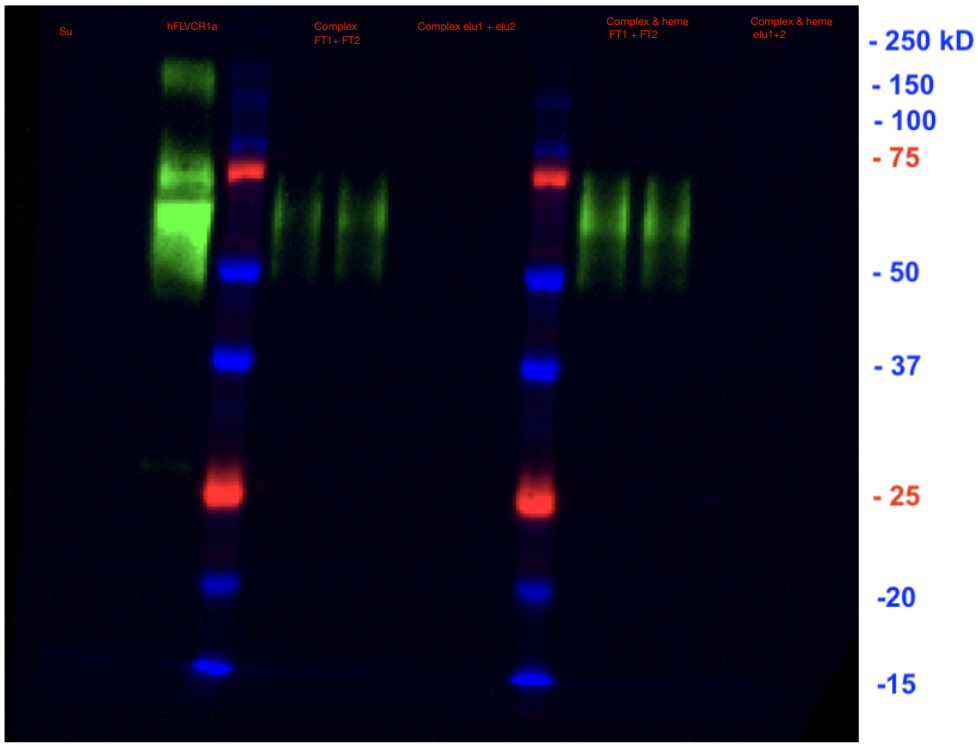


Figure 3.7. Western blot analysis of hFLVCR1a following magnetic pulldown in the absence and presence of heme. Samples from the magnetic pulldown assay were analyzed by western blotting with an anti-FLAG antibody to detect FLAG-tagged hFLVCR1a. From left to right, SU and hFLVCR1a were included as controls, and molecular-weight markers (M) were loaded at the indicated positions. Complex flow-through (FT) and eluate (ELU) fractions were analyzed in duplicate under both heme-free and heme-supplemented (40 µM heme) conditions. A FLAG-positive signal was detected in the hFLVCR1a control and in the flow-through fractions, whereas no detectable FLAG signal was observed in the complex eluates under either condition.

3.3 Cross-reactivity of bivalent scFv-Fc monoclonal antibodies with murine FLVCR1a (Data from Professor Francesca Magnani)

The preliminary characterisation of the FBE monoclonal antibody panel by western blotting, analytical SEC and epitope classification is presented in Section 1.6 (Figures 1.22 and 1.23, Table 1.1). This section describes the assessment of orthologue specificity of selected clones.

To assess orthologue specificity, a subset of clones was tested for recognition of murine FLVCR1a alongside human FLVCR1a. The aim was to determine whether antibodies raised against human FLVCR1a selectively recognised the human protein or also cross-reacted with its murine orthologue. Human and murine FLVCR1a were expressed and analysed in parallel for each antibody, and mock-transfected samples were included as negative controls to assess background signal and to determine whether the observed bands represented specific FLVCR1a recognition.

The antibodies tested were FBE339-C1, FBE339C8, FBE339D6, FBE339H11, FBE340C1, FBE341D4 and FBE339F1 (Figure 3.8). The clones showed distinct recognition profiles. FBE339C8 produced a detectable signal in the human FLVCR1a sample but not in the murine FLVCR1a sample, indicating preferential recognition of the human orthologue under the conditions tested. In contrast, FBE339D6 and FBE339H11 produced no detectable signal in either the human or murine samples, providing no evidence of FLVCR1a recognition in this assay. FBE340C1 and FBE341D4 detected both human and murine FLVCR1a, which was interpreted as cross-reactivity. The other antibodies displayed varying levels of recognition of human and/or murine FLVCR1a, indicating differences in their orthologue specificity.

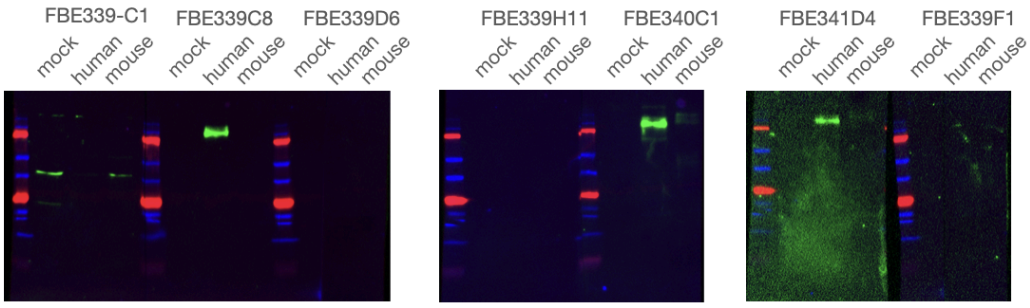


Figure 3.8. Assessment of monoclonal antibody recognition of human and murine FLVCR1a. Selected monoclonal antibodies were tested against both human and murine FLVCR1a to assess their orthologue specificity and potential cross-reactivity. For each antibody, mock-transfected samples and samples expressing human or murine FLVCR1a were analysed in parallel. The antibodies tested were FBE339-C1, FBE339C8, FBE339D6, FBE339H11, FBE340C1, FBE341D4 and FBE339F1.

FLVCR1a is a cell-surface membrane protein predicted to contain 12 transmembrane segments and six extracellular loops. Previous studies have shown that extracellular regions of FLVCR1 contribute to receptor function, with extracellular loops 1 and 6 being particularly important for FeLV-C receptor activity. Sequence differences between orthologues may therefore influence antibody binding, depending on the location and sequence of the recognised epitope [31].

3.4 Characterization of the hFLVCR1a–Fab 339F1 interaction

Among the antibody clones characterized in Section 3.3, Fab 339F1 formed a complex with native, detergent-solubilized hFLVCR1a by SEC but gave no western blot signal, making it a candidate conformational binder. Antibodies that recognize the folded receptor are the most useful for structural work. hFLVCR1a is a small (~60 kDa) membrane protein with little mass outside the detergent micelle, which makes particle alignment in cryo-EM difficult. A bound antibody fragment adds mass and recognizable features, and it can stabilize a single receptor conformation. Fab fragments are preferred over full IgG-like antibodies for this purpose because they are compact, less flexible and monovalent, so they do not cross-link receptors [35–37]. This section therefore tests whether the Fab derived from 339F1 retains binding to hFLVCR1a, both without heme and with heme present, since heme binds hFLVCR1a and increases its affinity for FeLV-C SU (Sections 3.1 and 3.2.1).

3.4.1 Complex formation assessed by gel filtration chromatography (SEC)

Having established that the full-length bivalent scFv-Fc mAb 339F1 binds hFLVCR1a (Sections 3.3), the corresponding antigen-binding fragment (Fab) was generated as a smaller, monovalent binding unit for structural studies, including cryo-EM. Fab fragments are widely used in cryo-EM as fiducial markers and conformational chaperones for membrane proteins because of their compact size, lower flexibility compared with bivalent scFv-Fc molecule, and lack of bivalent avidity effects [35, 36, 37]. However, the change of antibody format from IgG to Fab can negatively affect its affinity for the epitope. The interaction between Fab 339F1 and hFLVCR1a was assessed using analytical SEC runs. The experiment included individual protein controls, complex formation in the absence of heme, and corresponding runs performed with heme present throughout the running buffer (Figure 3.9).

- hFLVCR1a alone, no heme (Figure 3.9A (blue)). hFLVCR1a eluted as a dominant peak at 1.994 ml, representing 77.1% of the total area, together with a void-volume peak (19.3%) and a minor late-eluting species (3.6%). Importantly, hFLVCR1a eluted substantially earlier than Fab 339F1, at 1.994 ml compared with 2.480 ml. This difference is consistent with the larger hydrodynamic radius of the receptor–DDM/CHS micelle particle relative to the soluble Fab fragment of approximately 50 kDa [18, 19]. The clear separation between the two elution positions was important for interpreting the complex sample.

- Fab 339F1 alone, no heme (Figure 3.9A (orange)). Fab 339F1 eluted as a single, sharp, highly monodisperse peak at 2.480 ml, accounting for 87.2% of the total peak area. Only a minor void-volume peak (7.6%) and a small late-eluting species (5.2%) were observed, confirming that the Fab preparation was homogeneous and well-behaved.

- hFLVCR1a + Fab 339F1, no heme (Figure 3.9A (pink)). When hFLVCR1a and Fab 339F1 were co-incubated and analyzed in the absence of heme, the chromatogram resolved into two peaks of similar area at 2.003 ml (46.7%) and 2.496 ml (47.2%). These positions closely matched those of hFLVCR1a alone (1.994 ml) and Fab 339F1 alone (2.480 ml), respectively. No earlier-eluting species consistent with formation of an hFLVCR1a–Fab complex was detected. This profile is therefore most consistent with the two proteins eluting independently as largely uncomplexed species, indicating that stable complex formation was not detectable by SEC under heme-free conditions.

- hFLVCR1a + heme, receptor control (Figure 3.9B (blue)). When heme was present throughout the running buffer, hFLVCR1a produced a dominant peak at 2.088 ml (57.8%), together with additional species at 1.189 ml (12.1%) and a broad late-eluting peak at 3.827 ml (30.1%). As observed previously (Section 3.2.2), the heme-containing buffer generated a broad late-eluting species that appeared under all conditions tested with this buffer and was not specific to a particular protein species.

- Fab 339F1 + heme, Fab control (Figure 3.9B (orange)). Fab 339F1 displayed a markedly different profile when analyzed in heme-containing buffer. Instead of the sharp peak observed under standard conditions (panel B), three broad peaks were detected at 2.626 ml (22.8%), 3.338 ml (36.1%), and 3.650 ml (41.1%). The overall absorbance was also substantially lower than that observed for Fab alone in standard buffer. This shifted and broadened profile indicates that the heme-containing

buffer significantly perturbed the chromatographic behavior of Fab 339F1, making direct interpretation of the corresponding complex run more difficult.

- hFLVCR1a + Fab 339F1 + heme, complex sample (Figure 3.9B (pink)). The complex sample analyzed in heme-containing buffer produced a dominant peak at 2.019 ml (45.4%), a minor peak at 2.438 ml (2.3%), and a large late-eluting peak at 4.707 ml (52.3%). The main peak at 2.019 ml was close to, but not clearly earlier than, the hFLVCR1a + heme control peak at 2.088 ml (Figure 3.9B (blue)). The large late-eluting peak at 4.707 ml was also substantially shifted relative to the Fab + heme control peaks, which occurred between 2.6 and 3.7 ml.

Because Fab 339F1 displayed markedly abnormal chromatographic behavior in the heme-containing buffer, complex formation cannot be interpreted unambiguously from this run. In addition, no clearly resolved earlier-eluting peak was observed. Such a peak would be expected to elute earlier than hFLVCR1a alone, at approximately 1.994 ml, for an hFLVCR1a–Fab complex with a combined mass of roughly 210 kDa. Therefore, this run does not provide positive evidence for complex formation under heme-containing conditions. Under the conditions tested, analytical SEC did not detect stable complex formation between Fab 339F1 and hFLVCR1a in either the presence or absence of heme. Interpretation of the heme-containing runs was further complicated by the substantial effect of the buffer on the Fab elution profile.

Several factors may explain the difference between the Fab results and those obtained with the full-length bivalent scFv-Fc mAb 339F1 (Section 3.3). Unlike the full IgG, the Fab is monovalent and lacks the bivalent avidity effect that can enhance apparent binding strength [38]. In addition, as mentioned, conversion from the IgG to the Fab format may have reduced the affinity below the level required for stable complex detection by SEC. Analytical SEC often requires relatively high-affinity interactions, potentially in the low-nanomolar range, to maintain complexes during the time course of a chromatographic run [39]. Further affinity measurements, such as MST or BLI, will therefore be necessary to determine whether Fab 339F1 retains binding to hFLVCR1a and, if so, to quantify its affinity.

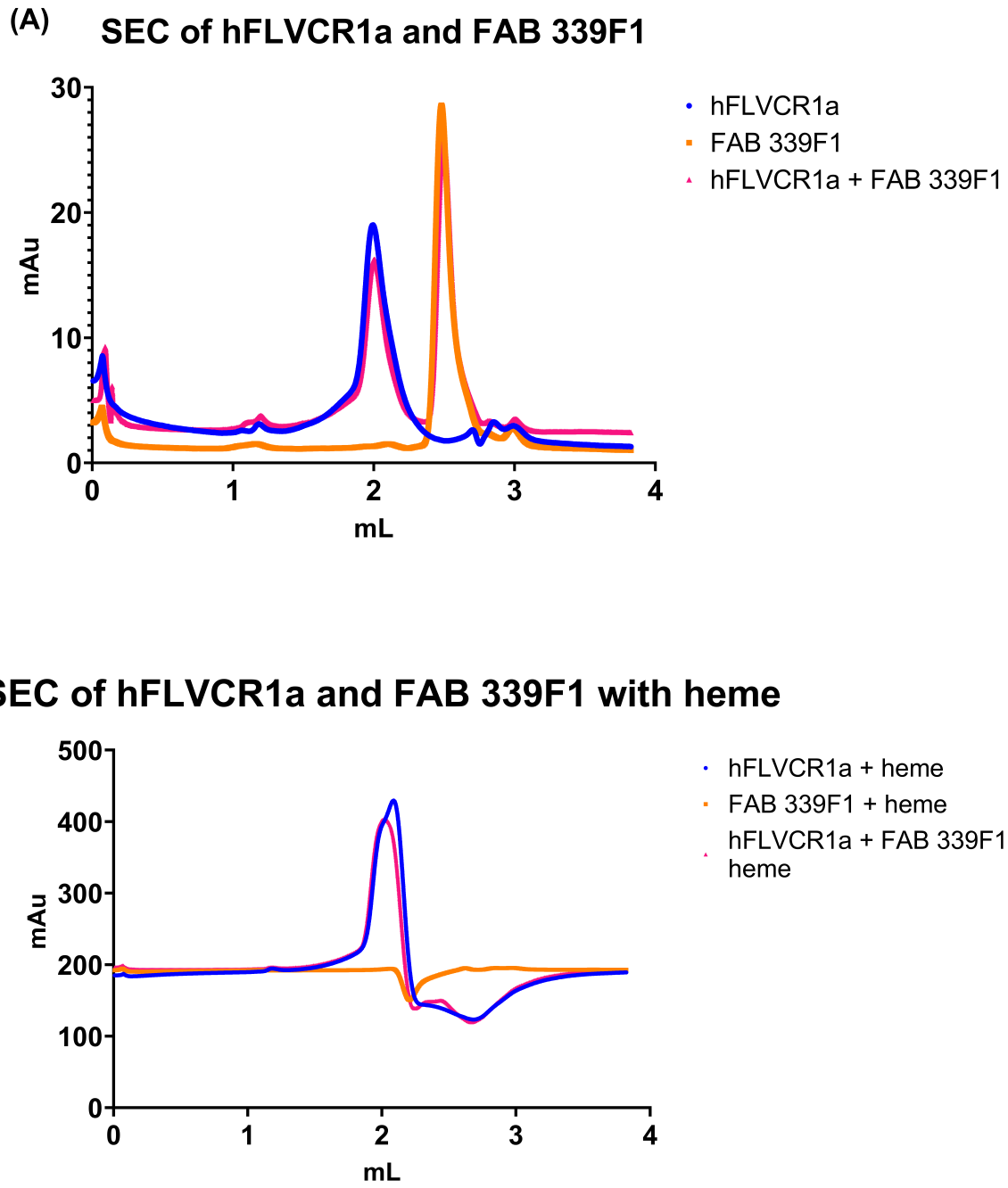


Figure 3.9. Analytical SEC characterization of the hFLVCR1a–Fab 339F1 interaction in the presence and absence of heme. (A) (blue) hFLVCR1a alone in standard buffer, (orange) Fab 339F1 alone in standard buffer, (pink) hFLVCR1a + Fab 339F1 complex in the absence of heme in standard buffer. (B) (blue) hFLVCR1a + heme receptor control with standard buffer and heme, (orange) Fab 339F1 + heme Fab control with standard buffer and heme, (pink) hFLVCR1a + Fab 339F1 complex with standard buffer and heme. All runs were performed in 50 mM HEPES pH 7.4, 150 mM NaCl, 0.026% DDM/CHS buffer, with heme included throughout the running buffer for part B. UV absorbance (mAU) is plotted against elution volume (ml). Peak positions and relative areas are summarized in the embedded peak tables.

3.5 Expression and purification of feline FLVCR1a

All binding experiments in Sections 3.1–3.4 were performed with hFLVCR1a. FeLV-C, however, is a feline virus, and fFLVCR1a is the receptor it uses in its natural host. The two orthologues share 85% sequence identity, and the differences between them, particularly in extracellular loops 1 and 6, which are important for FeLV-C receptor function [31], could influence SU recognition, its modulation by heme, or antibody binding. To allow these analyses, and ultimately structural studies, to be carried out on the cognate receptor, fFLVCR1a was expressed in mammalian cells and purified using the strategy established for hFLVCR1a. This section describes the construct, a small-scale expression test, scale-up and purification, and the SEC profile of the purified protein as an indicator of its suitability for downstream work.

3.5.1 Construct design

Feline FLVCR1a (fFLVCR1a) is a 555-residue, approximately 60 kDa polytopic membrane transporter of the SLC49/major facilitator superfamily (MFS) and shares 85.2% sequence identity with human FLVCR1a (hFLVCR1a). The fFLVCR1a gene was cloned into the pEG BacMam vector with a C-terminal TEV cleavage site and Twin-Strep tag, following the strategy described for hFLVCR1a (Section 2.1; full construct details in Materials and Methods, Section 2.1.3). A sequence alignment of the feline and human orthologues, annotated with the predicted transmembrane helices and N-glycosylation sites, is shown in Figure 3.10.

```
sp|Q9N1F2|FLVC1_FELCA      MVKLNDEEGAAMAPGHQPTNGYLLVPGGEPPGKVSAELQNGPKAVCLTLNGVSRDSLAAA 60
sp|Q9Y5Y0|FLVC1_HUMAN      MARPDDEEGAAVAPGHPLAKGYLPLPRGAPVGKESVELQNGPKAGTFPVNGAPRDSLAAA 60
                           *.: :******:****  ::*** :* * * ** *.********  : :**. *******

sp|Q9N1F2|FLVC1_FELCA      AEALCRPQTPLAPEEETQTRLLPTGPGEETPGTEGSPAPQTALSARRFVVLLIFSLYSLV 120
sp|Q9Y5Y0|FLVC1_HUMAN      SGVLGGPQTPLAPEEETQARLLPAGAGAETPGAESSPLPLTALSPRRFVVLLIFSLYSLV 120
                           : .*  ***********:****:* * ****:*.** * **** ***************

sp|Q9N1F2|FLVC1_FELCA      NAFQWIQYSVISNVFEGFYGVSSLHIDWLSMVYMLAYVPLIFPATWLLDTRGLRLTALLG 180
sp|Q9Y5Y0|FLVC1_HUMAN      NAFQWIQYSIISNVFEGFYGVTLLHIDWLSMVYMLAYVPLIFPATWLLDTRGLRLTALLG 180
                           *********:***********: ************************************

sp|Q9N1F2|FLVC1_FELCA      SGLNCLGAWVKCASVQQHLFWVTMLGQCLCSVAQVFILGLPSRIASVWFGPKEVSTACAT 240
sp|Q9Y5Y0|FLVC1_HUMAN      SGLNCLGAWIKCGSVQQHLFWVTMLGQCLCSVAQVFILGLPSRIASVWFGPKEVSTACAT 240
                           *********:**.************************************************

sp|Q9N1F2|FLVC1_FELCA      AVLGNQLGAAIGFLLPPVLVPNTQNNTDLLACNISTMFYGTSSVATFLCFLTIIAFKEKP 300
sp|Q9Y5Y0|FLVC1_HUMAN      AVLGNQLGTAVGFLLPPVLVPNTQNDTNLLACNISTMFYGTSAVATLLFILTAIAFKEKP 300
                           ********:*:*************:*:***************:***:* :** *******

sp|Q9N1F2|FLVC1_FELCA      QYPPSQAQAALQNSPPAKYSYKKSIRNLFRNVPFVLLLITYGIITGAFYSVSTLLNQMIL 360
sp|Q9Y5Y0|FLVC1_HUMAN      RYPPSQAQAALQDSPPEEYSYKKSIRNLFKNIPFVLLLITYGIMTGAFYSVSTLLNQMIL 360
                           :***********:*** :***********:*:**********:*****************

sp|Q9N1F2|FLVC1_FELCA      TYYKGEEVSAGKIGLTLVVAGMVGSILCGFWLDYTKIYKQTTLIVYILSFLGMVIFTFTL 420
sp|Q9Y5Y0|FLVC1_HUMAN      TYYEGEEVNAGRIGLTLVVAGMVGSILCGLWLDYTKTYKQTTLIVYILSFIGMVIFTFTL 420
                           ***:****.**:******************:****** *************:*********

sp|Q9N1F2|FLVC1_FELCA      DLGYGIVVFVTGGVLGFFMTGYLPLGFEFAVEITYPESEGTSSGLLNAAAQIFGILFTLA 480
sp|Q9Y5Y0|FLVC1_HUMAN      DLRYIIIVFVTGGVLGFFMTGYLPLGFEFAVEITYPESEGTSSGLLNASAQIFGILFTLA 480
                           ** * *:*********************************************:**********

sp|Q9N1F2|FLVC1_FELCA      QGKLTTDYSPKAGNIFLCVWLFLGIILTALIKSDLRRHNINIGIANGDIKAVPVEDTVED 540
sp|Q9Y5Y0|FLVC1_HUMAN      QGKLTSDYGPKAGNIFLCVWMFIGIILTALIKSDLRRHNINIGITNVDVKAIPA-----D 535
                           *****:**.**********:*:*********************:* *:**:*.     *

sp|Q9N1F2|FLVC1_FELCA      SPTDKESKTIVMSKQSESAI 560
sp|Q9Y5Y0|FLVC1_HUMAN      SPTDQEPKTVMLSKQSESAI 555
                           ****:* **:::*********
```

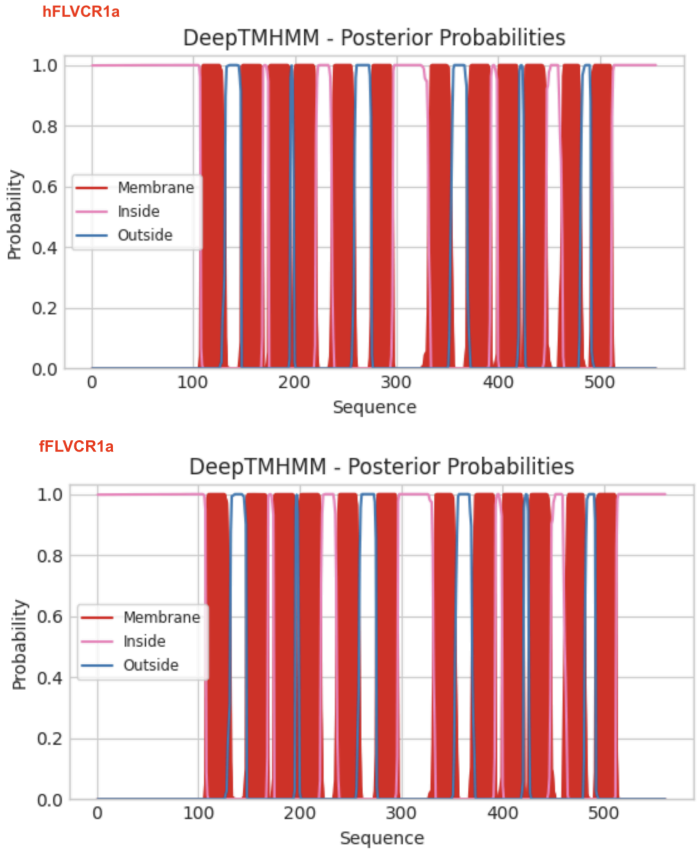


Figure 3.10. Pairwise alignment of fFLVCR1a and hFLVCR1a with predicted TM helices and N-glycosylation sites marked. Alignment was achieved using Clustal Omega, with TM prediction from DeepTMHMM and glycosylation sites from NetNGlyc. Identical residues are marked with asterisks (*), while conserved and semi-conserved substitutions are indicated by colons (:) and periods (.), respectively.

3.5.2 Small-scale expression by transient transfection

Expression of fFLVCR1a was first assessed by transient transfection of HEK293 cells with the plasmid and western blot analysis of the detergent-solubilised cell extract (Materials and Methods, Section 2.2.2). Probing with an HRP-conjugated Strep-Tactin conjugate detected a specific band in the lane loaded with the fFLVCR1a plasmid-transfected material at the size expected for the Twin-Strep-tagged protein (Figure 3.11). The apparent molecular weight, calculated with the imaging software, was 64.8 kDa. This is close to the predicted mass of approximately 60 kDa, with the modest upward shift commonly seen for glycosylated membrane proteins in SDS-PAGE. This result validated the construct and supported scale-up.

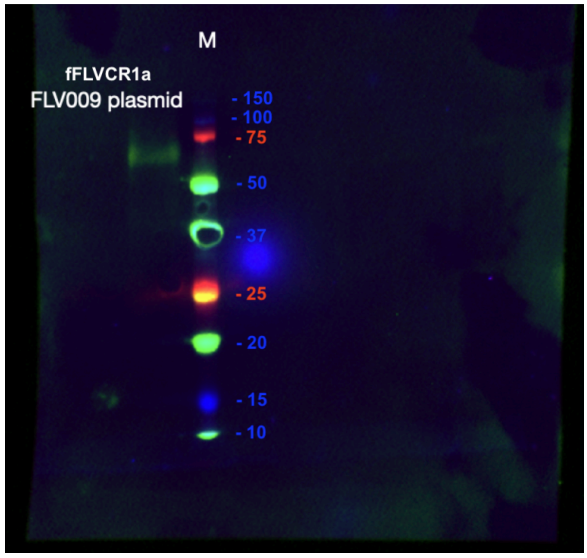


Figure 3.11. Western blot of HEK293 cells transiently transfected with the fFLVCR1a plasmid. Detergent extract of plasmid-transfected cells was run alongside a prestained molecular-weight marker (M) and probed with an HRP-conjugated Strep-Tactin conjugate. A specific band is detected at the expected molecular weight of the Twin-Strep-tagged protein.

3.5.3 Baculovirus generation

Attempts to generate recombinant baculovirus for BacMam-based expression have not yet been successful. They will be repeated, and transduction-based expression will be evaluated once viral stocks are available. The material characterised below was therefore produced exclusively by transient plasmid transfection.

3.5.4 Large-scale expression and purification

fFLVCR1a was produced at larger scale by transient transfection of 550 ml of HEK293 culture and purified from the clarified detergent extract by Strep-Tactin affinity chromatography, exploiting the C-terminal Twin-Strep tag (Materials and Methods, Section 2.3.3). The eluate was analysed by SDS-PAGE (Figure 3.12) and western blot (Figure 3.13). Both showed a prominent diffuse band in the upper region of the gel, together with a lower-molecular-weight smear, a migration pattern consistent with heterogeneous glycosylation (see Chapter 4 Discussion).

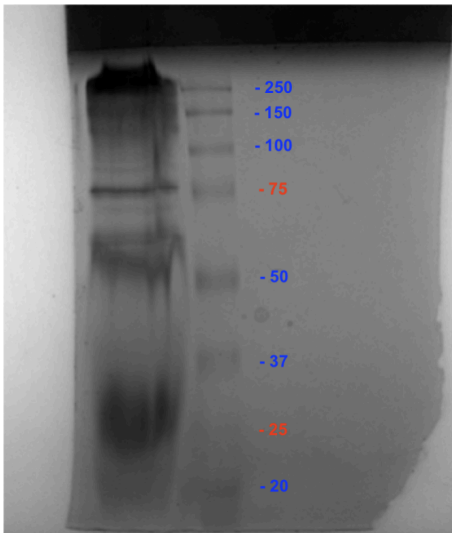


Figure 3.12. Gel analysis of purified fFLVCR1a. Coomassie-stained gel of the purified preparation run alongside a molecular-weight marker. The gel was run in native (SDS-free) running buffer in error, so migration does not reflect molecular mass and the marker is shown for reference only. The predominant species is consistent with enrichment of recombinant fFLVCR1a.

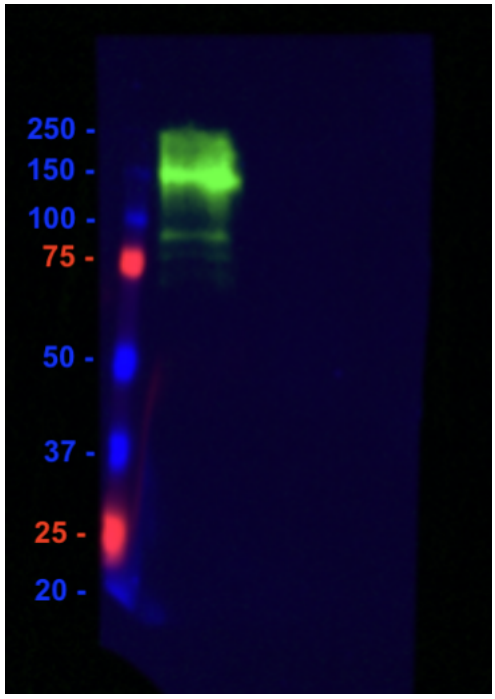


Figure 3.13. Western blot of purified fFLVCR1a probed with an HRP-conjugated Strep-Tactin conjugate. The gel was run in native (SDS-free) running buffer in error, so band positions do not reflect polypeptide mass. A prominent band is detected in the upper region, together with a lower-molecular-weight smear. The marker is in the leftmost lane and is for reference only.

Size-exclusion chromatography (SEC) of the eluate (Figure 3.14) showed two resolved species: a minor early-eluting peak at 1.18 ml, close to the void volume, and a substantially larger, symmetric peak at 2.02 ml (approximately 13.9 mAU) that accounted for most of the UV signal. This elution volume is identical to that of hFLVCR1a, indicating comparable behavior of the two orthologues in DDM/CHS.

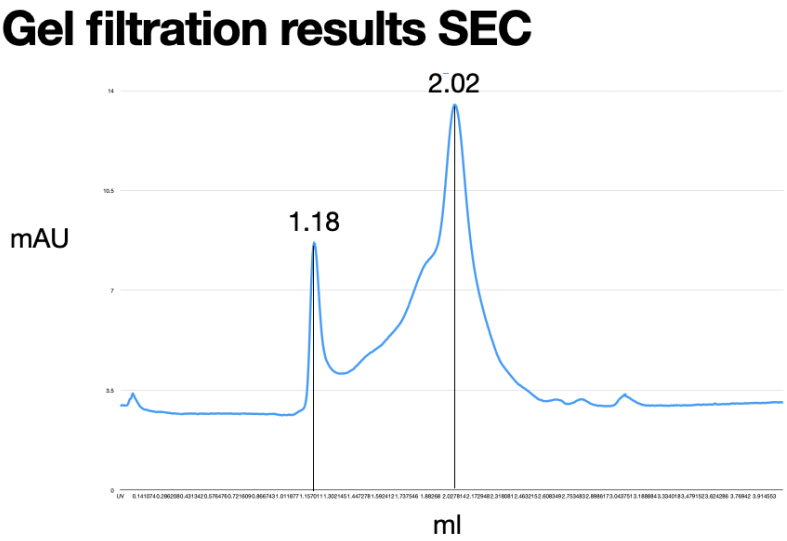


Figure 3.14. Size-exclusion chromatography profile of purified fFLVCR1a. Absorbance at 280 nm (mAU) is plotted against elution volume (ml). Two peaks were detected, at approximately 1.18 ml and 2.02 ml, the latter being the predominant species.

The final eluate had a protein concentration of 5.6 mg/ml in a volume of 60 µl post-SEC, corresponding to 336 µg of purified protein from the 550 ml transfected culture, i.e. a yield of approximately 0.61 mg per litre of culture.

3.6 Cloning, expression, and purification of FeLV-B SU RBD

This section describes the production of the receptor-binding domain (RBD) of the FeLV-B surface unit (SU), the second target protein of this thesis. The RBD is the region of the envelope glycoprotein that engages the host phosphate transporters and therefore determines receptor specificity; a soluble, purified RBD would allow receptor engagement to be studied independently of the full-length glycoprotein. The work proceeded in two stages: a first attempt based on the baculovirus–insect cell system, which did not yield an identifiable RBD (Sections 3.6.1–3.6.3), and

a revised strategy based on expression in mammalian cells, including a variant carrying a heterologous signal peptide (Sections 3.6.4–3.6.6).

3.6.1 Cloning strategy

The biophysical studies described later in this thesis required a soluble recombinant form of the FeLV-B SU receptor-binding domain (RBD). This protein needed to be produced in sufficient amounts and at a suitable level of purity for SEC and pulldown-based binding assays involving hFLVCR1a and PiT-1 (Sections 3.2 and 3.6–3.7). During this project, three constructs were generated. Each encoded the RBD defined structurally by Barnett et al. (2003) [84] (PDB 1LCS), and the constructs are referred to throughout this thesis as FeLV-B_RBD in pFastBac1, FeLV-B_RBD in pEG BacMam and μSP-FeLV-B_RBD (Section 2.1.1).

FeLV-B_RBD in pFastBac1 was the first construct to be generated. It consisted of the native FeLV-B RBD signal peptide, followed by the RBD ectodomain, a TEV protease cleavage site, and two tandem 6×His tags linked by a Gly-Ser sequence. The resulting Kozak-RBD-TEV site-6×His-GS-6×His-STOP STOP cassette was cloned into pFastBac1, between SalI and XbaI restriction sites, for expression using the conventional Bac-to-Bac baculovirus/insect-cell secretion system [48].

The construct encoded a 271-residue protein with a calculated molecular weight of 30,299.97 Da, an extinction coefficient of 72,015 $M^{-1}cm^{-1}$, and an $Abs_{0.1}\%$ (1 g/L) value of 2.401:

MEGPTHPKPSKDKTFSWDLMILVGVLLRLDVG |
MANPSPHQVYNVTWTITNLVTGTKANATSMLGTLTDAFPTMYFDLCDIIGNTWNPSDQEPF
PGYGCDQPMRRWQQRNTPFYVCPGHANRKQCGGPQDGFCAVWGCETTGETYWRPTSSW
DYITVKKGVTQGIYQCSGGGWCGPCYDKAVHSSTTGASEGGRCNPLILQFTQKGRQTSWD
GPKSWGLRLYRSGYDPIALFSVSRQVMTITPPQA

The sequence before the vertical line '|' represents the native 32-residue signal peptide. The sequence following the line corresponds to the mature ectodomain and matches the RBD used in the crystallographic structure of PDB 1LCS.

After the ExpiSf9/Bac-to-Bac secretion system failed to produce FeLV-B_RBD in pFastBac1 at levels that could be reliably detected by SDS-PAGE or anti-His immunodetection (Sections 3.6.1–3.6.3 and 4.6), the same Kozak-RBD-TEV site-6×His-GS-6×His-STOP STOP cassette was

transferred from pFastBac1 into an available pEG BacMam acceptor vector for expression in mammalian HEK293 cells, closer to the natural FeLV-B host. The acceptor vector was linearised at the corresponding SalI and XbaI sites, and the cassette was subcloned without any sequence changes [24]. The resulting mammalian-expression construct was designated FeLV-B_RBD in pEG BacMam. It retained the native signal peptide of the FeLV-B RBD and was generated to determine whether the poor expression of FeLV-B_RBD in pFastBac1 was caused by the insect-cell expression host rather than by an intrinsic problem with the RBD sequence itself (Section 4.6).

In parallel, a third construct, μSP-FeLV-B_RBD, was designed to investigate whether the native signal peptide was limiting secretion of the FeLV-B RBD. In this construct, the FeLV-B signal peptide was replaced with the heterologous μ-phosphatase secretion signal peptide (MGILPSPGMPALLSLVSLLSVLLMGCVA↓ETG; the arrow indicates the predicted signal peptidase cleavage site). This signal peptide was originally developed as part of a flexible secretion-vector system for mammalian and insect-cell expression [55]. Because the full signal-peptide sequence was too long to incorporate into a single primer, it was added to the 5′ end of the RBD coding sequence using three successive overlap-PCR reactions. The resulting fragment was then assembled into the same SalI/XbaI-linearised pEG BacMam vector by In-Fusion cloning (Section 2.1.1; Section 3.6.5). Unlike FeLV-B_RBD in pEG BacMam, which was maintained and propagated as plasmid DNA, μSP-FeLV-B_RBD was introduced into DH10Bac E. coli cells to produce a recombinant bacmid through Tn7-mediated transposition [48].

FeLV-B_RBD in pFastBac1, FeLV-B_RBD in pEG BacMam and μSP-FeLV-B_RBD in pEG BacMam all contain the same mature RBD–TEV cleavage site–6×His–GS–6×His tag arrangement. The constructs differ only in their expression systems—pFastBac1 in insect cells for FeLV-B_RBD in pFastBac1, compared with pEG BacMam in mammalian cells for FeLV-B_RBD in pEG BacMam and μSP-FeLV-B_RBD in pEG BacMam—and, in the case of μSP-FeLV-B_RBD in pEG BacMam, in the signal peptide used. FeLV-B_RBD in pFastBac1 and FeLV-B_RBD in pEG BacMam retain the native FeLV-B signal peptide, whereas μSP-FeLV-B_RBD in pEG BacMam contains the heterologous μ-phosphatase signal peptide. This design allowed the effects of expression platform and signal-peptide identity to be assessed independently within the same construct framework. The resulting comparisons form the basis of the expression-troubleshooting analysis presented in Sections 3.6.4–3.6.6 and discussed further in Section 4.6.

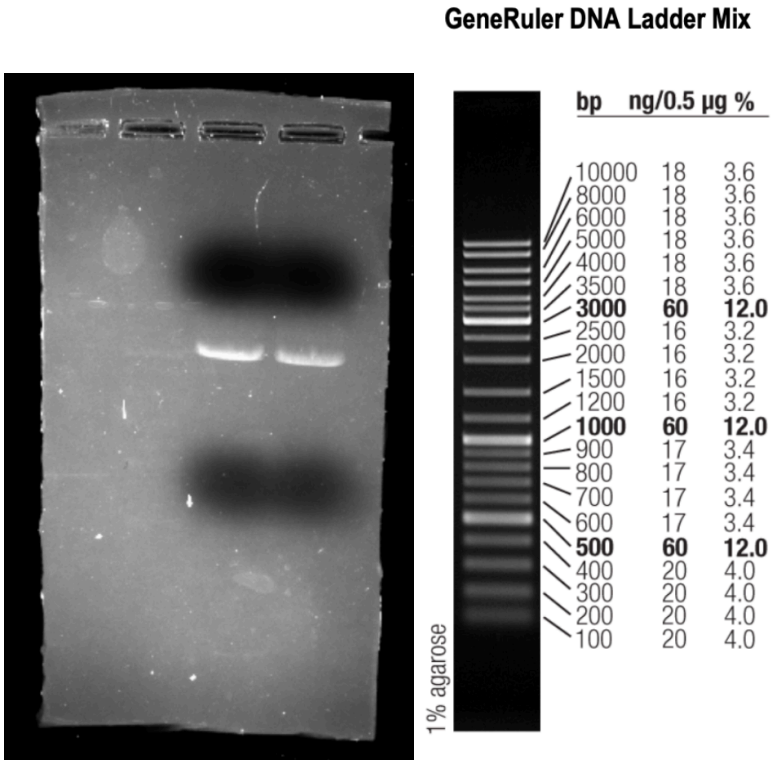


Figure 3.15. Agarose gel electrophoresis (1% agarose) of PCR products from colony screening of putative recombinant DH10Bac clones carrying the FeLV-B_RBD in pFastBac1 cassette, run alongside a GeneRuler DNA Ladder Mix for size reference. The two clones tested in the left panel produced the expected pair of amplicons, approximately 3.0 kb and 1.0 kb in size, consistent with successful Tn7-mediated transposition of the RBD expression cassette into the bacmid.

3.6.2 Expression optimization

Recombinant bacmid DNA was used to generate baculovirus in ExpiSf9 insect cells. Cultures with viability above 90% were seeded at 1×10^6 cells/mL and transfected the following day, at a density of 2×10^6 cells/mL, using ExpiFectamine–bacmid complexes containing 2 µg bacmid DNA and 10 µL ExpiFectamine prepared in transfection buffer (50 mM HEPES, pH 7.4, and 150 mM NaCl). After 96 hours of incubation, cell viability had decreased to the expected 60–70% range, as determined by trypan blue exclusion. The P0 viral stock was then harvested by centrifugation at 1,000 × g for 10 minutes and protected from light.

The P0 stock was used to infect a larger-scale ExpiSf9 culture (100 mL; 1×10^6 cells/mL) at a low inoculum of 500 µL. Following the same viability assessment and harvesting criteria, the clarified supernatant was retained as the amplified P1 viral stock and stored at 4 °C in the dark, consistent

with standard baculovirus handling practices given the photolability and general long-term instability of high-titre viral stocks.

The functional expression competence of the P1 stock was assessed by transducing HEK293-6E cells with increasing proportions of P1 stock (0.5%, 1%, and 2%; duplicate wells). One replicate set was additionally treated with 10 mM sodium butyrate, a histone deacetylase inhibitor routinely used to enhance baculovirus-mediated transgene expression in mammalian cells by counteracting epigenetic silencing of the transduced viral genome [50]. This assay was used primarily for P1 stock titration and quality control rather than as the production platform for the RBD.

For large-scale production, ExpiSf9 cultures were infected directly with baculovirus stocks from two independent P1 harvests, designated P1(1) and P1(2), and with a further-amplified P2 stock. Because the FeLV-B RBD construct is secreted into the culture medium, the cultures were harvested by low-speed centrifugation (1,200 × g, 10 minutes, 4 °C), and the clarified supernatants were retained for downstream purification rather than the cell pellets. This strategy is consistent with the established use of the baculovirus–insect cell system for producing secreted recombinant glycoproteins [51]. The RBD concentrations recovered from the P1(1), P1(2), and P2 ExpiSf9 expression and harvest batches, as determined after the initial affinity-capture step, were 0.412, 0.500, and 0.297 mg/mL, respectively. These measurements represent the total protein recovered at this stage and do not indicate sample purity, which was assessed separately (Section 3.6.3).

3.6.3 Purification and quality control

The purity of the recovered material was initially assessed by 14% SDS–PAGE across the three expression batches. None of the P1(1), P1(2), or P2 lanes showed a single, clearly enriched band at the expected molecular mass of approximately 30 kDa. Instead, all three lanes exhibited a broad, poorly resolved pattern of bands and smearing across a wide molecular-weight range, with no dominant species corresponding to the target RBD (Figure 3.16). This outcome was therefore considered unsatisfactory.

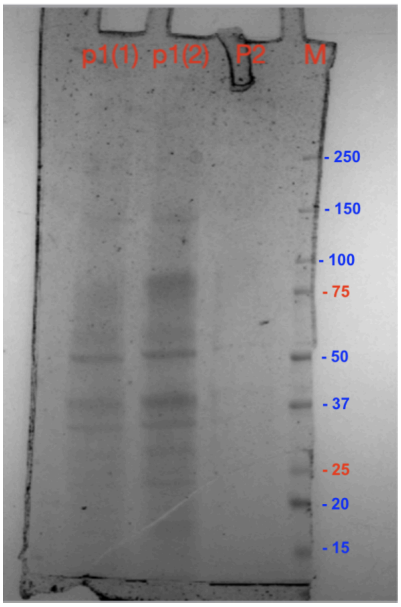


Figure 3.16. 14% SDS–PAGE analysis of RBD preparations from the insect-cell expression batches P1(1), P1(2), and P2, alongside a prestained protein ladder spanning 10–250 kDa. All three sample lanes displayed diffuse, multiple bands rather than a single prominent band at the expected molecular weight of approximately 30 kDa, indicating substantial sample impurity at this stage.

To determine whether a correctly sized His-tagged species was nevertheless present, the samples were analysed by western blot on two separate occasions using different detection strategies. In the first experiment, the membranes were blocked and probed conventionally with an anti-polyhistidine primary antibody prepared in milk/TBS, followed by standard immunoblot development. In the second experiment, detection was performed using a Ni-NTA–Atto550 fluorescent conjugate, which binds directly to polyhistidine tags and therefore eliminates the need for primary and secondary antibodies [52]. This workflow comprised SDS–PAGE, membrane transfer (1–2 h), blocking with 5% BSA in PBS (1–14 h), a PBST rinse, incubation with the Ni-NTA–Atto conjugate (1:1000–1:2500 for 1 h, protected from light), a further PBST wash, and fluorescent imaging. The total protocol time was approximately 3–18 h.

Both experiments included appropriate positive controls, namely anti-FLAG and a FeLV-B SU protein standard. In both cases, the blots showed only the red and blue bands corresponding to the prestained marker ladder; no discrete signal at the expected molecular weight of approximately 30 kDa was detected in the flow-through or RBD sample lanes from either P1(1) or P1(2) (Figures 3.17–3.18). A diffuse green signal was observed at the extreme left edge of the first blot, but this

most likely represented an artefact associated with the loading well or an adjacent control lane rather than a resolved RBD-specific band.

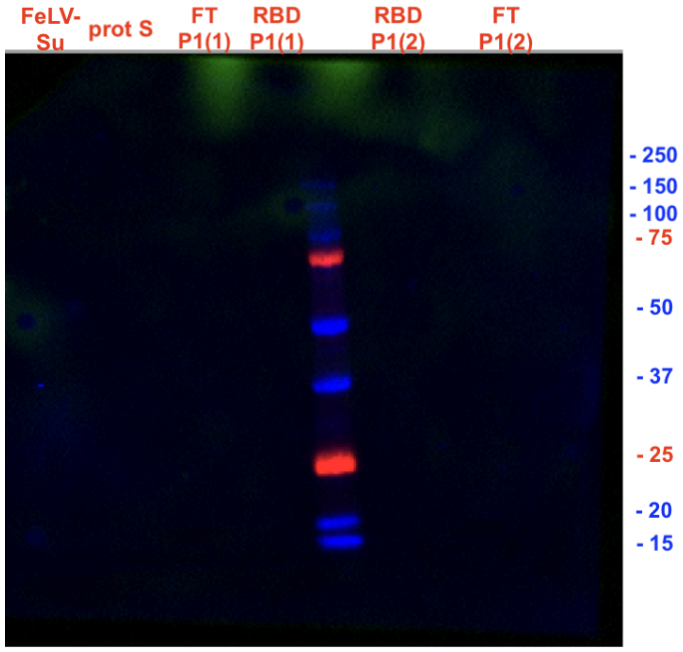


Figure 3.17. Anti-polyhistidine antibody western blot of RBD purification fractions from insect cells, performed using milk/TBS as the blocking solution. Positive controls included anti-FLAG and a FeLV-B SU protein standard, along with flow-through and eluate fractions from P1(1) and P1(2). Only the protein marker ladder was visible; no specific band was detected at the expected molecular weight of RBD in any sample lane.

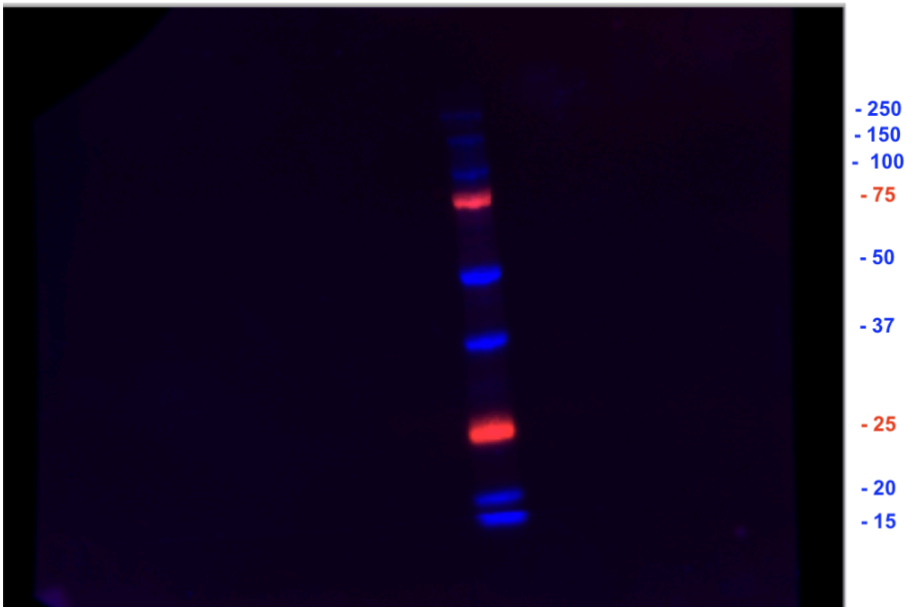


Figure 3.18. Repeat western blot analysis of RBD purification fractions from insect cells, using a Ni-NTA–Atto550 fluorescent conjugate for detection and the same positive controls. As shown in Figure 3.17, only the protein marker ladder was detected, with no discrete signal corresponding to the His-tagged RBD.

Therefore, the SDS-PAGE and anti-His western blot results indicated that the protein was neither recovered nor quantified from all three expression batches (Section 3.6.2), and that neither the purity nor the identity of a correctly sized, His-tagged FeLV-B RBD species could be confirmed by this method, suggesting that the virus titer was too low or the expression system unsuited for this target, at least in our hands. In response, the expression strategy was substantially revised. The RBD-encoding cassette was subcloned into the pEG BacMam vector [24] to enable direct expression in mammalian cells, more similar to the natural host for the FeLV-B virus than insect cells.

This recloning also provided an opportunity to investigate whether replacing the native FeLV-B SU signal peptide with a highly expressed heterologous signal peptides influenced RBD expression, secretion, and, in particular, receptor tropism. In other retroviral and lentiviral envelope glycoproteins, signal peptides have been shown to affect glycosylation and the antigenic and functional properties of the mature protein independently of the receptor-binding domain sequence itself [53]. This provided a rationale for examining their potential effects on FeLV-B RBD receptor engagement. The results obtained using the revised constructs and expression strategy are presented in the following section.

3.6.4 Recloning of the RBD cassette into pEG BacMam

Following the negative purification results obtained using the ExpiSf9/Bac-to-Bac secretion strategy (Sections 3.6.1–3.6.3), the FeLV-B SU RBD expression cassette (Kozak–RBD–TEV–6His–GS–6His–STOP STOP; 813bp) was recloned from the original pFastBac-based construct into an open pEG BacMam acceptor vector [24]. The acceptor vector was linearized between the same SalI and XbaI sites used previously to enable direct expression in mammalian cells. The recloned construct, FeLV-B-RBD in pEG BacMam, was 7678 bp long.

The RBD cassette was amplified by PCR from the pFastBac template using primers that add the SalI and XbaI sites and the overlap required for seamless cloning (primer sequences and PCR conditions are given in Methods). The expected amplicon was therefore longer than the cassette itself: the 813 bp cassette plus the 16 nt added to each end by the primers gives approximately 845 bp. Both replicate reactions yielded a single, clean band (Figure 3.19) [band migrates at ~ 800-900 bp against the ladder], consistent with this expected size and with no visible secondary products.

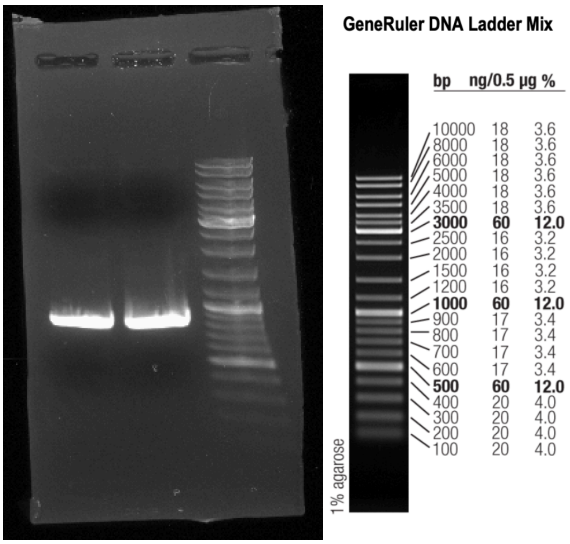


Figure 3.19. Agarose gel electrophoresis of the FeLV-B_RBD in pEG BacMam PCR products from two replicate reactions, alongside a GeneRuler DNA Ladder Mix. Both reactions produced a single, clean amplicon of the expected size (highlighted), which was subsequently excised from the gel for purification.

The band was excised from the gel and purified.

Seamless cloning into the SalI/XbaI-linearized pEG BacMam vector was performed using an In-Fusion-based cloning enzyme. The assembled product was transformed into chemically competent E. coli, and plasmid DNA was purified from individual colonies. To confirm correct assembly, an

aliquot containing 200 ng of plasmid DNA was digested with SalI and XbaI restriction enzymes. The correct size of the gene cassette excised was confirmed by agarose gel electrophoresis.

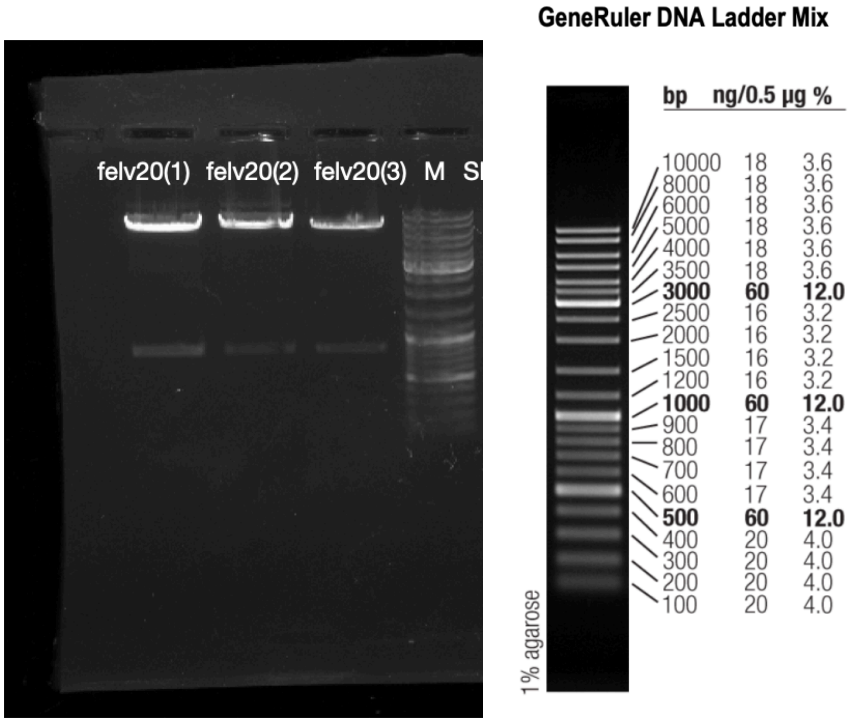


Figure 3.20. Agarose gel electrophoresis of SalI/XbaI-digested miniprep DNA from three independent FeLV-B_RBD in pEG BacMam clones, alongside a DNA ladder (M). All three clones displayed the expected two-band digestion pattern, consisting of a higher-molecular-weight vector backbone band and a lower-molecular-weight insert-release band of consistent size across clones. These results confirmed successful subcloning of the cassette into pEG BacMam.

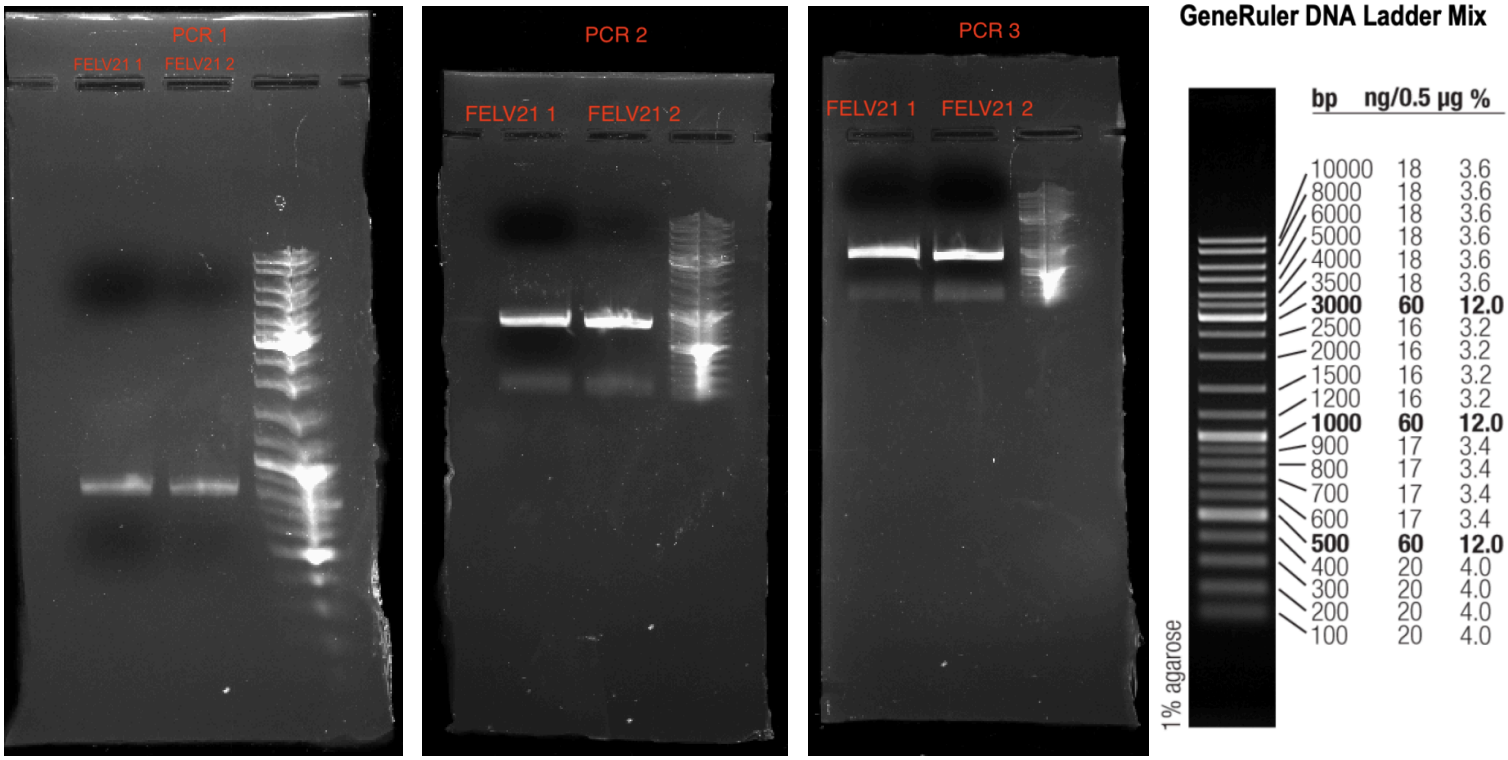
The plasmid DNA concentrations of the three verified clones were 190, 387, and 268 ng/µL, respectively. Each plasmid preparation was eluted in a final volume of 50 µL.

3.6.5 Signal peptide substitution: FeLV-B-RBD with the µ-phosphatase signal peptide

In parallel, a second construct was generated in which the native FeLV-B SU signal peptide was replaced with the heterologous µ-phosphatase secretion signal peptide (MGILPSPGMPALLSLVSLLSVLLMGCVA↓ETG; the arrow denotes the predicted eukaryotic signal peptidase cleavage site). This signal peptide was originally described as part of a versatile mammalian/insect secretion vector suite [55]. The resulting variant retained the same RBD–TEV–

6His–GS–6His–STOP STOP cassette and is referred to below as the μ-phosphatase SP construct, in contrast to the native SP construct described in Section 3.6.4.

Because the complete μ-phosphatase signal sequence could not be incorporated into a single primer, it was appended to the 5′ end of the RBD coding sequence through three sequential, overlapping PCR reactions. Each reaction used a progressively longer forward primer to extend the amplicon further in the 5′ direction, while the same reverse primer was retained throughout. Consequently, the C-terminal TEV–6His–GS–6His cassette remained unmodified.



Figures 3.21, 3.22, and 3.23. Agarose gel electrophoresis of the three sequential PCR steps (PCR1, PCR2, and PCR3) used to assemble the μSP-FeLV-B_RBD in pEG BacMam, with each reaction performed in duplicate (replicates 1 and 2). At each stage, both replicates produced a single amplicon of the expected size without prominent nonspecific products. This pattern was consistent with the successful, progressive extension of the signal-peptide-encoding sequence onto the RBD cassette across the three reactions.

Following the third PCR, the final full-length μ-phosphatase SP–RBD amplicon was gel-purified as described in Section 3.6.4, with the mass of the excised gel used to determine the appropriate purification reagent volumes. Seamless In-Fusion cloning was subsequently performed as described above, using the same SalI/XbaI-linearized pEG BacMam acceptor vector.

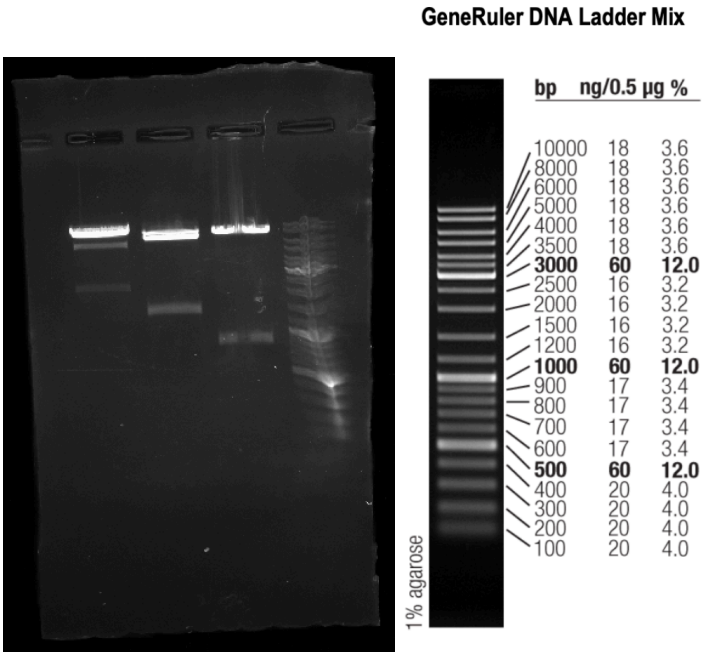


Figure 3.24. Diagnostic restriction digestion of the assembled µ-phosphatase SP construct using three enzyme combinations—XhoI/XbaI (Lane 1), XhoI/SalI (Lane 2), and SalI/XbaI (Lane 3)—alongside a DNA ladder. The SalI/XbaI digest (rightmost sample lane) produced the expected fragment pattern and was therefore selected for downstream clone screening, followed by standard SalI/XbaI-based verification of subsequent clones.

3.6.6 Small-scale expression and affinity-capture test of the native SP and µ-phosphatase SP constructs

Both constructs, carrying either the native or the µ-phosphatase signal peptide, were used for small-scale transient transfection of Expi293 (HEK293-derived) cells in order to evaluate which design expressed better.

For purification, 1.5 mL of each culture (corresponding to 4.5 million cells) was lysed and used for purification.

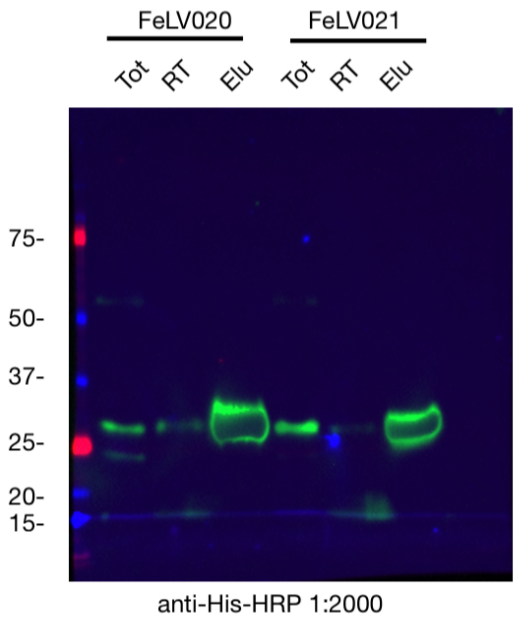


Figure 3.25. Anti-His–HRP (1:2000) western blot of the small-scale Expi293 expression and Ni-NTA capture assay for the FeLV-B_RBD in pEG BacMam and µSP-FeLV-B_RBD in pEG BacMam constructs. Total supernatant (Tot), Ni-NTA flow-through (RT), and imidazole eluate (Elu) fractions are shown for each construct alongside a prestained molecular-weight marker. Both constructs produced a distinct immunoreactive band at approximately 25–30 kDa, consistent with the calculated molecular mass of 30.3 kDa for the His-tagged RBD. The signal was markedly reduced in the corresponding flow-through fractions and strongly enriched as a single, well-resolved band in the eluate fractions for both constructs.

Both pEG BacMam-recloned FeLV-B-RBD constructs were purified successfully and to a similar yield (Figure 3.25). Since expression of the two constructs was comparable, the construct carrying the native signal peptide was selected for the subsequent experiments.

3.7 Cloning, expression, and purification of fSLC20A1 (PiT-1)

SLC20A1 is the cellular receptor for FeLV-B, and a purified, detergent-solubilised preparation of it is the second receptor needed to study FeLV Env recognition in vitro, alongside FLVCR1a. A soluble RBD (Section 3.6) and a purified receptor together would allow the same biophysical approaches used for the FLVCR1a–FeLV-C SU interaction to be applied to the FeLV-B system. This section therefore describes the production of fSLC20A1 in mammalian cells, using the same pEG BacMam platform, Twin-Strep affinity tag and DDM/CHS solubilisation strategy that worked for FLVCR1a. It also documents the first construct, which carried a C-terminal tag, and why it was

redesigned. Expression was detected with a general fluorescent western blot, but no specific Strep-tag signal could be confirmed, so a reciprocal N-terminally tagged construct (N-terminus fSLC20A1) was made. The two tag positions were then compared directly in a small-scale expression test, treating tag position as an open experimental variable rather than an assumption. The outcome determines which construct, if either, is carried forward to scale-up and quality assessment.

3.7.1 Cloning strategy

The third target investigated in this thesis was feline SLC20A1 (PiT-1), a ubiquitously expressed, 12-transmembrane-helix, type III sodium-dependent inorganic phosphate transporter. Both its N- and C-termini are positioned extracellularly, and the protein contains a characterized N-linked glycosylation site [58]. PiT-1 is particularly relevant to this thesis because, together with PiT-2/ SLC20A2, it serves as a principal cellular receptor for the FeLV-B SU RBD investigated in Section 3.6. Viral entry is mediated through direct interaction between the RBD and the transporter's fourth extracellular loop [46, 58].

The PiT-1 coding sequence (2,172 bp; EcoRI–Kozak–SLC20A1–TEV–Twin-STREP–STOP STOP–XbaI) was cloned into the same pEG BacMam expression platform used previously for the FLVCR1a construct fFLVCR1a (Section 3.5) [24]. When combined with the approximately 4,200 bp pEG BacMam backbone, the construct was predicted to have a total plasmid size of 6,372 bp. This calculated size was used as the primary criterion for identifying correctly assembled clones by agarose gel electrophoresis.

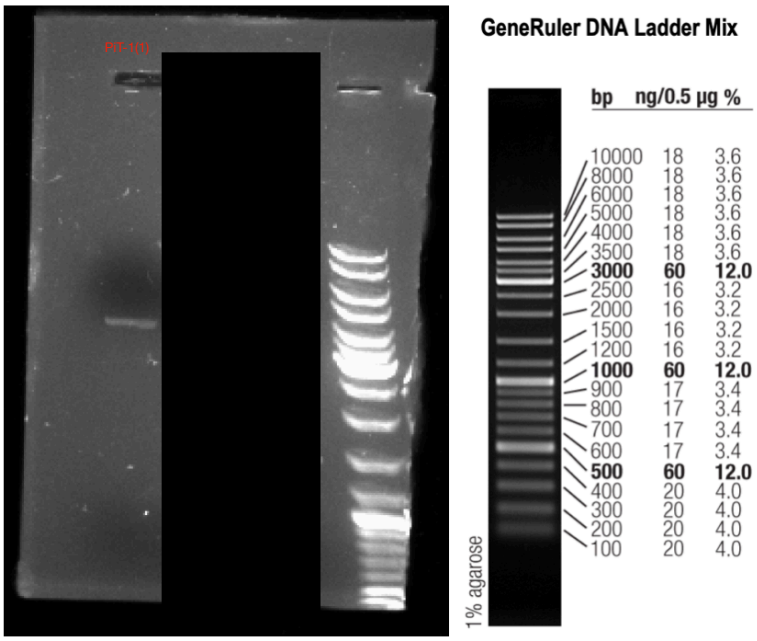


Figure 3.26. Agarose gel electrophoresis of the assembled pEG BacMam clone PiT-1(1), alongside a GeneRuler DNA Ladder Mix. The PiT-1(1) clone migrated at the expected size of approximately 6,372 bp, corresponding to the ~4,200 bp vector backbone plus the 2,172 bp PiT-1 insert.

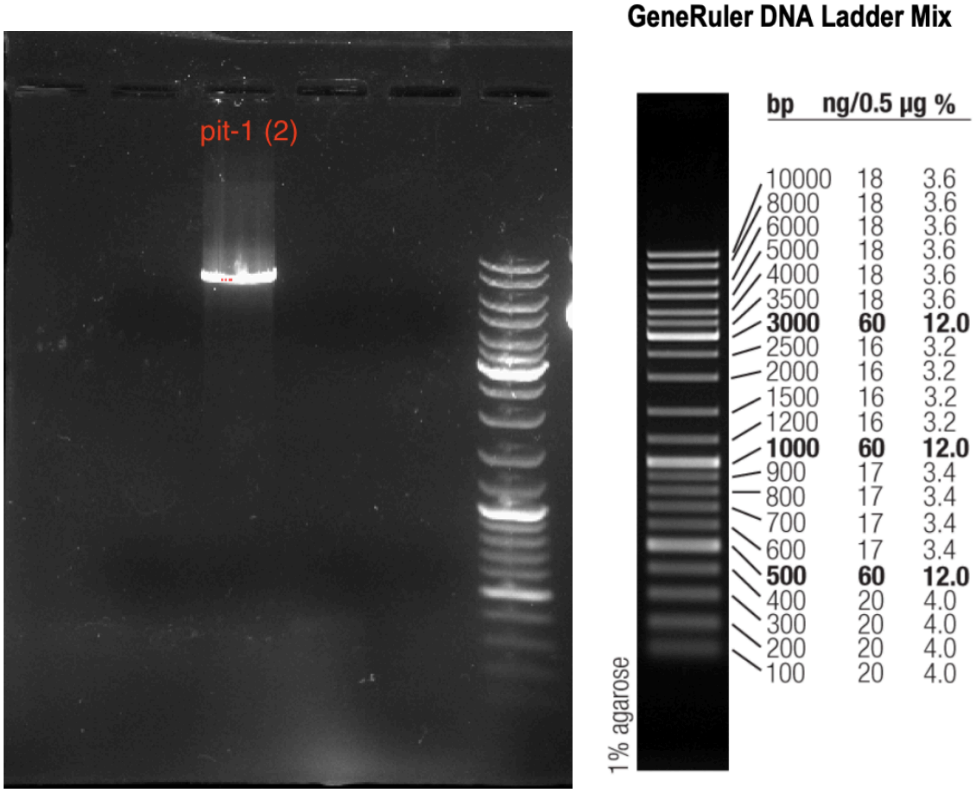


Figure 3.27. Agarose gel electrophoresis of a second independent PiT-1 clone, PiT-1(2), alongside a DNA ladder. The sample showed a single dominant high-molecular-weight species consistent with the assembled plasmid, confirming the successful isolation of a second candidate clone for downstream analysis.

Verified PiT-1 plasmid clones, comprising two independent isolates, were transformed into DH10Bac E. coli to generate recombinant bacmids through Tn7-mediated transposition [48]. Bacmid DNA was subsequently purified from selected white colonies.

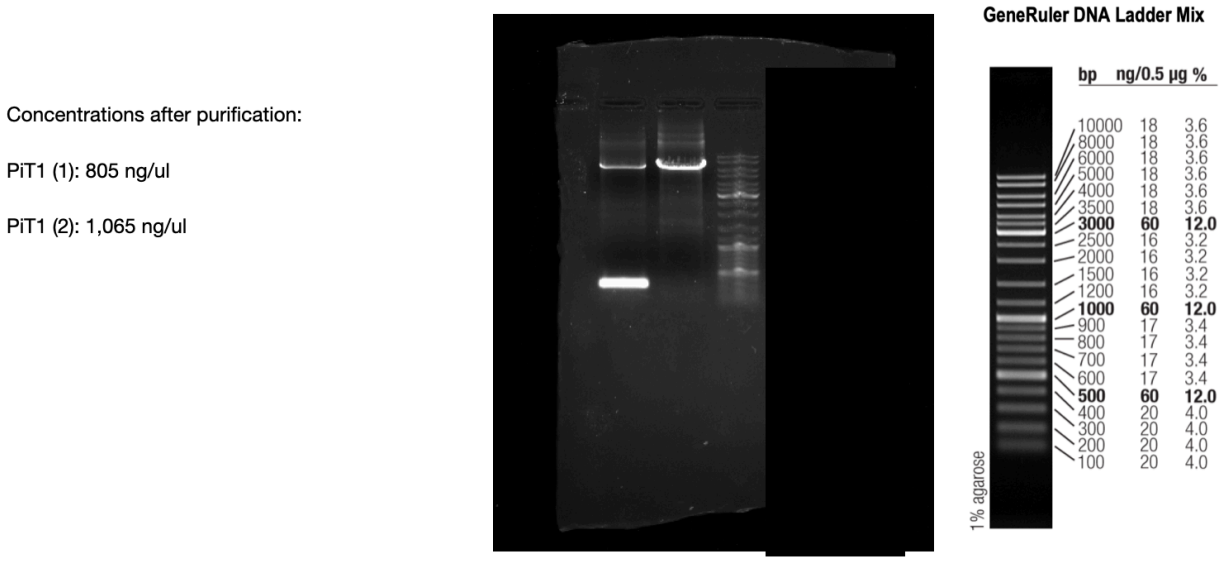


Figure 3.28. Agarose gel electrophoresis of bacmid DNA purified from two independent PiT-1 clones, alongside a DNA ladder. In each lane, the DNA migrated as a diffuse, high-molecular-weight species near the loading wells, consistent with the expected behaviour of intact bacmid DNA (>130 kbp) on a standard 1% agarose gel. The concentration and purity of each eluted bacmid preparation were assessed. All samples had an A260/280 ratio of ≥1.8, indicative of double-stranded DNA largely free from protein or RNA contamination. The measured concentrations were 805 ng/µL for PiT-1(1) and 1,065 ng/µL for PiT-1(2). A parallel concentration and purity assessment performed after transformation of the recombinant pEG BacMam–PiT-1 construct into DH10Bac yielded concentrations of 3.090 µg/µL for PiT-1(1) and 3.430 µg/µL for PiT-1(2).

3.7.2 Expression optimization

Expression of PiT-1 was screened in mammalian cells using the delivery route supported by the pEG BacMam system [24]: transduction with baculovirus generated from the corresponding recombinant bacmid DNA in insect cells. Expression was assessed by fluorescent western blot (Figure 3.29). Probing with Mab-Strep detected a dominant band in both lanes at approximately 60–65 kDa, below the expected size. A weaker band was detected at approximately 70 kDa, just below

the 75 kDa marker, together with a diffuse species at approximately 20 kDa. Full-length PiT-1 could therefore not be confirmed.

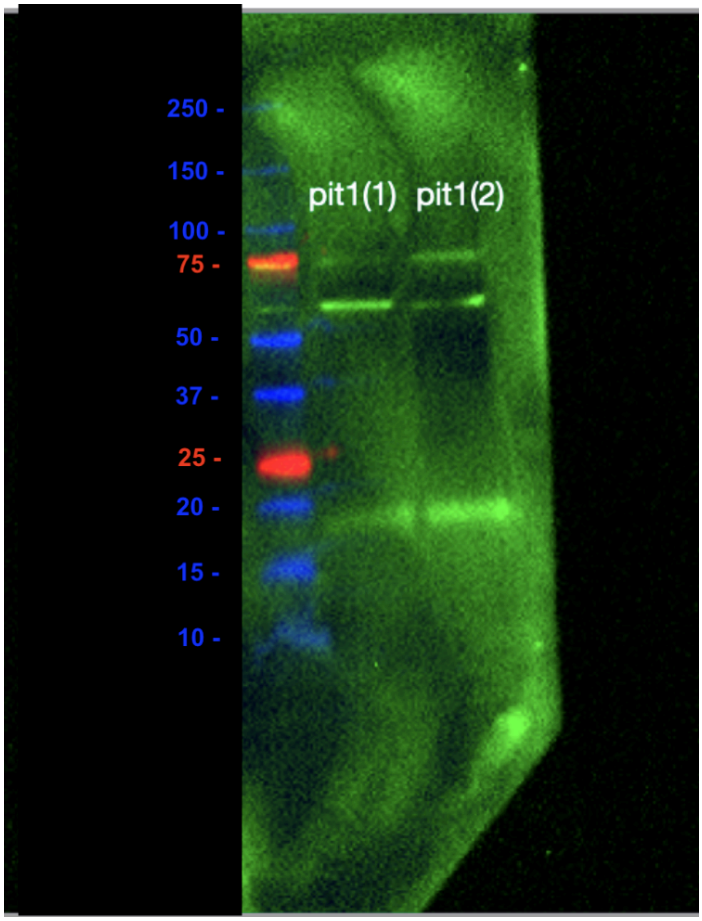


Figure 3.29. Western blot of small-scale PiT-1 expression probed with an anti-Strep-tag monoclonal antibody (Mab-Strep). Detergent-solubilised extracts from two independent PiT-1 clones, pit1(1) and pit1(2), were separated by SDS-PAGE and probed with Mab-Strep to detect the C-terminal Twin-Strep tag, with fluorescent detection. The expected molecular weight of PiT-1 is approximately 74 kDa. In both lanes the strongest signal was a band at approximately 60–65 kDa, below the expected size. A weaker band was detected at approximately 70 kDa, just below the 75 kDa marker, together with a diffuse species at approximately 20 kDa. Molecular-weight markers (kDa) are shown on the left, and lanes not relevant to this experiment were masked.

3.7.3 Purification and quality control

Because the previous result was inconclusive, the membrane was reprobed with an HRP-conjugated anti-Strep-Tactin antibody (procedure described in Methods). The blot showed no bands for PiT-1(1) and PiT-1(2), indicating that PiT-1 was poorly expressed in these samples (Figure 3.30).

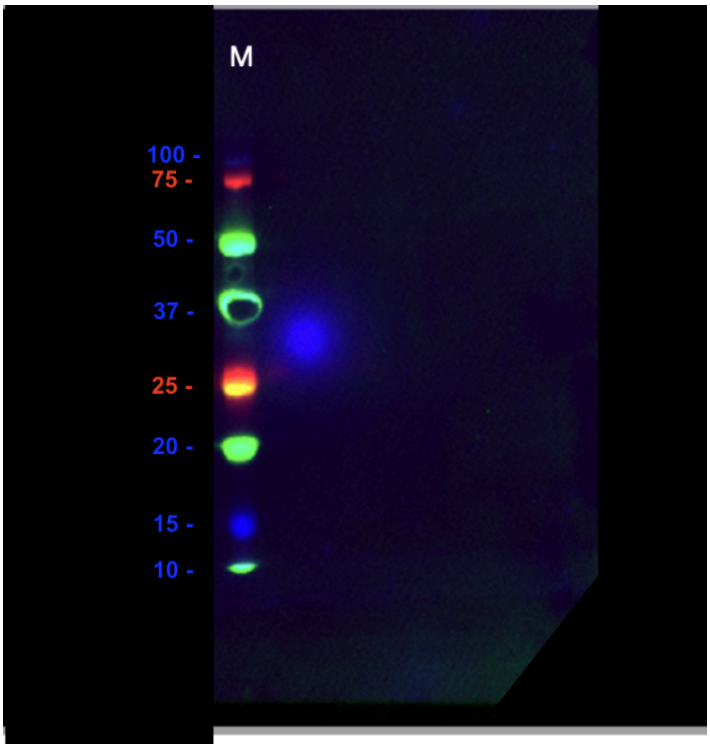


Figure 3.30. Reprobing of the PiT-1 membrane with an HRP-conjugated anti-Strep-Tactin antibody shows no specific bands. The membrane shown in Figure 3.29 (probed with Mab-Strep) was reprobed with an HRP-conjugated anti-Strep-Tactin antibody to detect the C-terminal Twin-Strep tag of PiT-1. No specific immunoreactive bands were detected in the sample lanes, including at the expected molecular weight of approximately 74 kDa, and only the molecular-weight marker (M) is visible. This result did not confirm the presence of Strep-tagged PiT-1 on the membrane, and did not resolve the unexpected bands seen with Mab-Strep. Molecular-weight markers (kDa) are shown on the left, and lanes not relevant to this experiment were masked.

As a final step in this initial testing phase, a fresh small-scale infection of newly prepared ExpiSf9 cells was performed using P1 baculovirus stocks for PiT-1, with two independent P1 harvests tested, and the resulting material was analysed by western blotting with an HRP-conjugated anti-Strep-Tactin antibody (Figure 3.31). In two independent P1 harvests, anti-Strep-Tactin detection revealed

only faint bands migrating below the expected molecular weight of PiT-1, so expression of the full-length protein in ExpiSf9 cells could not be confirmed.

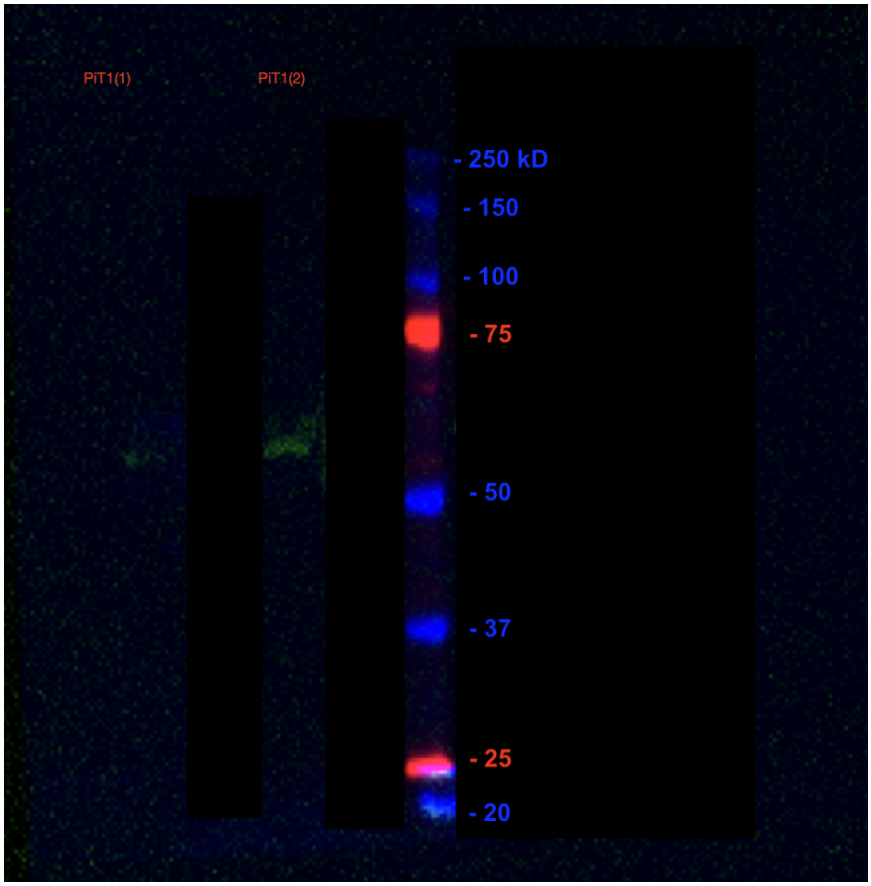


Figure 3.31. Western blot of PiT-1 expressed in ExpiSf9 cells from P1 baculovirus stocks shows bands below the expected molecular weight. Freshly prepared ExpiSf9 cells were infected on a small scale with P1 baculovirus stocks for PiT-1, and two independent P1 harvests, PiT1(1) and PiT1(2), were tested. The resulting material was analysed by western blotting with an HRP-conjugated anti-Strep-Tactin antibody to detect the Twin-Strep tag. Only faint signals were detected in the PiT1(1) and PiT1(2) lanes, at an apparent molecular weight of approximately 55–60 kDa. This is below the expected size of tagged PiT-1 (approximately 74 kDa), and no band was detected at the expected position. The result was therefore considered unsatisfactory, as the detected species could not be unambiguously assigned to full-length PiT-1. Molecular-weight markers (kDa) are shown on the right, and lanes not relevant to this experiment were masked.

Finally, the results presented in Sections 3.7.2 and 3.7.3 indicated that, although a signal consistent with PiT-1 expression was observed by general fluorescent detection (Figure 3.29), its identity as an intact, Strep-tagged fusion protein could not be confirmed in three independent detection attempts:

the initial anti-Strep-Tactin western blot, the reblot of the same membrane, and a subsequent small-scale ExpiSf9 infection test. Consequently, the cloning and expression approach was modified in a subsequent round of experiments, as described in the following section.

3.7.4 Redesign of the PiT-1 construct: repositioning the TwinStrep tag to the N-terminus

The original PiT-1 construct described in Sections 3.7.1–3.7.3 (EcoRI–Kozak–SLC20A1–TEV–TwinStrep–STOP STOP–XbaI) is referred to as fSLC20A1-C-terminus. This designation distinguishes it from the redesigned construct described below. Although general SLC20A1 expression was detected by fluorescent western blotting (Sections 3.7.2 and 3.7.3), a specific Strep-tag signal could not be confirmed in three independent detection attempts using an anti-Strep-Tactin antibody. Because the native SLC20A1 C-terminus is predicted to be extracellular but located close to the final transmembrane helix within the protein's 12-transmembrane topology [58], it was hypothesized that a C-terminal TwinStrep tag might be sterically inaccessible to the antibody or Strep-Tactin reagent and/or might compromise expression efficiency.

To address this uncertainty, a second construct carrying an N-terminal tag, N-terminus-fSLC20A1, was generated in parallel. The two constructs therefore allowed the effect of tag position on receptor folding, cell-surface expression, and epitope accessibility to be assessed experimentally rather than assumed. This strategy is consistent with earlier studies that used independently N- and C-terminally epitope-tagged Pit1 constructs to map functionally important receptor regions [93].

N-terminus-fSLC20A1 is the reciprocal construct, with the equivalent affinity and cleavage cassette positioned at the N-terminus of fSLC20A1. The expression cassette—SalI–Kozak–Twin-Strep–TEV–SLC20A1–STOP STOP–NotI—contains a 2,174 bp insert, measured from SalI to NotI and including both restriction sites, within the 9,040 bp full-length pEG BacMam vector. It encodes a 716-residue fusion protein with a calculated mass of approximately 78 kDa, in which the Twin-Strep-tag II affinity tag and TEV protease cleavage site precede the mature fSLC20A1 sequence. As expected for an N-terminal fusion, the native initiator methionine of fSLC20A1 is replaced by the upstream tag cassette, and translation begins at the methionine residue encoded within the tag cassette. The vector backbone and dual mammalian/baculovirus expression system provided by pEG BacMam are the same as those used for fSLC20A1 and fFLVCR1a [24, 41].

The redesigned construct, N-terminus-fSLC20A1, was assembled using the existing pEG BacMam-based vector EROS004 as a scaffold: the mEROS coding sequence was replaced with the full-length SLC20A1 coding sequence, and the Strep-FLAG-Strep tag cassette was simplified to a tandem TwinStrep tag, using overlap-extension PCR followed by seamless In-Fusion cloning (details are given in Methods). The final architecture was:

SalI – Kozak – STREP – STREP – TEV – SLC20A1 – STOP STOP – NotI (2174bp)

The resulting 9,040-bp construct was designated N-terminus-fSLC20A1.

3.7.5 Verification of N-terminus-fSLC20A1 clones and bacmid generation

Following transformation and plasmid miniprep, three independent N-terminus-fSLC20A1 clones were verified by double digestion with SalI and NotI, the two restriction sites flanking the assembled expression cassette. The digestions were performed in the same batch as those for three clones of the FeLV-B-RBD construct (Section 3.6.4) (Figure 3.32).

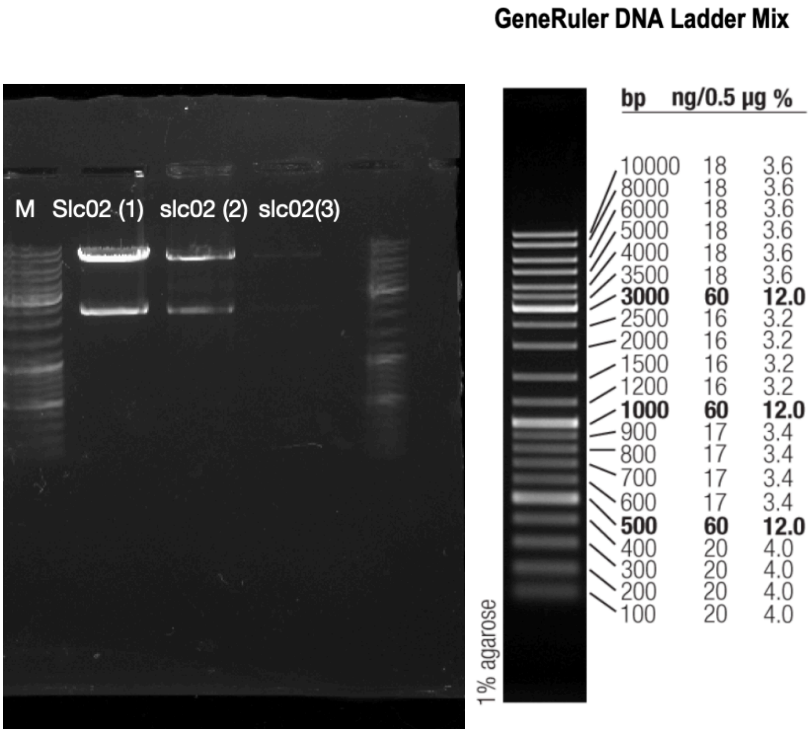


Figure 3.32. Agarose gel electrophoresis of SalI/NotI-digested miniprep DNA from three independent N-terminus-fSLC20A1 clones, Slc02(1)–(3), alongside a DNA ladder (M). Clones Slc02(1) and Slc02(2) displayed the expected digestion pattern, whereas Slc02(3) gave only a very faint signal.

Clones displaying the expected digestion pattern, Slc02(1) and Slc02(2), were selected for transformation into DH10Bac E. coli to generate recombinant bacmid through Tn7-mediated transposition [48]. Recombinant bacmid DNA was subsequently isolated for small-scale expression testing in mammalian cells.

3.7.6 Expression test of fSLC20A1-C-terminus and N-terminus-fSLC20A1

fSLC20A1-C-terminus and N-terminus-fSLC20A1 were compared directly in a small-scale Expi293 expression test (experimental details are given in Materials and Methods).

Because SLC20A1 is a multipass integral membrane protein rather than a secreted product, purification was initiated from the cell pellet rather than the culture supernatant. Cells were solubilized with DDM/CHS, clarified by centrifugation, and analysed by western blotting.

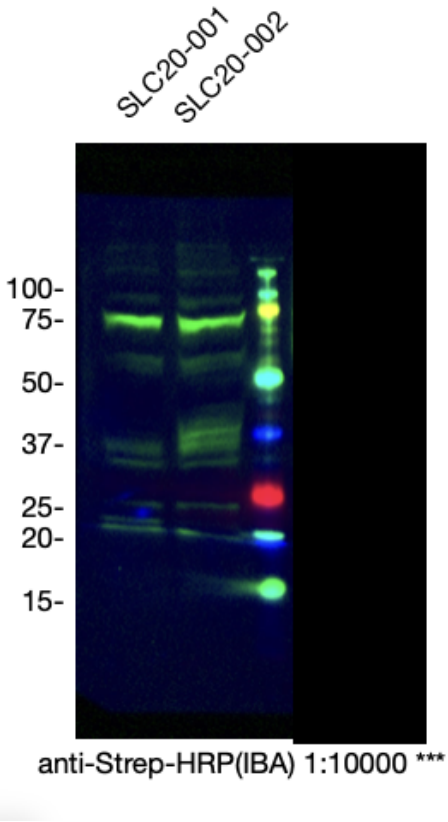


Figure 3.33. Anti-Strep-HRP (IBA, 1:10,000) western blot of small-scale Expi293 expression and DDM/CHS solubilization tests for fSLC20A1-C-terminus and N-terminus-fSLC20A1, alongside a prestained molecular-weight marker ladder. Specific bands were detected for both fSLC20A1-C-terminus and N-terminus-fSLC20A1 at approximately 75–100 kDa, consistent with the expected molecular mass of glycosylated SLC20A1 and with the approximately 74-kDa apparent molecular weight previously estimated for PiT-1 (Section 3.7.2). An additional lower-molecular-weight species of approximately 37 kDa was also detected in both lanes.

Unlike the earlier detection attempts using the Mab-Strep-Tactin antibody (Section 3.7.3), the revised approach—combining direct DDM/CHS-based solubilization of the cell pellet with a higher-titre anti-Strep-HRP (IBA) probe—produced a clear, specific signal for both the original C-terminally tagged fSLC20A1-C-terminus and the redesigned N-terminally tagged N-terminus-fSLC20A1 constructs. This represents the first successful confirmation of Strep-tagged SLC20A1 expression in this work and indicates that both tag placements are compatible with expression and Strep-tag-based detection under these conditions. These findings support scaling up the expression and purification of the 2 constructs for subsequent quality and functionality assessment.

4. Discussion

4.1 Overview

This thesis examined three related questions concerning feline leukemia virus subgroup B/C receptor engagement and the cellular receptors involved: (i) the substrate specificity and viral-receptor function of hFLVCR1a; (ii) the development of expression, purification, and antibody-based tools for the two receptors implicated in FeLV entry—FLVCR1a and PiT-1/SLC20A1—as well as the FeLV-B SU receptor-binding domain (RBD); and (iii) the identification of an alternative ligand or molecules as a possible route toward determining the structure of membrane proteins. Collectively, the results show that hemin binds and stabilises hFLVCR1a, and that heme increases the affinity of the FeLV-C SU RBD for the receptor, which suggests that the receptor's ligand-bound state influences viral engagement. The main obstacle to structural studies is therefore not a lack of potential ligands or binders, but the difficulty of producing homogeneous, stable protein and converting solution-phase interactions into sufficiently robust complexes for structural analysis.

4.2 hFLVCR1a substrate recognition: hemin binds and stabilises; coproporphyrin I does not

The MST and nDSF data in Sections 3.1.1–3.1.3 together indicate that hemin, but not coproporphyrin I, engages hFLVCR1a. Hemin titration gave a saturable binding curve with a Kd of 23 μM, and 100 μM hemin raised the melting temperature of hFLVCR1a by 2.2 °C, which is evidence of ligand-induced stabilisation. Coproporphyrin I gave an apparent Kd of 1.8 μM by MST, but the normalised fluorescence fell to near zero, a change much larger than that seen with hemin, and nDSF showed no thermal shift ($\Delta Tm \approx 0$ °C). The most likely explanation is that coproporphyrin I quenched the fluorescence of the labelled protein, so that the apparent binding in MST is a fluorescence artefact and not evidence of a tighter interaction (Section 3.1.2). The nDSF result is consistent with this interpretation, although an absence of thermal shift cannot by itself exclude weak binding that does not change stability. The two assays are therefore not in conflict, and the Kd for coproporphyrin I should not be used to rank the two porphyrins. This observation also shows why a fluorescence-based binding assay needs an orthogonal readout before a ligand is classified.

These results are consistent with hemin being a physiological substrate of hFLVCR1a. Its export is required for erythroid maturation and for maintaining systemic iron and heme homeostasis [2, 3, 17], but direct biophysical evidence that hemin binds the isolated, detergent-solubilised transporter has been limited. The data presented here provide such evidence. The key chemical difference between the two ligands is the central iron: hemin contains an iron(III) ion within its porphyrin ring, whereas coproporphyrin I is a metal-free porphyrin. It is possible that the iron is needed for productive engagement, for example through axial coordination by a conserved histidine, as proposed for other heme-handling transporters [3, 10]. ABCB6 provides a comparison, since hemin, together with glutathione, promotes a closed and functionally relevant state in that transporter whereas the metal-free porphyrin does not [5]. This remains a hypothesis, and resolving it will require structural studies at atomic resolution.

ABCB6 provides a useful comparison. This structurally unrelated porphyrin transporter can bind coproporphyrin III and hemin at overlapping sites, but the two ligands induce different conformational outcomes. In that system, hemin, together with glutathione, promotes a closed and functionally relevant state, whereas the metal-free porphyrin does not [5]. If hFLVCR1a behaves similarly, the thermal-shift data would suggest that hemin—but not coproporphyrin I—engages the iron-coordinating chemistry of the native substrate site and thereby affects the folding or conformational equilibrium of the transporter. One possible mechanism is axial coordination of the heme iron by a conserved histidine, as proposed for other heme-handling transporters [3,10]. Coproporphyrin I may bind non-productively within the same pocket or may occupy a separate, lower-specificity site. The two assays are therefore not necessarily in conflict. nDSF measures changes in protein folding stability, whereas MST can detect ligand-induced changes in size, charge, or hydration shell [70]. These results indicate that both types of measurement are needed before a porphyrin can be classified confidently as a bona fide hFLVCR1a substrate.

4.3 Heme as a switch for viral receptor engagement

The central biophysical finding of this thesis is that heme increases the affinity of the FeLV-C SU for hFLVCR1a by approximately sixfold, as measured by MST. The Kd decreased from 412 nM in the absence of heme to 66.7 nM in its presence (Section 3.2.1). To my knowledge, this is the first biophysical evidence that occupancy of the FLVCR1a substrate site can influence its activity as a retroviral receptor. The finding extends the genetic evidence showing that FLVCR1a functions both

as the FeLV-C receptor and as an essential heme exporter [3, 15, 16] into a ligand-dependent mechanistic framework.

hFLVCR1a is an MFS transporter expected to cycle between outward-open, occluded, and inward-open conformations through a rocker-switch mechanism [22, 23]. The viral vr1 determinant interacts with the extracellular face of the receptor [4, 15]. The simplest model is therefore that heme binding shifts the conformational equilibrium toward an outward-facing, or otherwise SU-accessible, state, stabilizing a receptor conformation favorable for high-affinity engagement of the viral spike. This would increase the proportion of receptor molecules displaying a competent viral docking surface at any given time, and would link substrate transport dynamics to viral receptor function. The model is consistent with, although not yet proven by, recent cryo-EM structures of FLVCR1/FLVCR1a captured in inward-facing state [10], which provide the first opportunity to test such a conformational mechanism at atomic resolution. It has not been tested in this work.

4.4 Heme-dependent co-elution of FeLV-C SU with hFLVCR1a in SEC

The SEC and pulldown experiments were performed with FeLV-C SU. In the first set of SEC runs, FeLV-C SU alone and hFLVCR1a alone eluted at 2.17 and 2.02 ml, respectively (Figure 3.3, red and blue respectively). Without heme, the mixture resolved into two peaks (1.98 and 2.16 ml) that closely matched the individual proteins, indicating that most of the receptor and SU remained uncomplexed (Figure 3.3, purple). In the presence of 40 μM heme, the free SU peak at about 2.17 ml was no longer detected, and the mixture produced a single, higher peak at 2.00 ml, coincident with the hFLVCR1a-alone peak (Figure 3.3, green). SU therefore no longer eluted as a free protein but co-eluted with the receptor, converting a largely uncomplexed mixture into a single co-eluting species (Section 3.2.2). These experiments should nevertheless be repeated. Repeating the series with larger amounts of each protein would also allow the peak fractions to be collected and analysed by SDS-PAGE. This would establish directly whether the co-eluting species contains both proteins, rather than inferring complex formation from peak position and amplitude alone.

No shift in the elution volume of hFLVCR1a was observed upon complex formation, as would be expected for a larger particle. This is most likely because the hFLVCR1a–lipid–detergent micelle is so large that binding of a protein of approximately 45 kDa (SU) barely changes the hydrodynamic size of the particle. Complex formation is thus detected as a change in peak amplitude

(disappearance of the separate SU peak and increase of the hFLVCR1a peak) rather than as a shift in peak position.

Two observations complicate the interpretation of the SEC data. First, heme itself absorbs strongly in the UV region, and part of the increase in peak amplitude may therefore reflect heme bound to or co-eluting with the proteins rather than increased complex formation alone. Analysis of the peak fractions by SDS-PAGE/western blot, together with orthogonal assays, would be required to confirm the composition of the co-eluting species.

Second, a subsequent SEC experiment, where heme was present in the running buffer rather than being added only during sample incubation, did not reproduce the clean co-elution observed in the first SEC experiment. The apparent complex peak (2.09 ml) eluted closer to free SU than to free receptor whose elution volume is dramatically altered (Figure 3.4, green), and a substantial late-eluting species of comparable abundance appeared in all samples. The same issue was observed in the Fab 339F1 SEC experiments (Section 3.4.1). These data therefore provide less direct evidence for complex formation and suggest that the receptor FLVCR1a might be degraded due to then presence of heme in the running buffer in ways that are not yet fully controlled.

In addition, the magnetic pulldown assay did not detect co-purification of hFLVCR1a with His-tagged SU under either heme condition. The assay nevertheless confirmed that both the bait and prey were detectable and functional: the bait was detected by anti-His blotting, while the prey was detected by anti-FLAG blotting in the flow-through (Section 3.2.3). This negative result should not simply be dismissed, but it also should not be interpreted as disproving the interaction. MST and SEC are equilibrium-based, non-immobilized, non-washing assays. By contrast, a bead pulldown introduces immobilization, dilution, and one or more wash steps. These additional manipulations can disrupt interactions with relatively rapid off-rates or with affinities in the sub-micromolar rather than nanomolar range [21]. The pulldown result may consequently indicate that the interaction is dynamic and conformation-sensitive rather than constitutively stable.

4.5 An antibody and Fab toolkit for hFLVCR1a

Since these monoclonal antibodies were intended to support structural studies of FLVCR1a, including cryo-electron microscopy (cryo-EM), their mode of antigen recognition was investigated in greater detail. Antibody epitopes are commonly classified as either linear (continuous) or

conformational (discontinuous). Linear epitopes are formed mainly by a contiguous sequence of amino acids, whereas conformational epitopes consist of residues that may be distant from one another in the primary sequence but are brought together by the three-dimensional folding of the antigen [32]. Antibody–antigen recognition is influenced not only by the static arrangement of these residues, but also by protein flexibility, conformational dynamics, and the thermodynamic properties of the interaction [33]. For structure determination, the most valuable antibodies are those that recognize a rigid, conformationally stable epitope, as such binding produces a well-defined antibody–antigen complex that reduces conformational heterogeneity and facilitates particle alignment and high-resolution reconstruction.

To determine whether recognition depended on the native conformation of FLVCR1a, the antibodies were evaluated by SDS-PAGE followed by western blotting, together with size-exclusion chromatography (SEC). These techniques provide complementary information. During SDS-PAGE, proteins are treated with SDS and become substantially unfolded and denatured before antibody detection. Antibodies that retain binding after this treatment are generally consistent with recognition of a linear or, less frequently, a denaturation-resistant epitope. Antibodies that depend on the native three-dimensional structure may lose access to their epitope after denaturation and therefore fail to produce a detectable signal. Consistent with this, Forsström et al. showed that antibodies directed against conformational epitopes frequently failed to detect their targets by western blotting, whereas antibodies recognizing linear epitopes were more likely to retain western blot reactivity [34].

SEC was used to assess antibody–FLVCR1a complex formation while maintaining the protein in a more native state. Unlike western blotting, SEC cannot directly establish whether an antibody recognizes a linear or conformational epitope. Instead, a change in the FLVCR1a elution profile after antibody addition indicates the formation of a species with altered hydrodynamic properties, consistent with complex formation. An antibody that forms a complex detected by SEC may therefore recognize either a linear sequence that remains accessible in the native protein or a discontinuous epitope created by the three-dimensional structure of FLVCR1a.

The two assays were therefore interpreted side by side. Clones that were positive in both were considered consistent with recognition of a linear or denaturation-resistant epitope. In contrast, antibodies that interacted with native FLVCR1a by SEC but produced no detectable western blot signal were considered candidates for conformational, structure-dependent epitopes, as antibodies

directed against such epitopes can retain recognition of native proteins while failing to detect the denatured proteins by western blotting [34].

Binding to native hFLVCR1a was assessed by analytical SEC for 15 of the 16 scFv-Fc clones (344C1 was not tested), alongside western blotting against denatured hFLVCR1a (Section 1.6, Table 1.1). Seven clones (339C1, 339F1, 339H11, 340C1, 340D3, 341F5 and 345E9) produced an unambiguous leftward shift consistent with complex formation. Of these seven, only 340C1 was also positive by western blot, consistent with a linear or denaturation-resistant epitope. Four (339F1, 339H11, 341F5 and 345E9) were SEC-positive but western-blot-negative, the pattern expected for a conformation-dependent epitope, and are therefore candidates for structural work. The remaining two (339C1, which gave a signal in the mock-transfected lane, and 340D3, which was not tested by western blot) could not be assigned. Five further clones were detected by western blot (339B6, 339B9, 339C8, 341D4 and 344C1) but were ambiguous by SEC (344C1 was not tested), and four (339D6, 339H8, 340E7 and 341A6) were ambiguous by SEC without a positive blot. Because samples were injected immediately after mixing, without pre-incubation, this ambiguity may reflect kinetics as much as epitope type: lower-affinity antibodies may not have reached equilibrium before the run [18]. Of the four conformational candidates, 339F1 was taken forward for reformatting as a Fab (Sections 3.3 and 3.4).

Distinguishing between these recognition modes was particularly important for the intended structural applications. Binding to a defined surface of the native protein may help stabilize or characterize a particular antigen conformation, although the effect of antibody binding on the conformation of FLVCR1a must be determined experimentally. The structural nature of an antibody–antigen interaction is defined by the molecular contacts formed at the interface, which may depend on both the spatial arrangement of the residues and their conformational dynamics [33]. The comparison of western blotting and SEC therefore provides only a preliminary classification, based on the apparent dependence of each antibody on the native structure of FLVCR1a. It indicates epitope character rather than definitive epitope mapping. Identifying the precise binding sites would require additional approaches, such as peptide mapping, site-directed mutagenesis, structural analysis, or other dedicated epitope-mapping techniques.

The orthologue cross-reactivity data provide an additional practical criterion for clone selection (Section 3.3). FBE339C8 recognized human but not murine FLVCR1a, whereas other clones showed broader or narrower cross-reactivity. Cross-reactive clones would be most useful for

mouse-model experiments or mouse-derived structural constructs, while human-restricted clones would be preferable when species specificity is required. Thus, there is no single "best" clone; the appropriate choice depends on the intended downstream application.

The most structurally relevant question was whether Fab 339F1, developed as a compact, monovalent, fiducial-sized binder for future cryo-EM studies (Section 2.4.2) [35, 37], retained binding after reformatting from its parent scFv-Fc. Under the conditions tested, SEC did not detect a complex between the Fab and hFLVCR1a (Section 3.4.1). At least three explanations are possible. The first is loss of avidity. The parent format is bivalent, and if the intrinsic affinity of 339F1 is only in the sub-micromolar range, removing the second binding arm could reduce the effective affinity below the level that analytical SEC can resolve. Such assays often require low-nanomolar or better affinity to retain a complex over the duration of the run [38, 71]. The second is that reformatting affected the Fab itself. Expression, folding, and disulfide pairing of the isolated VL-CL/VH-CH1 module may differ from those of the parent scFv-Fc, and a partially misfolded or heterogeneous Fab preparation could fail to form a detectable complex even if the parent antibody binds effectively. The third is an assay-specific artefact. As discussed in Section 4.4, the heme-containing buffer used in some runs visibly altered the Fab elution profile even in the absence of hFLVCR1a, which prevents a confident negative interpretation of the heme-containing complex runs. The available SEC data cannot distinguish between these explanations.

4.6 Successful optimization of RBD expression through expression in mammalian cells

The successful purification of both pEG BacMam-recloned constructs f or expression in HEK293 cells contrasts with the earlier ExpiSf9/Bac-to-Bac secretion strategy (Sections 3.6.1–3.6.3), in which neither SDS-PAGE nor anti-His detection confirmed the presence of a correctly sized or purified RBD species. Recloning the RBD cassette into the mammalian-optimized pEG BacMam vector, delivered either as plasmid DNA (native signal peptide) or as recombinant bacmid DNA (μ-phosphatase signal peptide), therefore constituted a successful modification of the expression strategy. These findings provided a positive basis for advancing both the native and heterologous signal-peptide constructs to larger-scale expression and comprehensive purification and quality-control analyses.

4.7 fFLVCR1a expression and purification

This thesis showed that the feline orthologue, fFLVCR1a, can be expressed by transient transfection of the pEG BacMam construct in HEK293 cells and purified using the DDM/CHS detergent conditions and Strep-Tactin-based capture established for hFLVCR1a (Sections 2.3.1–2.3.2, 3.5.2 and 3.5.4). Generation of recombinant baculovirus for transduction-based expression has not yet been successful (Section 3.5.3). Following affinity capture and size-exclusion chromatography (SEC) polishing, fFLVCR1a eluted predominantly as a single, symmetrical peak at 2.02 ml on a Superose 6 Increase 5/150 column, identical to hFLVCR1a, with a smaller species near the void volume consistent with a minor aggregate population. In total, 336 µg of purified protein was recovered from 550 mL of HEK293 culture, corresponding to a yield of 0.61 mg per litre (Section 3.5.4). This provides the first biochemically confirmed and purifiable feline receptor material generated in this project, and it shows that the pipeline developed for hFLVCR1a can be extended across orthologues.

However, direct heme binding or heme-transport activity has not yet been measured for fFLVCR1a, so the porphyrin-binding and thermal-stabilisation data in Section 3.1 remain specific to the human orthologue. The amount and purity obtained are sufficient for the same panel of biophysical assays (MST, nDSF and analytical SEC) already applied to hFLVCR1a. Testing whether hemin stabilises fFLVCR1a, and whether heme modulates SU binding to it, is an important next step (Sections 4.2 and 4.3). Such experiments would connect the biophysical findings directly to the natural FeLV-C–FLVCR1a virus–receptor pair in the cat.

4.8 fSLC20A1 (PiT-1) cloning and expression

The work in Section 3.7 therefore aimed to establish whether feline PiT-1 could be produced in mammalian cells with the pEG BacMam platform, Twin-Strep tag and DDM/CHS solubilisation that had worked for fFLVCR1a.

Cloning was straightforward. Two independent clones of the C-terminally tagged construct (fSLC20A1-C-terminus) gave plasmids of the expected size (about 6,372 bp) and yielded plasmid DNA of good concentration and purity (Section 3.7.1). The redesigned N-terminally tagged construct (N-terminus-fSLC20A1) was assembled by overlap-extension PCR and In-Fusion cloning. Two of three clones gave the expected SalI/NotI digestion pattern and were taken to

bacmid generation (Sections 3.7.4–3.7.5). Cloning was therefore not the limiting step. Expression detection was.

The first screen with Mab-Strep gave a dominant band at about 60–65 kDa and a weaker one at about 70 kDa, both below the expected size (78 kDa). Reprobing with an HRP-conjugated anti-Strep-Tactin antibody and a small-scale ExpiSf9 infection test also failed to detect a full-length, Strep-tagged protein (Sections 3.7.2–3.7.3). Three independent attempts therefore left expression unconfirmed. These bands cannot be assigned to PiT-1, and they may represent truncated or degraded species, a possibility that was not tested here. The failure could have been due to the construct, the host or the detection reagent. The tag-position hypothesis, that a C-terminal tag might be inaccessible or might impair expression, was reasonable given the topology of the protein [58], and it motivated the N-terminal construct. In the end, though, the signal came from a change in the experimental conditions, not from the tag position alone. Direct DDM/CHS solubilisation of Expi293 pellets, together with a higher-titre anti-Strep-HRP probe, gave specific bands for both constructs at about 75–100 kDa (Section 3.7.6). This range is consistent with a glycosylated transporter, given the characterised N-linked glycosylation site in PiT-1 [58], although the presence of glycosylation was not tested directly. A species of about 37 kDa was also seen in both lanes and has not been identified.

This result establishes that Strep-tagged PiT-1 can be expressed in mammalian cells and that both tag positions are compatible with expression and detection under these conditions. The comparison was qualitative, from a single small-scale test with no quantification, so neither construct can be preferred. The experiments also say nothing about folding, membrane localisation, solubilisation efficiency or function, and no PiT-1 has been purified yet. Thus, PiT-1 is at an earlier stage than fFLVCR1a (Section 4.7), for which purified protein with a monodisperse SEC profile is available. The next steps are to scale up both constructs, purify them by Strep-Tactin affinity capture and SEC, and assess their quality as was done for fFLVCR1a. Once purified material is available, the interaction with the FeLV-B RBD (Section 3.6) can be examined with the SEC and MST assays used for FLVCR1a. Both constructs should be carried forward until their yield and behaviour in detergent have been compared quantitatively.

4.9 Lessons from an iterative membrane-protein production pipeline

Sections 3.5–3.7 describe the production of three constructs: fFLVCR1a, the FeLV-B SU RBD and PiT-1/SLC20A1. The pattern across these projects is broadly applicable beyond any one target.

fFLVCR1a was the most straightforward: the pipeline established for hFLVCR1a gave a specific band at the expected size in a single small-scale expression test (Section 3.5.2), and this supported scale-up without further changes. The FeLV-B RBD presented a different problem. The original Bac-to-Bac/ExpiSf9 insect-cell secretion system produced material that was neither sufficiently pure by SDS-PAGE nor detectable using two independent anti-His formats (Sections 3.6.1–3.6.3). The solution was not a simple reagent adjustment but a complete change of expression platform. Recloning into the mammalian-optimised pEG BacMam vector, produced FeLV-B_RBD for both signal peptide-constructs, both of which showed clean capture on Ni-NTA beads (Section 3.6.6). For PiT-1, after changing the Western blotting detection of the Strep-tag, both constructs with the tag at either end of the protein produced specific signals (Section 3.7.6 and 4.8).

These troubleshooting paths suggest a useful diagnostic hierarchy for membrane-protein expression failures. Before concluding that a construct does not express, it is reasonable to test: (i) detection-reagent changes, such as switching antibody format or dilution; (ii) expression-platform changes, including insect versus mammalian hosts and plasmid versus bacmid delivery; and finally (iii) construct redesign, such as altering tag position or signal peptide identity. In this thesis, fFLVCR1a required none of these, the RBD required tiers (ii) and (iii), and PiT-1 required tiers (i) and (iii) combined. This sequence is consistent with established guidance for eukaryotic membrane-protein production [24, 41] and provides a practical example of why a staged troubleshooting strategy is valuable.

The final quality metrics obtained for fFLVCR1a, a dominant, monodisperse SEC peak with a minor void-proximal aggregate species and a yield of 0.61 mg per litre of HEK293 culture, are sufficient for preliminary biophysical studies. However, the yield remains modest compared with what is typically needed for routine biophysical and structural studies, although BacMam-expressed membrane proteins can reach low milligram-per-litre yields when the target is well behaved [24, 41].

5. Conclusions and Future Perspectives

5.1 Conclusions

This thesis aimed to determine whether the transport substrate of FLVCR1a influences its function as a retroviral receptor, and to develop the antibody and expression tools needed for structural studies of the FeLV receptors FLVCR1a and PiT-1/SLC20A1 (Section 1.7). Three main conclusions emerge from this work.

First, hemin binds and stabilises hFLVCR1a, whereas coproporphyrin I does not. Second, heme increased the affinity of the FeLV-C SU receptor-binding domain for hFLVCR1a about sixfold (Section 3.2.1). To my knowledge, this is the first biophysical evidence that occupancy of the FLVCR1a substrate site can modulate its activity as a retroviral receptor, and it is consistent with a conformational model in which heme favours a receptor state that is accessible to the viral spike (Section 4.3). This model has not been tested directly. Heme-dependent co-elution was seen in the first SEC experiment, but it was not reproduced in the repeat SEC run, and no complex was detected in the magnetic pulldown (Sections 3.2.2, 3.2.3 and 4.4). This is compatible with a dynamic, conformation-sensitive interaction, but it also reflects limits of the co-migration assays, including the effect of heme on chromatographic behaviour.

Third, the antibody and expression work provides tools for future structural studies. Clone 339F1 was SEC-positive but western-blot-negative, which is the pattern expected for a conformational epitope (Section 1.6, Section 4.5). However, the Fab derived from 339F1 formed no detectable complex under the conditions tested (Section 3.4.1), so its affinity and suitability as a fiducial remain unresolved. In parallel, fFLVCR1a was expressed by transient transfection and purified to a dominant, monodisperse SEC peak (336 µg from 550 ml of culture, about 0.61 mg/l), although recombinant baculovirus has not yet been generated (Sections 3.5 and 4.7). Two pEG BacMam constructs of the FeLV-B RBD expressed in mammalian HEK293 cells, with the native or the µ-phosphatase signal peptide, were successfully expressed and captured on Ni-NTA after the insect-cell strategy had failed (Sections 3.6 and 4.6). Expression of Strep-tagged PiT-1 was confirmed for both tag positions (N- or C-terminus), but PiT-1 expression has not yet been scaled up to enable its purification (Section 3.7.6).

5.2 Future Perspectives

1) Directly testing conformational changes during heme-dependent receptor engagement. The conformational model proposed in Section 4.3 should be tested with methods that report directly on receptor conformation, such as HDX-MS, a FRET-based conformational sensor [113], or cryo-EM of hFLVCR1a with and without heme and SU. The SEC measurement should also be repeated with FeLV-C SU with heme in the sample but not in the running buffer, so that the data can be placed on the same footing as the MST result. Purified fFLVCR1a now makes it possible to test whether hemin stabilises the feline receptor and whether heme modulates SU binding to it (Section 4.7).

(2) Completing the antibody and Fab toolkit. The ambiguous clones in the SEC panel (Section 1.6) should be repeated with a standardised pre-incubation step, because Section 4.5 attributes part of the ambiguity to kinetics. The affinity of Fab 339F1 should be measured directly by MST or BLI before deciding whether it can be kept as a structural tool (Section 3.4.1). In addition, the Fab should be tested without heme in the running buffer, since the buffer perturbed its SEC profile (Sections 3.4.1 and 4.5).

(3) Developing a mechanistic understanding of gammaretrovirus recognition of host receptors. The heme-dependent increase in affinity measured here for the FeLV-C SU RBD raises a broader question that this thesis has only begun to address: why do host range and tissue tropism differ so markedly among gammaretroviruses and host species? FeLV-A, FeLV-B, FeLV-C, GALV, and related viruses use overlapping but distinct receptor sets, including THTR1, PiT1/PiT2, and FLVCR1. Their tropism is also associated with sequence variation in the VRA–VRC regions of their SU RBDs (Section 1.2.4) [11, 13, 14]. A systematic comparison of RBD–receptor binding thermodynamics—including Kd, ΔTm, and, where feasible, the enthalpic and entropic contributions measured by ITC—across representative viral isolates and receptor orthologues would provide an important next step. Combining these measurements with structures of the corresponding complexes could move the field beyond the correlative relationships between sequence variation and phenotype described in Section 1.2.4, toward a genuinely mechanistic explanation of tropism. This work would also have direct translational relevance. Defining the precise epitope and conformational requirements for productive viral engagement, as this thesis has begun to do for the heme–hFLVCR1a–SU axis, is an essential prerequisite for developing molecular strategies to block receptor engagement. The same knowledge could also support gene-therapy and pseudotyping applications that seek to exploit gammaretroviral receptor interactions. In addition, a comparative

framework could help explain how naturally occurring or engineered RBD mutations across FeLV, GALV, and MLV subtypes redirect receptor tropism. This question is particularly relevant to the mosaic FeLV-A/C recombinant isolates discussed in Section 1.2.4 [14].

(4) Using the antibody and Fab panel as an independent strategy for increasing particle mass and asymmetry. The antibody and Fab work presented in this thesis (Section 4.5) should be considered not only an epitope-mapping and functional resource, but also an independent structural route to be pursued alongside the ligand-based strategies involving FeLV-C SU for FLVCR1a and PiT-1. Both FLVCR1a and PiT-1 are relatively small proteins. Their transmembrane domains also appear to have the internal twofold pseudo-symmetric architecture commonly found in MFS and SLC folds. Once embedded in a detergent micelle, this combination produces a particle that is both small and approximately symmetric. These characteristics can create significant challenges for single-particle cryo-EM by reducing the signal-to-noise ratio available for particle alignment and increasing the risk of symmetry-related misassignments during 2D classification, thereby compromising the accuracy of the final 3D reconstruction. Binding a Fab or antibody fragment can increase both the mass and asymmetry of the particle. It can also break the internal pseudo-symmetry and provide a well-defined, high-contrast feature to support particle alignment. This approach is now routinely used to make otherwise challenging small or symmetric membrane proteins more tractable for cryo-EM [35, 37, 66]. If the RBD- or SU-based strategies prove insufficient—for example, because the RBD or SU is too small or too flexibly attached to function as a reliable fiducial and mass-enhancing partner—the antibody panel characterised in this thesis provides an independent route toward the same structural goal. Clones 339F1, 339H11, 341F5 and 345E9 (SEC-positive, western-blot-negative; Table 1.1) are the conformational candidates. As the Fab 339F1 did not form a detectable complex (Section 3.4.1), the affinity of each Fab must be confirmed before grid preparation, and the other three candidates are the natural alternatives. These candidates could be used alone or in combination with an RBD/SU ligand to further increase particle size and asymmetry.

(5) PiT1/SLC20A1 as a Prospective Structural Target: Lessons from Related Syncytin–Receptor Systems. Before such studies can begin, the PiT-1 constructs must be scaled up and purified, since only expression has been confirmed so far (Section 3.7.6). Beyond the receptors characterized in this thesis, another member of the syncytin family presents a promising opportunity for future structural investigation. Mousseau et al. (2024) [72] recently identified the sodium-dependent phosphate transporter PiT1/SLC20A1 as the cellular receptor for mouse syncytin-B

(SynB), one of the two fusogenic retroviral envelope proteins required for syncytiotrophoblast formation in the mouse placenta. Using a cell–cell fusion screen based on a human ORFeome expression library, the authors showed that PiT1, but not the closely related transporter PiT2/ SLC20A2, supports SynB-mediated fusion. They further confirmed this interaction by co-immunoprecipitation from co-cultured cells. Experiments with PiT1/PiT2 chimeras and truncation constructs localized receptor specificity to the short extracellular N-terminus of PiT1 (residues 1–25). This region is dispensable for infection by other PiT1-using retroviruses, such as 10A1-MLV, but is essential for SynB binding. These findings suggest that PiT1 contains at least two mechanistically distinct entry sites: one used by gammaretroviruses through the EC4 loop and another used by SynB through the N-terminal region [72]. To date, no experimental structure of PiT1 has been reported, either in isolation or in complex with a ligand. The only available structural template for the SLC20 family is the bacterial homologue TmPiT (PDB 6L85) [73]. However, TmPiT shares limited sequence identity with mammalian SLC20 transporters and does not resolve their extracellular loops or N-terminal regions. This gap resembles the situation that motivated structural studies of the related placental receptor–syncytin pairs MFSD2A–syncytin-2 [74] and ASCT2–syncytin-1/suppressyn [75]. In both cases, consensus-sequence protein engineering, detergent-based binding assays, and cryo-EM were combined to resolve the transporter and its receptor-binding domain. These studies suggest a plausible strategy for determining the structure of the PiT1–SynB complex. In both systems, wild-type transporter and ligand constructs were often unstable in detergent. Replacing poorly conserved residues with consensus residues derived from vertebrate orthologues—producing ASCT2CO, MFSD2ACO, and SYNC2CO—substantially improved stability without disrupting function, as demonstrated by split-GFP fusion and substrate-transport assays [74, 75]. A similar consensus-design strategy could potentially be applied to PiT1, whose SynB-permissive orthologues include proteins from human, mouse, dog, and chicken [72]. Both studies also used detergent-phase affinity measurements to identify constructs suitable for cryo-EM and introduced point mutations or truncations to stabilize the receptor–ligand complex before structural analysis. When conformational heterogeneity limited resolution, targeted approaches were successful: individual components were extracted from a flexible oligomeric assembly in one study [74], whereas a conformation-selective nanobody was used as a fiducial in the other [75]. The PiT1–SynB interaction may be more experimentally tractable than the larger, multi-loop interfaces described for ASCT2 and MFSD2A. The SynB-binding site is confined to a short, topologically defined extracellular segment of 25 residues, and a membrane-anchored construct containing only this N-terminal region and the first transmembrane helix was sufficient to

support partial SynB-mediated fusion [72]. Resolving the PiT1–SynB complex would provide the first structural view of the PiT1 extracellular architecture, clarify the basis of SynB's strict receptor specificity relative to PiT2, and reveal whether receptor engagement stabilizes an outward-facing, inward-facing, or occluded transporter conformation. Such information would also inform our understanding of PiT1's broader roles in phosphate sensing, apoptosis, and cell proliferation [76, 77]. The PiT1–SynB complex therefore represents a natural extension of the present work and a promising target for future structural investigation.

6. References

1. Jerabek-Willemsen, M., Wienken, C. J., Braun, D., Baaske, P., & Duhr, S. (2011). Molecular interaction studies using microscale thermophoresis. *Assay and Drug Development Technologies*, 9(4), 342–353.
2. Yang, Z., Philips, J. D., Doty, R. T., Giraudi, P., Ostrow, J. D., Tiribelli, C., Smith, A., & Abkowitz, J. L. (2010). Kinetics and specificity of feline leukemia virus subgroup C receptor (FLVCR) export function and its dependence on hemopexin. *Journal of Biological Chemistry*, 285(37), 28874–28882.
3. Quigley, J. G., Yang, Z., Worthington, M. T., Phillips, J. D., Sabo, K. M., Sabath, D. E., Berg, C. L., Sassa, S., Wood, B. L., & Abkowitz, J. L. (2004). Identification of a human heme exporter that is essential for erythropoiesis. *Cell*, 118(6), 757–766.
4. Fiorito, V., & Tolosano, E. (2024). Unearthing FLVCR1a: tracing the path to a vital cellular transporter. *Cellular and Molecular Life Sciences*, 81(1), 166.
5. Wen, M., Liang, Y., Wang, Z., Sun, Y., Wu, T., Mao, Y., … & Gong, X. (2022). Structural insights into porphyrin recognition by the human ATP-binding cassette transporter ABCB6. *Science Advances*, 8(33), eabq8175.
6. Bai, N., Ramos, A. L., Bhatt, D. L., & Bhatt, D. (2019). *nDSF as a screening method for membrane proteins.*NanoTemper Technologies Application Note.
7. Reinhard, L., Mayerhofer, H., Geerlof, A., Mueller-Dieckmann, J., & Weiss, M. S. (2013). Optimization of protein buffer cocktails using Thermofluor. *Acta Crystallographica Section F*, 69(2), 209–214.
8. Niesen, F. H., Berglund, H., & Vedadi, M. (2007). The use of differential scanning fluorimetry to detect ligand interactions that promote protein stability. *Nature Protocols*, 2(9), 2212–2221.
9. Lo, M. C., Aulabaugh, A., Jin, G., Cowling, R., Bard, J., Malamas, M., & Ellestad, G. (2004). Evaluation of fluorescence-based thermal shift assays for hit identification in drug discovery. *Analytical Biochemistry*, 332(1), 153–159.
10. Son, L. et al. (2024). Structural and mechanistic insights into human choline and ethanolamine transport. *Nature*(published online; PDB: 8QCS, 8QCT).
11. Sarma, P.S. and Log, T. (1973) Subgroup classification of feline leukemia and sarcoma viruses by viral interference and neutralization tests. *Virology*, 54(1), 160–169. https://doi.org/10.1016/0042-6822(73)90125-6

12. Miyake, A., Watanabe, S., Hiratsuka, T., Ito, J., Ngo, M.H., Makundi, I., Kawasaki, J., Endo, Y., Tsujimoto, H. and Nishigaki, K. (2016) Novel Feline Leukemia Virus Interference Group Based on the env Gene. *Journal of Virology*, 90(9), 4832–4837. https://doi.org/10.1128/JVI.03229-15
13. Bolin, L.L. and Levy, L.S. (2011) Viral Determinants of FeLV Infection and Pathogenesis: Lessons Learned from Analysis of a Natural Cohort. *Viruses*, 3(9), 1681–1698. https://doi.org/10.3390/v3091681
14. Stewart, H., Adema, K.W., McMonagle, E.L., Hosie, M.J. and Willett, B.J. (2012) Identification of novel subgroup A variants with enhanced receptor binding and replicative capacity in primary isolates of anaemogenic strains of feline leukaemia virus. *Retrovirology*, 9, 48. https://doi.org/10.1186/1742-4690-9-48
15. Tailor, C. S., Willett, B. J., & Kabat, D. (1999). A putative cell surface receptor for anemia-inducing feline leukemia virus subgroup C is a member of a transporter superfamily. *Journal of Virology*, 73(8), 6500–6505.
16. Quigley, J. G., Burns, C. C., Anderson, M. M., Lynch, E. D., Sabo, K. M., Overbaugh, J., & Abkowitz, J. L. (2000). Cloning of the cellular receptor for feline leukemia virus subgroup C (FeLV-C), a retrovirus that induces red cell aplasia. *Blood*, 95(3), 1093–1099.
17. Khan, A. A., & Quigley, J. G. (2013). Heme and FLVCR-related transporter families SLC48 and SLC49. *Molecular Aspects of Medicine*, 34(2–3), 669–682.
18. Kunji, E. R. S., Harding, M., Butler, P. J. G., & Akamine, P. (2008). Determination of the molecular mass and dimensions of membrane proteins by size exclusion chromatography. *Methods*, 46(2), 62–72.
19. le Maire, M., Arnou, B., Olesen, C., Georgin, D., Ebel, C., & Møller, J. V. (2008). Gel chromatography and analytical ultracentrifugation to determine the extent of detergent binding and aggregation, and Stokes radius of membrane proteins using sarcoplasmic reticulum Ca^{2+}-ATPase as an example. *Nature Protocols*, 3(11), 1782–1795.
20. Gimpl, K., Klement, J., & Keller, S. (2016). Characterising protein/detergent complexes by triple-detection size-exclusion chromatography. *Biological Procedures Online*, 18, 4.
21. Louche, A., Salcedo, S. P., & Bigot, S. (2017). Protein–protein interactions: pull-down assays. In L. Journet & E. Cascales (Eds.), *Bacterial Protein Secretion Systems* (Methods in Molecular Biology, Vol. 1615, pp. 247–255). Humana Press.
22. Yan, N. (2013). Structural advances for the major facilitator superfamily (MFS) transporters. *Trends in Biochemical Sciences*, 38(3), 151–159.

23. Law, C. J., Maloney, P. C., & Wang, D.-N. (2008). Ins and outs of major facilitator superfamily antiporters. *Annual Review of Microbiology*, 62, 289–305.
24. Goehring, A., Lee, C. H., Wang, K. H., Michel, J. C., Claxton, D. P., Baconguis, I., … & Gouaux, E. (2014). Screening and large-scale expression of membrane proteins in mammalian cells for structural studies. *Nature Protocols*, 9(11), 2574–2585.
25. Pieprzyk, J., Pazicky, S., & Löw, C. (2018). Transient expression of recombinant membrane-eGFP fusion proteins in HEK293 cells. In D. Hacker (Ed.), *Recombinant Protein Expression in Mammalian Cells* (Methods in Molecular Biology, Vol. 1850, pp. 17–31). Humana Press.
26. Gorman, C. M., Howard, B. H., & Reeves, R. (1983). Expression of recombinant plasmids in mammalian cells is enhanced by sodium butyrate. *Nucleic Acids Research*, 11(21), 7631–7648.
27. Backliwal, G., Hildinger, M., Kuettel, I., Delegrange, F., Hacker, D. L., & Wurm, F. M. (2008). Valproic acid: a viable alternative to sodium butyrate for enhancing protein expression in mammalian cell cultures. *Biotechnology and Bioengineering*, 101(1), 182–189.
28. Walls, A. C., Park, Y. J., Tortorici, M. A., Wall, A., McGuire, A. T., & Veesler, D. (2019). Structure, function, and antigenicity of the SARS-CoV-2 spike glycoprotein. *Cell*, 181(2), 281–292.
29. Mishra, S., Verhalen, B., Bhatt, D., Bhatt, D. L., & Bhatt, D. (2011). High-efficiency screening of monoclonal antibodies for membrane protein crystallography. *PLOS ONE*, 6(9), e24653.
30. Dominik, P. K., & Bhatt, D. (2024). Generation of conformation-specific monoclonal antibodies for integral membrane proteins. *Current Protocols*, e70142.
31. Brown, J.K., Fung, C. and Tailor, C.S. (2006) Comprehensive mapping of receptor-functioning domains in feline leukemia virus subgroup C receptor FLVCR1. *Journal of Virology*, 80(4), 1742–1751.
32. Jespersen MC, Peters B, Nielsen M, Marcatili P. (2017). BepiPred-2.0: improving sequence-based B-cell epitope prediction using conformational epitopes. *Nucleic Acids Research*, 45(W1), W24–W29. https://doi.org/10.1093/nar/gkx346
33. Greenspan NS. (2023). Epitopes, paratopes, and other topes 30 years on: Understanding what we are talking about. *Human Immunology*, 84(9), 429–438. https://doi.org/10.1016/j.humimm.2023.06.006
34. Forsström B, Bisławska Axnäs B, Rockberg J, Danielsson H, Bohlin A, Uhlén M. (2015). Dissecting antibodies with regards to linear and conformational epitopes. *PLoS ONE*, 10(3), e0121673. https://doi.org/10.1371/journal.pone.0121673

35. Pardon, E., Laeremans, T., Triest, S., Rasmussen, S. G. F., Wohlkönig, A., Ruf, A., … & Steyaert, J. (2014). A general protocol for the generation of Nanobodies for structural biology. *Nature Protocols*, 9(3), 674–693.
36. Dominik, P. K., & Bhatt, D. (2024). Generation of conformation-specific monoclonal antibodies for integral membrane proteins. *Current Protocols*, e70142.
37. Uchański, T., Masiulis, S., Fischer, B., Kalichuk, V., López-Sánchez, U., Zarkadas, E., … & Bhatt, D. (2021). Megabodies expand the nanobody toolkit for protein structure determination by single-particle cryo-EM. *Nature Methods*, 18(1), 60–68.
38. Greenfield, E. A. (2010). Antibodies: A Laboratory Manual (2nd ed.). Cold Spring Harbor Laboratory Press.
39. Hulme, E. C., & Trevethick, M. A. (2010). Ligand binding assays at equilibrium: validation and interpretation. *British Journal of Pharmacology*, 161(6), 1219–1237.
40. Zanin Venturini, D.I. and Chiabrando, D. (2026) 'FLVCR1-related diseases: from clinical heterogeneity to mechanistic insights', *Brain Communications*, 8(3), fcag165.
41. Dukkipati, A., Park, H.H., Waghray, D., Fischer, S. and Garcia, K.C. (2008) 'BacMam system for high-level expression of recombinant soluble and membrane glycoproteins for structural studies', *Protein Expression and Purification*, 62(2), pp. 160–170.
42. Kapust, R.B., Tözsér, J., Fox, J.D., Anderson, D.E., Cherry, S., Copeland, T.D. and Waugh, D.S. (2001) 'Tobacco etch virus protease: mechanism of autolysis and rational design of stable mutants with wild-type catalytic efficiency', *Protein Engineering*, 14(12), pp. 993–1000.
43. Schmidt, T.G.M., Batz, L., Bonet, L., Carl, U., Holzapfel, G., Kiem, K., Matulewicz, K., Niermeier, D., Schuchardt, I. and Stanar, K. (2013) 'Development of the Twin-Strep-tag and its application for purification of recombinant proteins from cell culture supernatants', *Protein Expression and Purification*, 92(1), pp. 54–61.
44. Seddon, A.M., Curnow, P. and Booth, P.J. (2004) 'Membrane proteins, lipids and detergents: not just a soap opera', *Biochimica et Biophysica Acta (BBA) – Biomembranes*, 1666(1–2), pp. 105–117.
45. Fekete, S., Beck, A., Veuthey, J.L. and Guillarme, D. (2014) 'Theory and practice of size exclusion chromatography for the analysis of protein aggregates', *Journal of Pharmaceutical and Biomedical Analysis*, 101, pp. 161–173.
46. Boomer, S., Eiden, M., Burns, C.C. and Overbaugh, J. (1997) 'Three distinct envelope domains, variably present in subgroup B feline leukemia virus recombinants, mediate Pit1 and Pit2 receptor recognition', *Journal of Virology*, 71(11), pp. 8116–8123.

47. Hochuli, E., Bannwarth, W., Döbeli, H., Gentz, R. and Stüber, D. (1988) 'Genetic approach to facilitate purification of recombinant proteins with a novel metal chelate adsorbent', *Bio/ Technology*, 6, pp. 1321–1325.
48. Luckow, V.A., Lee, S.C., Barry, G.F. and Olins, P.O. (1993) 'Efficient generation of infectious recombinant baculoviruses by site-specific transposon-mediated insertion of foreign genes into a baculovirus genome propagated in *Escherichia coli*', *Journal of Virology*, 67(8), pp. 4566–4579.
49. Thermo Fisher Scientific (n.d.) Bac-to-Bac® Baculovirus Expression System User Guide (MAN0000414).
50. Condreay, J.P., Witherspoon, S.M., Clay, W.C. and Kost, T.A. (1999) 'Transient and stable gene expression in mammalian cells transduced with a recombinant baculovirus vector', *Proceedings of the National Academy of Sciences USA*, 96(1), pp. 127–132.
51. Kost, T.A., Condreay, J.P. and Jarvis, D.L. (2005) 'Baculovirus as versatile vectors for protein expression in insect and mammalian cells', *Nature Biotechnology*, 23(5), pp. 567–575.
52. Sigma-Aldrich (n.d.) *Ni-NTA-Atto Conjugates* [Technical Article]. Available at: sigmaaldrich.com.
53. Lambert, G.S. and Upadhyay, C. (2021) 'HIV-1 envelope glycosylation and the signal peptide', *Vaccines*, 9(2), p. 176.
54. Zhu, B., Cai, G., Hall, E.O. and Freeman, G.J. (2007) 'In-Fusion assembly: seamless engineering of multidomain fusion proteins, modular vectors, and mutations', *BioTechniques*, 43(3), pp. 354–359.
55. Berrow, N.S., Alderton, D., Sainsbury, S., Nettleship, J., Assenberg, R., Rahman, N., Stuart, D.I. and Owens, R.J. (2007) 'A versatile ligation-independent cloning method suitable for high-throughput expression screening applications', *Nucleic Acids Research*, 35(6), e45.
56. Qiagen (2015) QIAprep Spin Miniprep Kit: Quick-Start Protocol.
57. Pham, P.L., Perret, S., Cass, B., Carpentier, É., St-Laurent, G., Bisson, L., Kamen, A. and Durocher, Y. (2003) 'Large-scale transient transfection of serum-free suspension-growing HEK293 EBNA1 cells: peptone additives improve cell growth and transfection efficiency', *Biotechnology and Bioengineering*, 84(3), pp. 332–342.
58. Farrell, K. B., Tusnady, G. E., & Eiden, M. V. (2009). New structural arrangement of the extracellular regions of the phosphate transporter SLC20A1, the receptor for gibbon ape leukemia virus. *Journal of Biological Chemistry*, 284(43), 29979–29987.

59. Kawate, T. and Gouaux, E. (2006) 'Fluorescence-detection size-exclusion chromatography for precrystallization screening of integral membrane proteins', *Structure*, 14(4), pp. 673–681.
60. Graham, F.L., Smiley, J., Russell, W.C. and Nairn, R. (1977) 'Characteristics of a human cell line transformed by DNA from human adenovirus type 5', *Journal of General Virology*, 36(1), pp. 59–74.
61. Thermo Fisher Scientific (2018) ExpiSf™ Expression System: User Guide (Publication No. MAN0017532).
62. Yeliseev, A., Zoubak, L. and Schmidt, T.G.M. (2017) 'Application of Strep-Tactin XT for affinity purification of Twin-Strep-tagged CB2, a G protein-coupled cannabinoid receptor', *Protein Expression and Purification*, 131, pp. 109–118.
63. Laemmli, U.K. (1970) 'Cleavage of structural proteins during the assembly of the head of bacteriophage T4', *Nature*, 227(5259), pp. 680–685.
64. Fazekas de St Groth, S., Webster, R.G. and Datyner, A. (1963) 'Two new staining procedures for quantitative estimation of proteins on electrophoretic strips', *Biochimica et Biophysica Acta*, 71, pp. 377–391.
65. Towbin, H., Staehelin, T. and Gordon, J. (1979) 'Electrophoretic transfer of proteins from polyacrylamide gels to nitrocellulose sheets: procedure and some applications', *Proceedings of the National Academy of Sciences USA*, 76(9), pp. 4350–4354.
66. Bloch, J.S., Pesciullesi, G., Boilevin, J., Nosol, K., Irobalieva, R.N., Darbre, T., Reymond, J.L., Kossiakoff, A.A. and Locher, K.P. (2021) 'Development of a universal nanobody-binding Fab module for fiducial-assisted cryo-EM studies of membrane proteins', *Proceedings of the National Academy of Sciences USA*, 118(45), e2115435118.
67. Wienken, C.J., Baaske, P., Rothbauer, U., Braun, D. and Duhr, S. (2010) 'Protein-binding assays in biological liquids using microscale thermophoresis', *Nature Communications*, 1, p. 100.
68. Steinke, S., Roth, K.D.R., Ruschig, M., Langreder, N., Polten, S., Schneider, K.T., Ballmann, R., Russo, G., Zilkens, K.J.K., Schubert, M., Bertoglio, F. and Hust, M. (2023) 'Antibody selection via phage display in microtiter plates', *Methods in Molecular Biology*, 2702, pp. 247–260.
69. Tsien, R.Y. (1998) 'The green fluorescent protein', *Annual Review of Biochemistry*, 67, pp. 509–544.
70. Wienken, C. J., Baaske, P., Rothbauer, U., Braun, D., & Duhr, S. (2010). Protein-binding assays in biological liquids using microscale thermophoresis. *Nature communications*, *1*, 100. https://doi.org/10.1038/ncomms1093

71. Hulme, E.C. and Trevethick, M.A. (2010), Ligand binding assays at equilibrium: validation and interpretation. British Journal of Pharmacology, 161: 1219-1237. https://doi.org/10.1111/j.1476-5381.2009.00604.x
72. Mousseau, G., Préault, N., Souquere, S., Bireau, C., Cassonnet, P., Bacquin, A., … & Heidmann, T. (2024). Sodium-dependent phosphate transporter PiT1/SLC20A1 as the receptor for the endogenous retroviral envelope syncytin-B involved in mouse placenta formation. *Journal of Virology*, 98(10), e00915-24.
73. Tsai, J. Y., Chu, C. H., Lin, M. G., Chou, Y. H., Hong, R. Y., Yen, C. Y., … & Sun, Y. J. (2020). Structure of the sodium-dependent phosphate transporter reveals insights into human solute carrier SLC20. *Science Advances*, 6(41), eabb4024.
74. Martinez-Molledo, M., Nji, E., & Reyes, N. (2022). Structural insights into the lysophospholipid brain uptake mechanism and its inhibition by syncytin-2. *Nature Structural & Molecular Biology*, 29, 604–612.
75. Khare, S., Villalba, M. I., Canul-Tec, J. C., Cajiao, A. B., Kumar, A., Backovic, M., Rey, F. A., Pardon, E., Steyaert, J., Perez, C., & Reyes, N. (2024). Cryo-EM structures of ASCT2 in complexes with syncytin-1 and suppressyn reveal a common receptor recognition mechanism. *Nature Structural & Molecular Biology*, 31, 1368–1376.
76. Beck, L., Leroy, C., Beck-Cormier, S., Forand, A., Salaün, C., Paris, N., … & Friedlander, G. (2010). The phosphate transporter PiT1 (Slc20a1) revealed as a new essential gene for mouse liver development. *PLoS ONE*, 5(1), e9148.
77. Salaün, C., Leroy, C., Rousseau, A., Boitez, V., Beck, L., & Friedlander, G. (2010). Identification of a novel transport-independent function of PiT1/SLC20A1 in the regulation of TNF-induced apoptosis. *Journal of Biological Chemistry*, 285(45), 34408–34418.
78. Greenwood, A.D., Ishida, Y., O'Brien, S.P., Roca, A.L. and Eiden, M.V. (2018) 'Transmission, evolution, and endogenization: lessons learned from recent retroviral invasions', *Microbiology and Molecular Biology Reviews*, 82(1), e00044-17.
79. Hogan, V. and Johnson, W.E. (2023) 'Unique structure and distinctive properties of the ancient and ubiquitous gamma-type envelope glycoprotein', *Viruses*, 15(2), p. 274.
80. Fass, D., Davey, R.A., Hamson, C.A., Kim, P.S., Cunningham, J.M. and Berger, J.M. (1997) 'Structure of a murine leukemia virus receptor-binding glycoprotein at 2.0 Å resolution', *Science*, 277(5332), pp. 1662–1666.
81. Battini, J.L., Danos, O. and Heard, J.M. (1995) 'Receptor-binding domain of murine leukemia virus envelope glycoproteins', *Journal of Virology*, 69(2), pp. 713–719.

82. Sugai, J., Eiden, M., Anderson, M.M., Van Hoeven, N., Meiering, C.D. and Overbaugh, J. (2001) 'Identification of envelope determinants of feline leukemia virus subgroup B that permit infection and gene transfer to cells expressing human Pit1 or Pit2', *Journal of Virology*, 75(15), pp. 6841–6849.
83. Anderson, M.M., Lauring, A.S., Robertson, S., Dirks, C. and Overbaugh, J. (2001) 'Feline Pit2 functions as a receptor for subgroup B feline leukemia viruses', *Journal of Virology*, 75(22), pp. 10563–10572.
84. Barnett, A.L., Wensel, D.L., Li, W., Fass, D. and Cunningham, J.M. (2003) 'Structure and mechanism of a coreceptor for infection by a pathogenic feline retrovirus', *Journal of Virology*, 77(4), pp. 2717–2729.
85. Overbaugh, J., Riedel, N., Hoover, E.A. and Mullins, J.I. (1988) 'Transduction of endogenous envelope genes by feline leukaemia virus in vitro', *Nature*, 332, pp. 731–734.
86. Tailor, C.S., Lavillette, D., Marin, M. and Kabat, D. (2003) 'Cell surface receptors for gammaretroviruses', *Current Topics in Microbiology and Immunology*, 281, pp. 29–106.
87. Chiabrando, D., Scietti, L., Prajica, A. G., Bertino, F., Tolosano, E., & Magnani, F. (2020). Expression and purification of the heme exporter FLVCR1a. *Protein Expression and Purification*, 172, 105637. https://doi.org/10.1016/j.pep.2020.105637
88. Chiabrando, D., Marro, S., Mercurio, S., Giorgi, C., Petrillo, S., Vinchi, F., Fiorito, V., Fagoonee, S., Camporeale, A., Turco, E., Merlo, G. R., Silengo, L., Altruda, F., Pinton, P., & Tolosano, E. (2012). The mitochondrial heme exporter FLVCR1b mediates erythroid differentiation. *Journal of Clinical Investigation*, 122(12), 4569–4579. https://doi.org/10.1172/JCI62422
89. Kavanaugh, M.P., Miller, D.G., Zhang, W., Law, W., Kozak, S.L., Kabat, D. and Miller, A.D. (1994) 'Cell-surface receptors for gibbon ape leukemia virus and amphotropic murine retrovirus are inducible sodium-dependent phosphate symporters', *Proceedings of the National Academy of Sciences*, 91(15), pp. 7071–7075. doi: 10.1073/pnas.91.15.7071.
90. Johann, S. V., Gibbons, J. J., & O'Hara, B. (1992). GLVR1, a receptor for gibbon ape leukemia virus, is homologous to a phosphate permease of Neurospora crassa and is expressed at high levels in the brain and thymus. *Journal of virology*, *66*(3), 1635–1640. https://doi.org/10.1128/JVI.66.3.1635-1640.1992
91. Bøttger, P., & Pedersen, L. (2011). Mapping of the minimal inorganic phosphate transporting unit of human PiT2 suggests a structure universal to PiT-related proteins from all kingdoms of life. *BMC biochemistry*, *12*, 21. https://doi.org/10.1186/1471-2091-12-21

92. Salaün, C., Rodrigues, P. and Heard, J.M. (2001) 'Transmembrane topology of PiT-2, a phosphate transporter–retrovirus receptor', *Journal of Virology*, 75(12), pp. 5584–5592. doi: 10.1128/JVI.75.12.5584-5592.2001.
93. Farrell, K.B., Russ, J.L., Murthy, R.K. and Eiden, M.V. (2002) 'Reassessing the role of region A in Pit1-mediated viral entry', Journal of Virology, 76(15), pp. 7683–7693. doi: 10.1128/JVI.76.15.7683-7693.2002.
94. Tailor, C.S., Takeuchi, Y., O'Hara, B., Johann, S.V., Weiss, R.A. and Collins, M.K. (1993) 'Mutation of amino acids within the gibbon ape leukemia virus (GALV) receptor differentially affects feline leukemia virus subgroup B, simian sarcoma-associated virus, and GALV infections', Journal of Virology, 67(11), pp. 6737–6741. doi: 10.1128/JVI.67.11.6737-6741.1993.
95. Eiden, M.V., Farrell, K.B. and Wilson, C.A. (1996) 'Substitution of a single amino acid residue is sufficient to allow the human amphotropic murine leukemia virus receptor to also function as a gibbon ape leukemia virus receptor', *Journal of Virology*, 70(2), pp. 1080–1085.
96. Lundorf, M.D., Pedersen, F.S., O'Hara, B. and Pedersen, L. (1999) 'Amphotropic murine leukemia virus entry is determined by specific combinations of residues from receptor loops 2 and 4', *Journal of Virology*, 73(4), pp. 3169–3175.
97. Leverett, B.D., Farrell, K.B., Eiden, M.V. and Wilson, C.A. (1998) 'Entry of amphotropic murine leukemia virus is influenced by residues in the putative second extracellular domain of its receptor, Pit2', *Journal of Virology*, 72(6), pp. 4956–4961.
98. Feldman, S.A., Farrell, K.B., Murthy, R.K., Russ, J.L. and Eiden, M.V. (2004) 'Identification of an extracellular domain within the human PiT2 receptor that is required for amphotropic murine leukemia virus binding', *Journal of Virology*, 78(2), pp. 595–602.
99. Chaudry, G.J. and Eiden, M.V. (2000) 'A 13-amino-acid Pit1-specific loop 4 sequence confers feline leukemia virus subgroup B receptor function upon Pit2', *Journal of Virology*, 74(6), pp. 2926–2929.
100. Ackle, F., Thavarasah, S., Earp, J.C. and Seeger, M.A. (2025) 'Rigid enlargement of sybodies with antibody fragments for cryo-EM analyses of small membrane proteins', Scientific Reports, 15, p. 9460. doi: 10.1038/s41598-025-92950-5.
101. Kumar, A., Planchais, C., Fronzes, R., Mouquet, H. and Reyes, N. (2020) 'Binding mechanisms of therapeutic antibodies to human CD20', Science, 369(6505), pp. 793–799. doi: 10.1126/science.abb8008.

102. Harris, L.J., Larson, S.B., Hasel, K.W. and McPherson, A. (1997) 'Refined structure of an intact IgG2a monoclonal antibody', Biochemistry, 36(7), pp. 1581–1597. doi: 10.1021/bi962514+.

103. Harris, L.J., Skaletsky, E. and McPherson, A. (1998) 'Crystallographic structure of an intact IgG1 monoclonal antibody', Journal of Molecular Biology, 275(5), pp. 861–872. doi: 10.1006/jmbi.1997.1508.

104. Nelson, A.L. (2010) 'Antibody fragments: hope and hype', mAbs, 2(1), pp. 77–83. doi: 10.4161/mabs.2.1.10786.

105. Chen, Q., Menon, R., Calder, L.J., Tolar, P. and Rosenthal, P.B. (2022) 'Cryomicroscopy reveals the structural basis for a flexible hinge motion in the immunoglobulin M pentamer', Nature Communications, 13, article 6314. doi: 10.1038/s41467-022-34090-2.

106. Van Regenmortel, M.H.V. (1996) 'Mapping epitope structure and activity: from one-dimensional prediction to four-dimensional description of antigenic specificity', Methods, 9(3), pp. 465–472. doi: 10.1006/meth.1996.0054.

107. Sela-Culang, I., Kunik, V. and Ofran, Y. (2013) 'The structural basis of antibody–antigen recognition', Frontiers in Immunology, 4, p. 302. doi: 10.3389/fimmu.2013.00302.

108. Thermo Fisher Scientific. ExpiSf9™ Cells (Gibco, Cat. No. A35243), product information. https://www.thermofisher.com/order/catalog/product/A35243

109. Vaughn JL, Goodwin RH, Tompkins GJ, McCawley P. The establishment of two cell lines from the insect *Spodoptera frugiperda* (Lepidoptera; Noctuidae). *In Vitro*. 1977;13(4):213–217. doi:10.1007/BF02615077

110. Summers MD, Smith GE. A manual of methods for baculovirus vectors and insect cell culture procedures. *Texas Agricultural Experiment Station Bulletin* No. 1555. 1987.

111. Smith GE, Summers MD, Fraser MJ. Production of human beta interferon in insect cells infected with a baculovirus expression vector. *Mol Cell Biol*. 1983;3(12):2156–2165. doi:10.1128/mcb.3.12.2156-2165.1983

112. Chaudry, G. J., & Eiden, M. V. (1997). Mutational analysis of the proposed gibbon ape leukemia virus binding site in Pit1 suggests that other regions are important for infection. *Journal of virology*, *71*(10), 8078–8081. https://doi.org/10.1128/JVI.71.10.8078-8081.1997

113. Gu, H., Lalonde, S., Okumoto, S., Looger, L. L., Scharff-Poulsen, A. M., Grossman, A. R., Kossmann, J., Jakobsen, I., & Frommer, W. B. (2006). A novel analytical method for in vivo phosphate tracking. FEBS Letters, 580(25), 5885–5893. https://doi.org/10.1016/j.febslet.2006.09.048